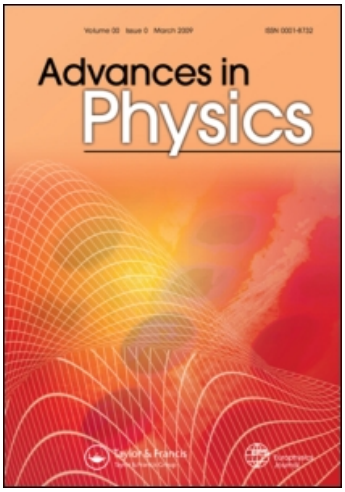

Advances in Physics
Publication details, including instructions for authors and subscription information:
http://www.informaworld.com/smpp/title~content=t713736250

Decoherence in solid-state qubits

Luca Chirolli[a]; Guido Burkard
[a] Department of Physics, University of Konstanz, D-78457 Konstanz, Germany

To cite this Article Chirolli, Luca and Burkard, Guido(2008) 'Decoherence in solid-state qubits', Advances in Physics, 57: 3, 225 — 285
To link to this Article: DOI: 10.1080/00018730802218067
URL: http://dx.doi.org/10.1080/00018730802218067

Advances in Physics
Vol. 57, No. 3, May–June 2008, 225–285

Taylor & Francis
Taylor & Francis Group

Decoherence in solid-state qubits

Luca Chirolli and Guido Burkard*

Department of Physics, University of Konstanz, D-78457 Konstanz, Germany; Institute of Theoretical Physics C, RWTH Aachen University, D-52054 Aachen, Germany

(*Received 10 December 2007; final version received 20 May 2008*)

The interaction of solid-state qubits with environmental degrees of freedom strongly affects the qubit dynamics, and leads to decoherence. In quantum information processing with solid-state qubits, decoherence significantly limits the performances of such devices. Therefore, it is necessary to fully understand the mechanisms that lead to decoherence. In this review, we discuss how decoherence affects two of the most successful realizations of solid-state qubits, namely, spin qubits and superconducting qubits. In the former, the qubit is encoded in the spin 1/2 of the electron, and it is implemented by confining the electron spin in a semiconductor quantum dot. Superconducting devices show quantum behaviour at low temperatures, and the qubit is encoded in the two lowest energy levels of a superconducting circuit. The electron spin in a quantum dot has two main decoherence channels, a (Markovian) phonon-assisted relaxation channel, due to the presence of a spin–orbit interaction, and a (non-Markovian) spin bath constituted by the spins of the nuclei in the quantum dot that interact with the electron spin via the hyperfine interaction. In a superconducting qubit, decoherence takes place as a result of fluctuations in the control parameters, such as bias currents, applied flux and bias voltages, and via losses in the dissipative circuit elements.

Keywords: decoherence; quantum dots; spin qubits; spin coherence; superconducting qubits

Contents

*Corresponding author. Email: guido.burkard@uni-konstanz.de

ISSN 0001–8732 print/ISSN 1460–6976 online

DOI: 10.1080/00018730802218067
http://www.informaworld.com

1. Introduction

1.1. *What is coherence and why is it interesting?*

Coherence is a defining property of quantum mechanics. It can be argued that quantum coherence is the property that draws a line between the 'quantum world' and the 'classical world'. However, what exactly is coherence? In physics, the term coherence refers to the property of waves to interfere, showing well-known interference patterns. Two waves, depending on their relative phase, can produce a constructive interference, characterized by an enhancement of the amplitude of the wave, or destructive interference, accompanied by a suppression of its amplitude. Only the relative phase of the two waves makes the difference. To be precise we should therefore speak about phase coherence of quantum states.

By quantum states here we mean states of a quantum system, which in turn can be constituted by more than one quantum object. The same rules of quantum mechanics that allow us to explain and predict interference of one object with itself, as the case of an electron through a double slit, predict that a system composed by two quantum subsystems can be in a state that has no classical counterpart, being a superposition with a precise phase of two or more quantum states of the whole system. This property of quantum states goes under the name of entanglement, and entangled states need to be phase coherent. In particular, coherence, as a property of quantum mechanical phenomena, disappears in the classical world, and it is therefore of fundamental interest to study it in theory and experiment. It is never completely possible to isolate a quantum system from the surrounding world. The system and its surroundings interact and, as a result, a randomization of the phase of the quantum system takes place, resulting in a loss of information. This process is known as decoherence.

Only in recent years, thanks to the advances in technology, has it become possible to study quantum effects involving single quantum objects, such as single photons, ions, electron spins, etc. Particular attention has been paid to observing coherence from an experimental point of view, and to understand its limitations. In fact, although remarkable improvements have been achieved, nowadays, to see coherence, a lot of effort must be spent on understanding how to preserve coherence. Over the last few decades, the idea of joining quantum physics laws and information science gave birth to a new and intriguing branch of science, quantum information theory, which studies the possibilities that quantum rules offer to information processing. In particular, the superposition principle opens the possibility to perform new and fast algorithms. The physical implementation of quantum information processing represents a challenge because one has to deal with the competition between fast and reliable quantum control, that requires interaction with the outside world, and good isolation of the quantum devices in order to ensure long coherence times.

Therefore, it is important to understand theoretically how decoherence happens in the systems under study (here, solid-state systems) in order to make progress towards this ambitious goal (that is, implementing quantum information).

1.1.1. *The quantum bit*

Classical information is based on binary logic, in which information is encoded in a series of bits (binary digits) that can assume only two values, 0 or 1. A typical example is

a switch, with its two possible states 'on' and 'off'. All classical logical operations can be implemented as algorithms based on one- and two-bit operations, the so-called gates.

The building block of quantum information is the quantum bit, or qubit. Using the Dirac notation, the two states that characterize the qubit are $|0\rangle$ and $|1\rangle$ and they represent the quantum counterpart of the classical 0 and 1. The most important property of a quantum bit is the possibility to be in a coherent superposition state

$$|\psi\rangle = \alpha|0\rangle + \beta|1\rangle, \tag{1}$$

with α and β complex numbers, characterized by a relative phase and by $|\alpha|^2 + |\beta|^2 = 1$. According to the postulates of quantum mechanics, $|\alpha|^2$ represents the probability for the qubit to be in the state $|0\rangle$, whereas $|\beta|^2$ represents the probability to be in the state $|1\rangle$. This means that if we prepare many copies of the same system in the state $|\psi\rangle$, a measurement of the state of the qubit will produce the outcome 0 with rate $|\alpha|^2$ and the outcome 1 with rate $|\beta|^2$. In the following the two logical states are the spin up $|\uparrow\rangle$ and the spin down $|\downarrow\rangle$. The two states $|0\rangle$ and $|1\rangle$ form a basis of the Hilbert space $\mathcal{H} = \text{span}\{|0\rangle, |1\rangle\}$ of the qubit.

A good example of a qubit is the spin 1/2. In order to explain the necessity to use complex numbers α and β to characterize the state of the qubit, we describe an interference procedure for a spin-1/2 particle. Suppose that we prepare the spin in the state $|\psi_0\rangle = |\uparrow\rangle$, that is, with probability 1 to find it parallel with respect to a certain direction z in the space, which we choose as the quantization axis. We then rotate the spin by an angle $\pi/2$ about an axis perpendicular to z, that is, the y-axis. The result is the state

$$|\psi_1\rangle = e^{-i(\pi/4)\sigma_y}|\uparrow\rangle = \frac{1}{\sqrt{2}}(|\uparrow\rangle + |\downarrow\rangle). \tag{2}$$

We then let the spin cross a region in which there is a magnetic field that points in the positive z direction, $\mathbf{B} = (0, 0, B)$. Owing to the presence of the magnetic field, the two states $|\uparrow\rangle$ and $|\downarrow\rangle$ accumulate a relative phase 2φ, that depends on the magnitude of the magnetic field and the time t spent in the region with the $\mathbf{B}$ field, and that for simplicity we leave unspecified. Up to an overall phase, the state of the system that comes out from the region with a magnetic field is given by

$$|\psi_2\rangle = \frac{1}{\sqrt{2}}(|\uparrow\rangle + e^{2i\varphi}|\downarrow\rangle). \tag{3}$$

Now, we again rotate the spin of $\pi/2$ about the y direction, and obtain

$$|\psi_3\rangle = e^{-i(\pi/4)\sigma_y}|\psi_2\rangle = e^{i\varphi}[\cos(\varphi)|\uparrow\rangle + i\sin(\varphi)|\downarrow\rangle]. \tag{4}$$

If we now measure the state of the spin, we obtain $|\uparrow\rangle$ with probability $\cos^2(\varphi)$ and $|\downarrow\rangle$ with probability $\sin^2(\varphi)$. We clearly see, now, that the relative phase can really affect the state of a quantum system. This procedure is known as Ramsey interference [1] and it is used in experiments to detect coherent oscillations in the transverse spin component.

1.1.2. *One qubit as an environment*

Decoherence is a consequence of the interaction of the qubit with the surrounding environment. As an instructive example we consider the case in which the environment is

constituted by another qubit. For the Hamiltonian describing the interaction between the two qubits we choose ($\hbar = 1$)

$$H = \frac{J}{4}\sigma_1^z \otimes \sigma_2^z, \tag{5}$$

where the operator $\sigma_1^z \otimes \sigma_2^z$ is a two-qubit operator, given by the tensor product of two single-qubit operators, and it acts in the tensor product space $\mathcal{H} = \mathcal{H}_1 \otimes \mathcal{H}_2$. We note that our general argument does not depend on the specific form of H, as long as it describes an interaction between the qubits. As the initial state for the two qubit system we choose a product state $|{+}{+}\rangle = |+\rangle_1 \otimes |+\rangle_2$, where the single qubit state is $|+\rangle = (|0\rangle + |1\rangle)/\sqrt{2}$, written in the basis diagonal with respect to σ_z, $\sigma_z|0\rangle = |0\rangle$, and $\sigma_z|1\rangle = -|1\rangle$. We let the system evolve according to the unitary evolution generated by the Hamiltonian (5) for a time t, after which we perform a trace operation on the second qubit and have a look at how the state of the first qubit has evolved during the time t in which it has interacted with the second qubit. We re-write the initial state of the first qubit as a pure state density matrix, $\rho_1 = |+\rangle_1\langle+|$. In the $\{|0\rangle, |1\rangle\}$ basis it is found to be

$$\rho_1(0) = \frac{1}{2}\begin{pmatrix} 1 & 1 \\ 1 & 1 \end{pmatrix}. \tag{6}$$

The state of the two-qubit system after a time t is given by $|\psi(t)\rangle = U(t)|{+}{+}\rangle$, with $U(t) = \exp(-iJt\sigma_1^z\sigma_2^z/2)$. After some algebra the state of the first qubit at time t is given by

$$\rho_1(t) = \mathrm{Tr}_2[|\psi(t)\rangle\langle\psi(t)|] = \frac{1}{2}\begin{pmatrix} 1 & \cos(Jt/2) \\ \cos(Jt/2) & 1 \end{pmatrix}. \tag{7}$$

The diagonal element of the first qubit density matrix is left unchanged by the interaction with the second qubit, whereas the off-diagonal elements change in time. The coherence of a state is encoded in the off-diagonal element of the density matrix. After a time $t = \pi/J$ the coherence is completely lost (full decoherence). However, owing to the smallness of the environment considered, the first qubit periodically recovers its original state. It is therefore clear that the interaction with the environment strongly affects the qubit coherence.

1.2. *Quantum open systems*

According to the axioms of quantum mechanics the dynamics of a closed conservative system is described as a unitary time evolution. In such a picture the system is considered to be decoupled from the surrounding environment, which has no influence on the dynamics of the closed system. Strictly speaking this is never the case. However, under certain conditions the coupling to the environment can be considered to be weak and, to a good approximation, neglected.

In condensed phases, the coupling to the environment can be relatively strong, and the system under consideration cannot be separated from its surrounding. However, often a rather complex physical situation can be modelled by a system that consists of few dynamical variables in contact with a huge environment, constituted by a very large or even infinite number of degrees of freedom. In this case, the small relevant system alone has to be described as an open system.

In general, an open system is a quantum system S which is coupled to an other quantum system B called the environment. It can, therefore, be thought to be a subsystem of the combined system $S+B$, which, in turn, is considered in many cases to be a closed system, governed by Hamiltonian dynamics. The system S will, in turn, change according to its internal dynamics, and as a consequence of the interaction with the environment. Certain system–environment correlations will be established between the two parts and, as a consequence, the dynamics of a quantum open system cannot, in general, be described in terms of a unitary time evolution.

Denote by $\mathcal{H}_S$ the Hilbert space of the system S and by $\mathcal{H}_B$ the Hilbert space of system B. The dynamics of the combined system $S+B$ takes place in the Hilbert space given by the tensor product space $\mathcal{H}_{SB}=\mathcal{H}_S\otimes\mathcal{H}_B$. The total Hamiltonian can be chosen to have the general form

$$H = H_S + H_B + H_I, \tag{8}$$

where H_S describes the evolution of the system S alone, H_B is the free Hamiltonian of the environment B, and H_I describes the interaction between the system and the environment. Usually when speaking about the *environment* of the system S, the term *reservoir* may appear, which refers to an environment with an infinite number of degrees of freedom, such that the frequency modes associated with it form a continuum spectrum. Occasionally, the term *heat bath* or simply *bath* refers to a reservoir which is in thermal equilibrium.

The presence of an environment is meant to model the communication of the open system with the external world. However, the attention is focused on the subsystem under study S, and all observations of interest refer to the subsystem S. Formally this means that all observables of interest act on the Hilbert space $\mathcal{H}_S$. Denoting the state of the total system by ρ, the expectation values of all observables may be written as

$$\langle\mathcal{O}\rangle = \mathrm{Tr}_S[\mathcal{O}\rho_S], \quad \rho_S = \mathrm{Tr}_B[\rho], \tag{9}$$

where $\mathcal{O}$ is the Hermitian operator describing the observable, ρ_S is the reduced density matrix of the open system S, and $\mathrm{Tr}_{S(B)}$ denotes a partial trace on the system $S(B)$.

The description of the open system S is contained in the reduced density matrix ρ_S. Since the total system evolves unitarily in time, $\rho_S(t)$ is obtained as a partial trace over the environment B of $\rho(t)$,

$$\rho_S(t) = \mathrm{Tr}_B\big[U(t,t_0)\rho_S(t_0)U^\dagger(t,t_0)\big], \tag{10}$$

where $U(t,t_0)$ is the unitary evolution operator of the total system. The equation of motion for the open system reduced density matrix $\rho_S(t)$ is

$$\frac{\mathrm{d}}{\mathrm{d}t}\rho_S(t) = -i\mathrm{Tr}_B[H(t),\rho_S(t)]. \tag{11}$$

1.3. *Generalized master equation*

In many cases it is useful to model the dynamics of an open system by means of an appropriate equation of motion for its density matrix, the so-called quantum

master equation. The evolution in time of the total system ρ is governed by the well-known Liouville equation of motion

$$\dot{\rho} = -i[H(t), \rho(t)] \equiv \mathcal{L}\rho(t), \tag{12}$$

where the second equality defines the Liouville operator $\mathcal{L}$. As the Hamiltonian can be divided into three terms that describe the dynamics of the two systems alone, H_S and H_B, and an interaction between the two parts, H_I, the Liouville operator can be written as the sum of three contributions

$$\mathcal{L} = \mathcal{L}_S + \mathcal{L}_B + \mathcal{L}_I. \tag{13}$$

Without going into details that are beyond the scope of this review, we just mention the fact that the Liouvillian is a superoperator, which maps operators into operators. The initial state for the combined system $S+B$ can typically be chosen to be a product state, $\rho(0) = \rho_S(0) \otimes \rho_B$.

We have already introduced the reduced density matrix ρ_S of the open subsystem S. It can be formally obtained from the density matrix of the total system ρ by means of a projection operation, which contains a partial trace over the system B,

$$\rho_S = \mathcal{P}\rho = \mathrm{Tr}_B[\rho] \otimes \rho_B. \tag{14}$$

Here, ρ_B is a fixed density matrix for the environment. Mapping operators into operators, the projector $\mathcal{P}$ is also a superoperator. We may thus decompose ρ as

$$\rho(t) = \rho_S(t) + (1 - \mathcal{P})\rho(t), \quad \mathcal{P}^2 = \mathcal{P}. \tag{15}$$

Substituting this decomposition in the Liouville equation of motion for the total system (12), choosing the projector in such a way that the inhomogeneous term that depends on the initial state can be disregarded, and using that the operator $\mathcal{P}$ defined in (14) commutes with the Liouvillian of the open system $\mathcal{L}_S$, after some algebra, the equation of motion for the reduced density matrix $\rho_S(t)$ can be cast in the form of an exact generalized master equation, the *Nakajima–Zwanzig equation* [2–4]

$$\dot{\rho}_S(t) = \mathcal{L}_S\rho_S(t) + \int_0^t \mathrm{d}t' \Sigma(t - t')\rho_S(t'), \tag{16}$$

$$\Sigma(t)\rho_S = -i\mathrm{Tr}_B\left[\mathcal{L}_I e^{(1-\mathcal{P})\mathcal{L}t}\mathcal{L}_I\rho_S \otimes \rho_B\right], \tag{17}$$

where $\Sigma(t)$ is the self-energy superoperator. The first term describes the reversible evolution of the open system S, while the second term produces irreversibility.

1.3.1. *Born approximation*

The generalized master Equation (16) is a formally exact and closed description of the dynamics of the state of the system ρ_S, but it is very complicated from a mathematical point of view and rather unpractical. Usually, in order to handle it some approximations are made. In fact, the kernel of (16) contains all powers of $\mathcal{L}_I$, and the dynamics of ρ_S at time t depends on the whole history of the density matrix. If the coupling between system and reservoir is weak, that is, $\|\mathcal{L}_I\| \ll \|\mathcal{L}_S + \mathcal{L}_B\|$, the exponential can be expanded in the

power of $\mathcal{L}_I$ in a perturbative way. In lowest-order Born approximation, the interaction Liouvillian is disregarded in the exponent and $\mathcal{L}_I$ is retained only to second order

$$\tilde{\Sigma}(t)\rho_S = -i\mathrm{Tr}_B\left[\mathcal{L}_I e^{(1-\mathcal{P})(\mathcal{L}_S+\mathcal{L}_B)t}\mathcal{L}_I\rho_S\otimes\rho_B\right]. \tag{18}$$

The applicability of the master equation in the Born approximation is strictly restricted to those cases in which the coupling between the system and environment is weak, with the decoherence and relaxation times large compared with the relevant timescales of the reversible dynamics.

1.4. *Quantum Markov process*

The master equation in the Born approximation (18), although much simpler than the exact Nakajima–Zwanzig Equation (16), is still an integro-differential equation that is very difficult to handle. Assuming that the temporal correlations in the bath are short lived and typically lead to exponential decay of the coherence and populations, the master equation in the Born approximation (18) can be further simplified. In the Born–Markov approximation the master equation for the reduced density matrix of system S assumes the form

$$\dot{\rho}_S(t) = -i\mathcal{L}_S\rho_S(t) + \tilde{\Sigma}^R(t)\rho_S(t), \tag{19}$$

$$\tilde{\Sigma}^R(t) = -i\int_0^t \mathrm{d}t'\tilde{\Sigma}(t')e^{it'\mathcal{L}_S}. \tag{20}$$

In an eigenstate basis of H_S, the master equation in the Born–Markov approximation can be written as the so-called Redfield equation [5–7]

$$\dot{\rho}_{nm} = -i\omega_{nm}\rho_{nm}(t) - \sum_{k,l} R_{nmkl}\rho_{kl}(t), \tag{21}$$

where $\rho_{nm} = \langle n|\rho_S|m\rangle$, $\omega_{nm} = \omega_n - \omega_m$, $H_s|n\rangle = \omega_n|n\rangle$ and we have introduced the Redfield tensor

$$R_{nmkl} = \int_0^\infty \mathrm{d}t\,\mathrm{Tr}_B\left[\langle n|\left[H_I^{\mathrm{int}}(t),\ \left[H_I^{\mathrm{int}}(0),\ |k(t)\rangle\langle l(t)|\rho_B\right]\right]|m\rangle\right], \tag{22}$$

where we have used the interaction picture Hamiltonian and the system eigenstates in the interaction picture

$$H_I^{\mathrm{int}}(t) = e^{i(H_S+H_B)t}H_I e^{-i(H_S+H_B)t}, \quad |k(t)\rangle = e^{iH_S t}|k\rangle = e^{i\omega_k t}|k\rangle. \tag{23}$$

The first term of (21) represents the reversible motion in terms of the transition frequencies ω_{nm}, while the second term describes the relaxation. The Redfield tensor can be expressed as

$$R_{nmkl} = \delta_{nm}\sum_r \Gamma^{(+)}_{nrrk} + \delta_{nk}\sum_r \Gamma^{(-)}_{lrrm} - \Gamma^{(+)}_{lmnk} - \Gamma^{(-)}_{lmnk}, \tag{24}$$

in terms of rates given by the golden rule expression

$$\Gamma^{(+)}_{lmnk} = \int_0^\infty \mathrm{d}t\, e^{-i\omega_{nk}t}\, \mathrm{Tr}_B\big[\tilde{H}_I(t)_{lm}\tilde{H}_I(0)_{nk}\rho_B\big], \tag{25}$$

$$\Gamma^{(-)}_{lmnk} = \int_0^\infty \mathrm{d}t\, e^{-i\omega_{lm}t}\, \mathrm{Tr}_B\big[\tilde{H}_I(0)_{lm}\tilde{H}_I(t)_{nk}\rho_B\big], \tag{26}$$

with $\tilde{H}_I(t)_{lm} = \langle n|e^{itH_B}H_I e^{-itH_B}|m\rangle$, and $(\Gamma^{(+)}_{lmnk})^* = \Gamma^{(-)}_{lmnk}$.

We have already pointed out that the dynamics of an open system cannot be described as a unitary evolution. However, the mapping describing the evolution is required to be completely positive [8], implying $\rho \to \sum_n O_n \rho O_n^\dagger$, where $\{O_n\}$ is a set of linear operators on the reduced state space that satisfy $\sum_n O_n^\dagger O_n = 1$, such to preserve the trace of ρ. In the framework of Lindblad theory [8], the master equation can be cast in the form

$$\dot{\rho}(t)_S = -i[H_S, \rho_S(t)] + \frac{1}{2}\sum_j \Big\{\Big[L_j\rho_S(t), L_j^\dagger\Big] + \Big[L_j, \rho_S(t)L_j^\dagger\Big]\Big\}. \tag{27}$$

The Lindblad operators L_j describe the effect of the environment in the Born–Markov approximation.

1.4.1. *Two-level systems and Bloch equations*

The aim of this review is to provide a overview on the mechanisms that affect qubit dynamics and induce decoherence in solid-state realizations of qubits. Therefore, we concentrate on two-level systems and their coupling to the surrounding environment.

The density operator of a two-state system is a two-dimensional positive Hermitian operator with trace one. It can thus be expressed in terms of a basis of Hermitian operators given by the three Pauli operators $\boldsymbol{\sigma} = (\sigma_x, \sigma_y, \sigma_z)$ and the 2×2 identity,

$$\rho = \frac{1}{2}(1 + \mathbf{p}\cdot\boldsymbol{\sigma}), \quad \mathbf{p} = \mathrm{Tr}[\rho\boldsymbol{\sigma}] = \begin{pmatrix} \rho_{01} + \rho_{10} \\ i(\rho_{01} - \rho_{10}) \\ \rho_{00} - \rho_{11} \end{pmatrix}. \tag{28}$$

The vector $\mathbf{p}$ is known as the Bloch vector, and for a spin-1/2 object it represents the expectation values of the spin components $\mathbf{p}/2 \equiv \langle\mathbf{S}\rangle = \mathrm{Tr}[\mathbf{S}\rho]$, where $\mathbf{S} = \boldsymbol{\sigma}/2$, with σ_z diagonal in the $|0\rangle$ $|1\rangle$ basis, $\sigma_z|0\rangle = |0\rangle$ and $\sigma_z|1\rangle = -|1\rangle$. Combining the last equation with the Redfield Equation (21) in the case that $n, m, k, l = 0, 1$, the master equation within the Born–Markov approximation for the density matrix of a two-level system can be expressed as a first-order time differential equation for the expectation value of the spin component $\langle\mathbf{S}\rangle = (\langle S_x\rangle, \langle S_y\rangle, \langle S_z\rangle)$,

$$\langle\dot{\mathbf{S}}\rangle = \boldsymbol{\omega} \times \langle\mathbf{S}\rangle - R\langle\mathbf{S}\rangle + \langle\mathbf{S}_0\rangle, \tag{29}$$

with $\boldsymbol{\omega} = (0, 0, \omega_{01})$. In case of a spin-1/2 particle in a magnetic field defining the z direction, ω_{01} represents the Zeeman splitting. The inhomogeneous term $\langle\mathbf{S}_0\rangle$ and the relaxation matrix R depend on the rates (25) and (26). If $\omega_{01} \gg R_{nmkl}$, it is possible to make

a secular approximation, retaining only terms R_{nmkl} with $n-m=k-l$ (see [9]) such that the Redfield tensor can be approximated by the diagonal form

$$R \approx \begin{pmatrix} T_2^{-1} & 0 & 0 \\ 0 & T_2^{-1} & 0 \\ 0 & 0 & T_1^{-1} \end{pmatrix}, \tag{30}$$

where the relaxation time T_1 and the decoherence time T_2 are given by

$$\frac{1}{T_1} = 2\mathrm{Re}\left(\Gamma^{(+)}_{0110} + \Gamma^{(+)}_{1001}\right), \tag{31}$$

$$\frac{1}{T_2} = \frac{1}{2T_1} + \frac{1}{T_\phi}, \tag{32}$$

with the pure dephasing time T_ϕ, given by

$$\frac{1}{T_\phi} = \mathrm{Re}\left(\Gamma^{(+)}_{0000} + \Gamma^{(+)}_{1111} - 2\Gamma^{(+)}_{0011}\right). \tag{33}$$

For a system–environment coupling given by a simple bilinear form $H_I = \mathcal{O}_S \otimes \mathcal{X}_B$, with $\mathcal{O}_S$ an operator acting in the system space $\mathcal{H}_S$, and $\mathcal{X}_B$ an operator acting in the environment space $\mathcal{H}_B$, the relaxation and dephasing times T_1 and T_ϕ can be written as

$$\frac{1}{T_1} = 4|\langle 0|\mathcal{O}_S|1\rangle|^2 S(\omega_{01}) \coth\frac{\omega_{01}}{2k_\mathrm{B}T}, \tag{34}$$

$$\frac{1}{T_\phi} = |\langle 0|\mathcal{O}_S|0\rangle - \langle 1|\mathcal{O}_S|1\rangle|^2 \frac{S(\omega)}{\omega}\bigg|_{\omega\to 0} 2k_\mathrm{B}T, \tag{35}$$

where the spectral density $J(\omega)$ is the Fourier transform of the environment time correlator

$$S(\omega) = \int_{-\infty}^{\infty} \mathrm{d}t \mathrm{Tr}_B[\mathcal{X}_B \mathcal{X}_B(t)\rho_B] e^{-i\omega t}. \tag{36}$$

The first term in (29) produces a rotation of the Bloch vector along the z direction. If $R=0$ we have the classical picture of a magnetic moment precessing along the externally applied magnetic field. The second term proportional to R describes an exponential damping of the component of the Bloch vector. Here T_1 describes the decay of the longitudinal component of the Bloch vector, while T_2 describes the decay of the transverse component.

We remark that the Markovian results (32) satisfy the expected fundamental Korringa relation [10].

1.5. *Theory of noise-induced qubit decoherence*

In the previous section we have seen that the spectral density $S_\mathcal{X}(\omega)$ of the bath variable $\mathcal{X}_B$ enters the decay rates $1/T_1$ and $1/T_\phi$ in the Markovian approximation. Fluctuations in the bath variable $\mathcal{X}_B$ coupled to a system variable $\mathcal{O}_S$ can be seen as noise induced in the parameters entering the qubit Hamiltonian. Each noise source affecting the parameter X is

described in terms of its quantum spectral density $S_X(\omega) \equiv (1/2\pi)\int \mathrm{d}t\, \langle \delta\hat{X}(0)\delta\hat{X}(t)\rangle e^{-i\omega t}$, that quantifies the ability of the source to absorb an energy quantum $\hbar|\omega|$ from the system (positive $\delta\omega_z$), and emit it towards the system (negative ω). Relaxation processes involve absorption of energy at a frequency ω_{01}, where $\hbar\omega_{01}$ is the unperturbed energy gap of the qubit, therefore involving $S_X(+\omega_{01})$, while dephasing, involving no energy exchange, is characterized by $S_X(\omega \approx 0)$.

We consider the free evolution of the qubit governed by the Hamiltonian $H = -\mathbf{B}\cdot\boldsymbol{\sigma}/2$, which experiences the pseudo-spin freely precessing in the field $\mathbf{B}$. Following [11], we expand the qubit Hamiltonian around the value X_0 of the control parameter X, up to second order in the fluctuations δX,

$$\mathcal{H} = -\frac{1}{2}\left(\mathbf{B}(X_0) + \frac{\partial \mathbf{B}}{\partial X}\delta X + \frac{1}{2}\frac{\partial^2 \mathbf{B}}{\partial X^2}\delta X^2 + \cdots\right)\cdot\boldsymbol{\sigma}. \tag{37}$$

Defining the three-component vectors $\mathbf{D}_X = (1/\hbar)\partial\mathbf{B}/\partial X$ and $\mathbf{D}_{X,2} = (1/\hbar)\partial^2\mathbf{B}/\partial X^2$, the Hamiltonian of the qubit can be rewritten in the basis of $\mathbf{B}(X_0)\cdot\boldsymbol{\sigma}$ as

$$\mathcal{H} = -\frac{\hbar}{2}[(\omega_{01} + \delta\omega_z)\sigma_z + \delta\omega_\perp\sigma_\perp], \tag{38}$$

where $\sigma_\perp$ denotes the transverse spin component, which can be any combination of σ_x and σ_y, and $D_{X,\perp}$ denotes the variation of transverse component $\mathbf{B}$ with respect to the parameter X, $D_{X,\perp} = (1/\hbar)\partial B_\perp/\partial X$, $\delta\omega_\perp = D_{X,z}\delta X + D_{X2,z}\delta X^2/2 + \cdots$, and $\delta\omega_\perp = D_{X,\perp}\delta X + \cdots$. The coefficients D can be written as

$$D_{X,z} = \frac{\partial\omega_{01}}{\partial X}, \tag{39}$$

$$D_{X2,z} = \frac{\partial^2\omega_{01}}{\partial X^2} - \frac{D_{X,\perp}^2}{\omega_{01}}. \tag{40}$$

As already discussed, in the Bloch–Redfield approach the decay is assumed to be exponential and it is associated with weak and short-correlated noise (white noise). In the general case the decay can be non-exponential, particularly when the main contribution to decoherence is due to noise that is singular close to $\omega \approx 0$. In many cases, however, it is possible to factorize a contribution due to relaxation, obtaining a decay law such as $f_z(t)\exp(-\Gamma_1 t/2)$.

As seen in the previous section, the relaxation processes produce a decay of the longitudinal component of the pseudo-spin, and the decay rate, irrespective of the statistics of the fluctuations, in lowest order in $D_{X,\perp}$, is given by

$$\frac{1}{T_1} = \frac{\pi}{2}S_{\delta\omega_\perp}(\omega_{01}) = \frac{\pi}{2}D_{X,\perp}^2 S_X(\omega_{01}). \tag{41}$$

For a noise source linearly and longitudinally coupled to the qubit, with a spectral density short-correlated in time, such that the Markovian approximation is valid, and regular near $\omega \approx 0$, the pure dephasing rate is given by

$$\frac{1}{T_\varphi} = \pi S_{\delta\omega_z}(\omega = 0) = \pi D_{X,z}^2 S_X(\omega = 0), \tag{42}$$

and the Korringa relation holds, $1/T_2 = 1/2T_1 + 1/T_\varphi$.

We consider now a noise spectral density that is singular at the origin $\omega \approx 0$. For Gaussian noise, the random phase accumulated after a time t is

$$\Delta\phi = D_{X,z} \int_0^t \mathrm{d}t'\, \delta X(t'), \tag{43}$$

is also Gaussian distributed. The decay law of the free induction, that experimentally corresponds to the Ramsey signal, in which the coherence time is inferred by the decay of the signal between two $\pi/2$ pulses, can be calculated as $f_{z,R}(t) = \langle \exp(i\Delta\phi) \rangle = \exp(-\langle \Delta\phi^2 \rangle/2)$, and it gives

$$f_{z,R}(t) = \exp\left(-\frac{t^2}{2} D_{X,z}^2 \int_{-\infty}^{\infty} \mathrm{d}\omega\, S_X(\omega) \frac{\sin^2(\omega t/2)}{(\omega t/2)^2} \right). \tag{44}$$

In an echo experiment an extra π pulse is added at the middle of the sequence. In this case the phase acquired is the difference between the two free evolution periods,

$$\Delta_E = -\Delta\phi_1 + \Delta\phi_2 = -D_{X,z} \int_0^{t/2} \mathrm{d}t'\, \delta X(t') + D_{X,z} \int_{t/2}^{t} \mathrm{d}t'\, \delta X(t'). \tag{45}$$

In this case, the decay is given by

$$f_{z,E}(t) = \exp\left(-\frac{t^2}{2} D_{X,z}^2 \int_{-\infty}^{\infty} \mathrm{d}\omega\, S_X(\omega) \frac{\sin^4(\omega t/4)}{(\omega t/4)^2} \right). \tag{46}$$

1.6. *Oscillator bath versus spin bath*

We have so far introduced a general formalism that allows us to study and understand how decoherence arises as the effect of the interaction between the system under consideration and its surrounding environment, under the particular assumptions of weak system–environment coupling (Born approximation), and short-lived temporal correlations in the bath (Markov approximation). However, we have not yet approached the description of the kinds of bath that are physically important.

Remarkably, only two types of baths appear to play a significant role, the oscillator bath and the spin bath. The former was introduced by Feynman and Vernon [12] to describe a quantum system weakly interacting with a dissipative environment. A mapping to a linear bath can be made rigorously only if the coupling is weak. As a result, oscillator modes are the best suited for N *delocalized* environmental modes, the coupling being automatically proportional to $\sim 1/N^{1/2}$, and therefore small in the large N regime.

As opposed to the linear oscillator environment, the spin bath plays a fundamental role in describing low-energy dynamics dominated by *localized* environmental modes, such as nuclear and paramagnetic spins, defects, and impurity spins. The coupling is in general strong and independent on N. One of the main differences between the two types of environment is that the Markov approximation is no longer valid, and that the spin bath can cause decoherence even in the limit $T \to 0$, involving no dissipation. The central spin model, in which a central spin couples to a bath of spins, has application in describing magnetic and superconducting systems.

An exhaustive treatment of the spin–boson model and the central spin model is beyond the scope of this review, and we refer to [13–15] and references therein for an extensive treatment.

1.6.1. *Spin–boson model*

Here, we describe a particular example of a qubit coupled to a dissipative linear environment in the Born–Markov approximation. We consider a generic two-level system described by the Hamiltonian

$$\mathcal{H}_S = \frac{\Delta}{2}\sigma_x + \frac{\epsilon}{2}\sigma_z. \tag{47}$$

In order to include the effect of dissipation in the quantum formalism, it is customary to follow the Caldeira–Leggett [13–15] approach. A bath of harmonic oscillators at thermal equilibrium at temperature T is introduced to describe the degrees of freedom of the environment. The 'system + bath' Hamiltonian is

$$H = H_S + H_B + H_{SB}, \tag{48}$$

$$H_B = \frac{1}{2}\sum_\alpha \omega_\alpha \left(b_\alpha^\dagger b_\alpha + \frac{1}{2}\right), \tag{49}$$

$$H_{SB} = \mathcal{O}_S \otimes \mathcal{X}_B = \sigma_z \sum_\alpha c_\alpha (b_\alpha + b_\alpha^\dagger), \tag{50}$$

where $\mathcal{H}_S$ is the quantized Hamiltonian of the system (47) and $\mathcal{H}_B$ is the bath Hamiltonian, described by independent bosonic degrees of freedom with frequencies ω_α. The coupling between the system and the bath degrees of freedom is described by $\mathcal{H}_{SB}$, where $\mathcal{O}_S = \sigma_z$, $\mathcal{X}_B = \sum_\alpha c_\alpha (b_\alpha + b_\alpha^\dagger)$, and c_α are coupling parameters.

A rigorous treatment of the spin–boson model in the Born approximation without making use of the Markov approximation is presented in [16,17]. The eigenstates of the Hamiltonian (47) are

$$|0\rangle = \frac{1}{\sqrt{2}}\left(\sqrt{1 + \frac{\epsilon}{\omega_{01}}}|+\rangle + \sqrt{1 - \frac{\epsilon}{\omega_{01}}}|-\rangle \right), \tag{51}$$

$$|1\rangle = \frac{1}{\sqrt{2}}\left(\sqrt{1 - \frac{\epsilon}{\omega_{01}}}|+\rangle - \sqrt{1 + \frac{\epsilon}{\omega_{01}}}|-\rangle \right), \tag{52}$$

where $|\pm\rangle$ are eigenstates of σ_z, $\sigma_z|\pm\rangle = \pm|\pm\rangle$, and $\omega_{01} = \sqrt{\Delta^2 + \epsilon^2}$. The initial state of a system of quantum harmonic oscillators in thermal equilibrium is

$$\rho_B = \mathcal{Z}_B^{-1} \exp(-\beta \mathcal{H}_B), \quad \mathcal{Z}_B = \mathrm{Tr} \exp(-\beta \mathcal{H}_B). \tag{53}$$

The entire information of the bath, such as the bath frequencies ω_α and the coupling parameters c_α appearing in the Hamiltonian, are contained in the spectral density $S(\omega)$

of the system–bath coupling,

$$S(\omega) = \frac{\pi}{2}\sum_{\alpha} c_{\alpha}^2 \delta(\omega - \omega_{\alpha}). \tag{54}$$

Here, we limit our attention to the Markovian case, and make use of the general Redfield theory described in the previous section. From the formulae (34) and (35), the relaxation and dephasing rates take the form

$$\frac{1}{T_1} = \left(\frac{\Delta}{\omega_{01}}\right)^2 J(\omega_{01}) \coth \frac{\omega_{01}}{2k_{\mathrm{B}}T}, \tag{55}$$

$$\frac{1}{T_{\phi}} = \left(\frac{\epsilon}{\omega_{01}}\right)^2 \frac{J(\omega)}{\omega}\bigg|_{\omega\to 0} 2k_{\mathrm{B}}T. \tag{56}$$

1.6.2. *Central spin model*

The derivation of a complete Hamiltonian for the central spin problem is not an easy task, and it strongly depends on the system under consideration. As already mentioned, the interaction between the central spin and the environmental spins cannot be treated perturbatively.

Here, we are in particular interested in giving an idea of the effects that can arise when the central spin interacts with a bath that is in a static random state. We consider, as a very simple but instructive example, a spin 1/2 that interacts with the total spin of the spin bath, in a magnetic field defining the z-direction, B^z,

$$\mathcal{H} = B^z S^z + J I^z_{\mathrm{tot}} S^z + J\left(I^-_{\mathrm{tot}} S^+ + I^+_{\mathrm{tot}} S^-\right)/2. \tag{57}$$

For a sufficiently large magnetic field, the transverse part of the interaction can be neglected, and as an effective Hamiltonian we can choose

$$\mathcal{H} = J I^z_{\mathrm{tot}} S^z, \tag{58}$$

where I^z_{tot} is the z-component of the total spin of the spin bath, and calculate the decay under Hamiltonian evolution of the initial product state

$$|+\rangle|\psi_I\rangle = \frac{1}{\sqrt{2}}(|\uparrow\rangle + |\downarrow\rangle)\int \mathrm{d}I^z \left(\frac{1}{\pi a^2}\right)^{1/4} e^{-(1/2a^2)(I^z - I_0)^2} |I^z\rangle, \tag{59}$$

where the central spin is prepared along the x-direction and the spin bath is in a superposition of I^z_{tot} eigenstates, Gaussian distributed, with mean I_0 and variance a. The choice of a pure state or a mixed state gives the same result, provided that the diagonal entries of the pure state are the same as the diagonal entries of the mixed state, in the basis where the mixed state is diagonal. Direct calculation yields

$$|\langle +|\langle\psi_I|e^{-i\mathcal{H}t}|\psi_I\rangle|+\rangle|^2 = \cos^2\left(\frac{JI_0 t}{2}\right)\exp\left[-\frac{a^2}{32}J^2t^2\right]. \tag{60}$$

The temporal Gaussian decay arise from the choice of Gaussian distributed eigenstates of I^{z}_{tot}. What results from this simple example is that the time decay is not exponential, as it would be if the dynamics were Markovian.

2. Spin qubits

Per antonomasia, the two-state system that nature provides us with is the intrinsic angular momentum of the electron: the spin 1/2. It is therefore natural to choose the electron spin as the two-state system that encodes the qubit. The spin of the electron can have a much longer decoherence time than the charge degrees of freedom. Nevertheless, isolating the spin degree of freedom of an electron to a degree required for quantum computation is not an easy task at all. Moreover, in order to be used for quantum computational purposes, electron spin-based qubits must be designed as scalable devices that can be externally controlled, coupled, manipulated, and read out, that is, they must satisfy the DiVincenzo criteria [18]. A successful and promising device for the physical implementation of electron spin-based qubits is the semiconductor quantum dot [19].

2.1. *Semiconductor quantum dots*

The quantum dots owe their name to the zero-dimensional character of such devices. They can be considered as a quantum box that can be filled with electrons (or holes) which occupy the available discretized states of the system. The electrons can tunnel on and off the dot, which is coupled to a large reservoir via tunnel barriers. The height of the barriers, and consequently the rates for tunnelling through the barriers on and off the dot, can be controlled via the application of gate electrodes. Electrostatic gates can also be used to tune the electrostatic potential of the dot with respect to the reservoirs, such that the ladder of energy levels in the dot can be shifted up or down with respect to the energy of the reservoir. External bias voltages can be applied and transport properties can be measured.

Quantum dots are basically characterized by the quantized level structure, for which they are considered as artificial atoms, and by the transport state of the dot, that can be active or blocked, and depends on the combination of bias and gate voltages applied. In fact, the Coulomb repulsion between the electrons in the dot determines an energy cost for adding an extra electron in the dot. At low temperatures, the tunnelling of electrons on and off the dot can be drastically suppressed, and the dot is in the so-called Coulomb blockade.

Many kinds of quantum dots have been realized so far. Here, we focus our attention on lateral III–V semiconductor quantum dots, such as those in Figure 1. These devices are fabricated from heterostructures of GaAs and AlGaAs grown by molecular beam epitaxy. The energy potential along the growth direction of such a structure has a minimum at the interface of the two layers, which is also asymmetric with respect to the growth direction. Free electrons are introduced by doping the AlGaAs layer with Si, which accumulate at the GaAs/AlGaAs interface, deep down in the minimum of the vertical potential, that provides strong confinement of the electrons along the growth direction. At the same time, the electrons are free to move along the interface, where they form a two-dimensional electron gas (2DEG), that can have a high mobility and a relatively low electron density (typically $10^{5}-10^{7}\,\mathrm{cm^{2}/V\,s}$ and approximately $10^{15}\,\mathrm{m^{-2}}$). The low-density results in a relatively long Fermi wavelength ($\approx$40 nm) and a large screening length, such that via the

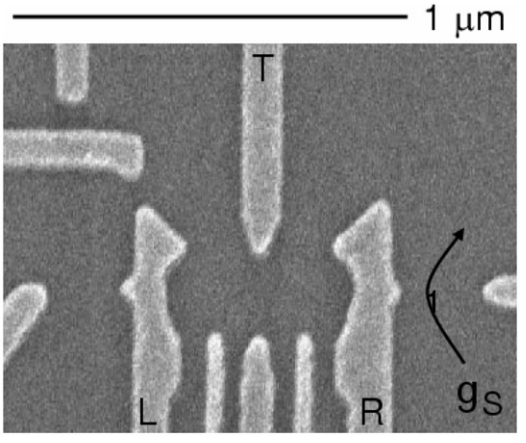

Figure 1. Scanning electron micrograph of a double quantum dot. Reprinted with permission from [18]. © 2008 by the American Physical Society.

application of an electric field, obtained through negatively charged metal gate electrodes, placed on top of the heterostructure, the 2DEG can be locally depleted. Therefore, by suitable designing the gate structure it is possible to isolate small islands of the 2DEG, thus creating a dot. When the lateral size of the dot is compared to the Fermi wavelength, the energy level structure of the dot becomes discretized, and at temperatures of tens of millikelvin, the energy separation of the levels becomes much higher than the temperature, such that quantum phenomena start to play a significant role.

2.2. *Spin relaxation and spin dephasing mechanisms in quantum dots*

The electron spin in semiconductor quantum dots can be isolated and controlled with a high accuracy, but it still suffers from decoherence due to the unavoidable coupling with the surrounding environment. In order to implement quantum computation algorithms with electron spin-based qubits in semiconductor quantum dots, it is necessary to engineer the devices in such a way as to preserve the coherence of the electron spin states for sufficiently long timescales. In addition to the fundamental interest, it is therefore important to theoretically understand which sources of dissipation and decoherence affect the electron spin in quantum dots, and to find ways to reduce their influence on the spin–qubit dynamics as much as possible.

Two kinds of environment turn out to mainly affect the dynamics of an electron spin in a quantum dot, the phonons in the lattice, and the spins of atomic nuclei in the quantum dot.

Phonon-induced relaxation in semiconductor quantum dots has attracted some attention from a theoretical point of view for the first time in [21,22]. The lattice phonons do not couple directly to the spin degree of freedom. However, even without the application of external electric fields, the breaking of inversion symmetry in GaAs gives rise to spin–orbit (SO) interaction, which couples the spin and the orbital degrees of freedom. These orbital degrees of freedom, being coupled to the phonons, provide an indirect coupling between the electron spin and the phonons, which constitute a large dissipative bosonic reservoir and provide a source of decoherence and relaxation.

Short time correlations in the phonon bath induce a Markovian dynamics of the electron spin, with well-defined relaxation and decoherence times T_1 and T_2. It turns out that effectively the phonon-induced pure dephasing time T_ϕ of an electron spin in a quantum dot in the presence of a magnetic field diverges. In the Bloch picture, pure dephasing arises from longitudinal fluctuations of the magnetic field, while a perturbative treatment of the SO interaction gives rise, within first order, to a fluctuating magnetic field perpendicular to the applied magnetic field. As a consequence the decoherence time T_2 is limited only by its upper bound T_1, $T_2 = 2T_1$. In turn, the relaxation time T_1 shows a strong dependence on the magnetic field, $T_1 \propto B^5$, that has been confirmed experimentally, where a very long relaxation time up to $T_1 \approx 1$ s has been measured for a magnetic field of $B = 1$ T (see [23]).

Hyperfine interaction was first taken into consideration as a source of decoherence for an electron spin confined in a quantum dot in [24]. In GaAs there are approximately 5×10^{21} atoms in $1\,\mathrm{cm}^3$. Therefore, the linear extension of a typical GaAs quantum dot, that is of order of the Fermi wavelength of around 40 nm, encompasses roughly 200 atoms, from which it can be estimated that the wavefunction of an electron in a GaAs quantum dot overlaps with approximately 10^5 nuclei. The electron spin and the nuclear spins in the dot couple via the Fermi contact hyperfine interaction, which creates entanglement between them and strongly affect the electron spin dynamics. It turns out that long-time correlations in the nuclear spin system induce a non-Markovian dynamics of the electron spin, with non-exponential decay in time of the expectation values of the electron spin components. In a large applied magnetic field B, the dynamics in the nuclear field due to the hyperfine interaction can be treated perturbatively and it turns out that flip–flop dynamics starts to affect the nuclear field in a time that scales as the number of nuclear spins ($\propto N$). For shorter times the nuclear field is static and the transverse component shows a Gaussian decay, that is due to the statistical distribution of nuclear spin states.

We remark that the phonon-induced relaxation rate of the electron spin is enhanced by an applied magnetic field, whereas the influence of the hyperfine interaction is reduced by a large Zeeman splitting.

2.3. *Hyperfine-induced decoherence in spin qubits*

2.3.1. *Hyperfine interaction*

The spin of an electron and the atomic nuclear spin can interact through the hyperfine Fermi contact interaction, a spin–spin interaction that takes place when the electron and the nucleus occupy the same position in space, for which we use the term 'contact'. The origin of the hyperfine coupling can be understood considering the electromagnetic interaction of an electron with the magnetic field produced by a nucleus. Without loss of generality the magnetic properties of a nucleus can be described as those of a magnetic dipole $\boldsymbol{\mu}_N = \mu_\mathrm{N}\hbar\mathbf{I}$, where μ_N is the nuclear magneton, and $\mathbf{I}$ is the nuclear spin operator. The interaction of a nuclear dipole $\boldsymbol{\mu}_N$ with the electronic shell gives a rather small effect, and can be treated using a perturbative method. In the non-relativistic Pauli description of the electron, the Hamiltonian of an electron in a magnetic field $\mathbf{B} = \nabla \times \mathbf{A}$ produced by a vector potential $\mathbf{A}$ is given by

$$\mathcal{H} = \frac{1}{2m}\left(\mathbf{p} + \frac{e}{c}\mathbf{A}\right)^2 + 2\mu_\mathrm{B}\mathbf{S} \cdot (\nabla \times \mathbf{A}), \tag{61}$$

where $\mathbf{S}$ is the electron spin operator. The vector potential produced by a magnetic dipole $\boldsymbol{\mu}$ at position $\mathbf{r}$ is, according to classical electromagnetism, $\mathbf{A} = (\boldsymbol{\mu} \times \mathbf{r})/r^3 = \nabla \times (\boldsymbol{\mu}/r)$. Neglecting the quadratic term in the vector potential and replacing $\hbar\mathbf{L} = \mathbf{r} \times \mathbf{p}$ for the electron orbital momentum operator, the Hamiltonian (61) can be written as

$$\mathcal{H} = 2\mu_B \frac{\mathbf{L} \cdot \boldsymbol{\mu}}{r^3} + 2\mu_B (\mathbf{S} \cdot \nabla)(\boldsymbol{\mu} \cdot \nabla)\frac{1}{r} - 2\mu_B (\mathbf{S} \cdot \boldsymbol{\mu})\nabla^2 \frac{1}{r}. \tag{62}$$

The magnetic interaction of the nuclear spin and the electron spin is contained in the second and the third term of (62), and it is obtained after integration over the orbital degrees of freedom, that is, it has to be understood as applied to an electron orbital state $\psi_{\mathrm{el}}(\mathbf{r})$. For $\mathbf{r} \neq 0$, the terms involving the electron spin $\mathbf{S}$ in (62) behave regularly, the last term vanishes identically, while the second term produces a usual dipole–dipole interaction $2\mu_B[3(\mathbf{S} \cdot \mathbf{r})(\boldsymbol{\mu} \cdot \mathbf{r})/r^5 - \mathbf{S} \cdot \boldsymbol{\mu}/r^3]$. The case $\mathbf{r} = 0$ needs to be treated more carefully. It can be shown [10] that the dominant contribution of the spin dependent part of (62) reduces to $(16\pi/3)\mu_B(\mathbf{S} \cdot \boldsymbol{\mu})\delta(\mathbf{r})$, and once applied on the electron orbital wavefunction is given by

$$\mathcal{H}_{\mathrm{hy}} = \frac{16}{3}\pi\mu_B |\psi_{\mathrm{el}}(0)|^2 \mathbf{S} \cdot \boldsymbol{\mu}, \tag{63}$$

which is finite for s electrons and zero for others. The Hamiltonian for the magnetic interaction of the electron with the nucleus can be written as

$$\mathcal{H} = 2\mu_B \mu_N \hbar \mathbf{I} \cdot \left[\frac{\mathbf{L}}{r^3} - \frac{\mathbf{S}}{r^3} + 3\frac{\mathbf{r}(\mathbf{S} \cdot \mathbf{r})}{r^5} + \frac{8}{3}\pi \mathbf{S}\delta(\mathbf{r}) \right]. \tag{64}$$

2.3.2. *Hyperfine interaction in semiconductor quantum dots*

In a semiconductor quantum dot an electron is confined in a two-dimensional region of space whose linear extension is of the order of the Fermi wavelength, about 100 nm for GaAs, which is much larger than the typical lattice spacing of the crystal (of the order of Ångstroms). As a result a discretization of the energy levels in the dot appears, with an orbital level spacing that, for lateral quantum dot containing single electrons, is much greater than the typical energy scale of the hyperfine interaction. As opposed to the case of single atoms, the electron orbital wavefunction in a quantum dot extends over a region much larger than the lattice size, such that the electron spin couples to many nuclear spins, as shown schematically in Figure 2. Taking into consideration only the main contribution of the total Hamiltonian (64) that comes from the diverging part, the effective hyperfine Hamiltonian describing the interaction of a single electron with the nuclei in the dot can be written as

$$\mathcal{H} = \mathbf{S} \cdot \mathbf{h}, \quad \mathbf{h} = A v_0 \sum_{k=1}^{N} |\psi_0(\mathbf{r}_k)|^2 \mathbf{I}_k \equiv \sum_{k=1}^{N} A_k \mathbf{I}_k, \tag{65}$$

where $\mathbf{S}$ is the electron spin operator, $\mathbf{h}$ is the so-called Overhauser field, given by the sum of all of the $\mathbf{I}_k$ nuclear spin operators, weighted by the position-dependent coupling strength $A_k = v_0 A |\psi_0(\mathbf{r}_k)|$, where the square modulus of the electron envelope wavefunction at the kth lattice site. Typically the electron can be assumed to be in the quantum dot

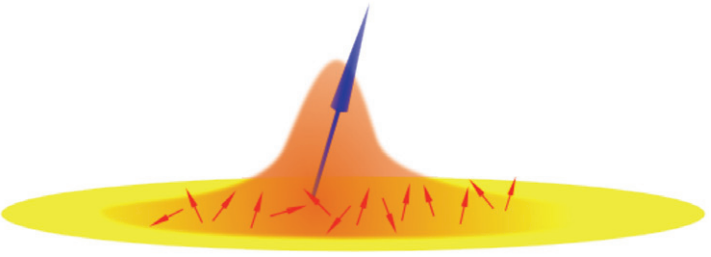

Figure 2. Schematic representation of the orbital wavefunction of an electron in a quantum dot. Owing to the spatial extension of the wavefunction, the electron spin (big blue arrow) couples to many nuclear spins (small red arrows). See online version for colour.

orbital ground state. Here, v_0 is the volume of the crystal unit cell containing one nuclear spin and $A = 16\pi\mu_B\mu_N\hbar/3$ is the contact hyperfine coupling strength. In GaAs the nuclear spin is $I = 3/2$ and an estimate of the interaction strength, weighted by the abundances of the three isotopes naturally present (^{69}Ga, ^{71}Ga, and ^{75}Ga), yields $A \approx 90\,\mu$eV.

The inhomogeneity of the electron wavefunction results in a non-uniform hyperfine coupling strength A_k, which depends on the probability to find the electron in the nuclear lattice site k, resulting in a subtle and complex many-body quantum mechanical behaviour, with the nuclear spin affecting the electron spin time evolution, and the electron spin acting back on the dynamics of each of the nuclei in turn.

From the point of view of the electron spin, entanglement with the degrees of freedom of nuclear spins arising from the hyperfine coupling constitutes a decoherence mechanism.

Since the Overhauser field **h** appearing in (65) is composed by the sum of a large number of spins, it is natural to question whether the nuclear field can be approximated as a classical object and to what extent this approximation gives correct results. In a relatively recent work by Coish et al. [25], it has been theoretically shown that, for the special case of a uniform hyperfine coupling constants $A_k = A/N$, arising from a constant wavefunction in the dot $\psi_0 = 1/\sqrt{v_0 N}$, the dynamics obtained in the mean field approximation and the quantum evolution show agreement up to the transverse-spin correlation time τ_c, which diverges in the zero external magnetic field case (unphysical result due to the assumption of constant coupling), but that saturates to a finite value in case of a finite external magnetic field.

2.3.3. *Fluctuation timescales of the nuclear field*

The nuclear field is a quantum many-body interacting spin system whose field orientation and magnitude change over time. This change is due to the combined effect of the inter-nuclear dipole–dipole interaction and the hyperfine interaction between electron and the nuclei. The dipolar interaction does not conserve the total nuclear spin and thus can be responsible for changes in the nuclear spin configuration. Those changes, combined with the spatial variation of the hyperfine coupling constant, lead to a different value of the nuclear field seen by the electron spin and thus to its decoherence. Here, we briefly outline the timescales in which those mechanisms take place, in order of decreasing timescales.

The strength of the effective magnetic dipole–dipole interaction between neighbouring nuclei in GaAs is directly given by the width of the nuclear magnetic resonance (NMR) line to be approximately $(100\,\mu s)^{-1}$ (see [26]) and its inverse can be taken as an estimate for the timescale in which a change in the nuclear configuration due to dipolar interaction takes place, that is, $T_{d-d} \approx 100\,\mu s$, which is just the period of precession of a nuclear spin in the local magnetic field generated by its neighbours. This timescale is so long that a great number of other decoherence mechanisms start to play a significant role before nuclear dipole effects start to matter.

In addition to spin diffusion driven by nuclear dipole–dipole interaction, the nuclear field can undergo a change due to the flip–flop term in the Hamiltonian (65). In a large external field B, the flip–flop term can be treated within the framework of perturbation theory, as it will be explained in the next section. We anticipate here that the hyperfine mediated dynamics in the nuclear field has a timescale given by $\propto A/N$. This means that up to this timescale the nuclear field can be considered as static.

2.4. *Decoherence due to hyperfine-induced electron spin dynamics*

The interaction in a quantum dot of the electron spin with the nuclear field via the hyperfine interaction belongs to the class of central spin problems briefly introduced in section 1.6.2. An early treatment of the hyperfine interaction as a decoherence mechanism for single electron spins confined in quantum dots whose carried out in [24]. There, a second-order time-dependent perturbation expansion of the hyperfine interaction in a magnetic field was performed with respect to the flip–flop transverse term $A(h_+S_- + h_-S_+)/2$ for a constant hyperfine coupling A, and an asymptotic electron spin-flip probability of approximately $1/p^2N$ is obtained, where p is the nuclear spin polarization. As a result, in addition to a large external magnetic field, a large polarization p and a large number of nuclei in the dot would suppress the spin-flip probability.

The first signature of the non-Markovian dynamics of the electron spin in a quantum dot coupled to the nuclear spin bath appeared in [27]. There, an exact solution for the fully polarized case $p = 1$ is provided. The Hamiltonian describing an electron spin $\mathbf{S}$ coupled to the nuclear spin bath $\mathbf{h}_N = \sum_i A_i \mathbf{I}_i$ via the hyperfine coupling, in presence of an external magnetic field $\mathbf{B}$ is

$$\mathcal{H} = g\mu_B \mathbf{S}\cdot\mathbf{B} + \mathbf{S}\cdot\mathbf{h}_N, \tag{66}$$

with $A_i = Av_0|\Psi(\mathbf{r}_i)|^2$. The fully polarized initial state is $\Psi_0 = |\Downarrow;\uparrow,\uparrow,\ldots,\uparrow\rangle$. At a later time $t > 0$ the wavefunction will have the exact form

$$\Psi(t) = \alpha(t)\Psi_0 + \sum_k \beta_k(t)|\Uparrow;\uparrow,\uparrow,\downarrow_k,\uparrow,\ldots\rangle. \tag{67}$$

Via inserting the ansatz wavefunction in the Schrödinger equation, a system of coupled first-order differential equation for α and β_k can be written. For large Zeeman field ($|\epsilon_z| \gg A$, with $\epsilon_z = g\mu_B B_z$), the correlator $C_0(t) = \langle\Psi_0|\delta\hat{S}_z(t)\hat{S}_z|\psi_0\rangle$, with $\delta\hat{S}_z(t) = \hat{S}_z(t) - \hat{S}_z$ and $\hat{S}_z(t)$ being the z-component of the electron spin operator in the Heisenberg representation, is found to asymptotically decay algebraically, that is, $C_0(t) - C_0(\infty) \sim 1/t^{3/2}$. The reason of this non-exponential decay lies in the non-uniform couplings A_i, which depend on the probability for the electron to be located at different nuclear sites.

According to long-time power-law decay, the longitudinal electron spin component decays of a fraction of around $1/N$, in a time of approximately N/A.

2.4.1. *Single-electron spin decoherence in large Zeeman splitting*

A detailed and comprehensive treatment of the hyperfine interaction [28] provides an analytical result for the electron spin dynamics for arbitrary nuclear spin I and nuclear polarization p. A generalized master equation (GME) approach allows a treatment of the transverse electron spin–nuclear spin flip–flop terms in the Hamiltonian with an external field in a well-controlled perturbative way. An expansion of the self-energy in the exact Nakajima–Zwanzig GME shows a rich electron spin dynamics, with exponential and non-exponential decaying contributions and undamped oscillations. The form of the decay of the transverse and longitudinal electron spin component is obtained in high magnetic field up to fourth order in perturbation theory.

The hyperfine Hamiltonian in an external magnetic field is

$$\mathcal{H} = bS_z + \epsilon_{nz} I_z + \mathbf{h} \cdot \mathbf{S}, \tag{68}$$

where $b = g^* \mu_B B_z$ ($\epsilon_{nz} = g_I \mu_N B_z$) is the electron (nuclear) Zeeman splitting in a magnetic field defining the z-axis B_z, g^* (g_I) the effective electron (nuclear) g-factor, and μ_B (μ_N) the Bohr (nuclear) magneton. In the rotating frame, with respect to the nuclear Zeeman term, the Hamiltonian can be separated into a longitudinal (unperturbed) and transverse (perturbation) term,

$$\mathcal{H} = \underbrace{(b + h_z) S_z}_{\mathcal{H}_0} + \underbrace{(h_+ S_- + h_- S_+)/2}_{V}. \tag{69}$$

In absence of V, $\langle S_z \rangle_t$ is constant, since $[\mathcal{H}_0, S_z] = 0$, but the transverse component $\langle S_\pm \rangle_t$ evolves in time in a non-trivial way. For a large number of nuclear spins $N \sim 10^5$ (GaAs dot) a direct application of the central limit theorem gives a Gaussian distribution for the eigenvalues of h_z with mean $h_0 = \langle h_z \rangle$ and variance $\sigma \approx A/\sqrt{N}$. The transverse correlator for an initial state given by the product state of the initial electron spin state $\rho_S(0)$ and incoherent Gaussian distributed nuclear mixture state is

$$\langle S_+ \rangle_t \approx \langle S_+ \rangle_0 \exp[-t^2/2\tau^2 + i(b + h_0)t], \quad \tau = \frac{1}{\sigma} = \frac{2\hbar}{A} \sqrt{\frac{N}{1 - p^2}}. \tag{70}$$

Choosing as the nuclear initial state the pure state

$$|\psi_I(0)\rangle = \prod_j \left(\sqrt{1 + p} |\uparrow_j\rangle + e^{i\phi_j} \sqrt{1 - p} |\downarrow_j\rangle \right) / \sqrt{2},$$

for a certain polarization p, the same result (70) with $h_0 = pN$ comes out.

The reason for this decay lies in the choice of the initial nuclear state containing many h_z eigenstates and can also be obtained choosing the nuclear field in an h_z eigenstate, but with the electron spin in a transverse initial state. This decay is reversible and can be removed with a standard spin echo technique [29,30]. Such an experiment therefore reveals only the decay due to the transverse flip–flop term V (see (68)). A more suitable procedure for a quantum computation algorithm would be a strong Von Neumann measurement of

the nuclear field that would then prepare an h_z eigenstate, leading to simple precession with no decay [31,32].

Analysis of the GME in the Born approximation for a very high magnetic field ($|B_z| \gg |A/g^*\mu_B|$) provides an asymptotic form to leading orders in $1/\omega_n = 1/(b + h_n^z)$,

$$\langle S_+\rangle_t \approx \sigma_+^{\rm osc}(t) + \sigma_+^{\rm dec}(t), \quad \langle S_z\rangle_t \approx \langle S_z\rangle_\infty + \sigma_z^{\rm dec}(t). \tag{71}$$

The transverse component $\langle S_+\rangle_t$ splits up into the sum of an oscillating term $\sigma_+^{\rm osc}(t) \propto \langle S_+\rangle_0 e^{i\omega_n t}$, that is proportional to the initial value of the transverse component $\langle S_+\rangle_0$ and oscillates at frequency ω_n, and a decaying term $\sigma_+^{\rm dec}(t)$, that, for a parabolic confinement in the dot, reads as $\sigma_+^{\rm dec}(t) \propto \delta/t^{3/2}$, with $\delta = N/\omega_n \ll 1$. The long-time behaviour of the longitudinal component $\langle S_z\rangle_t$ splits up into the sum of a constant term and a decaying term $\sigma_z^{\rm dec}(t) \propto \delta/t^{3/2}$, showing that it saturates to an asymptotic value that is proportional to the initial expectation value $\langle S_z\rangle_\infty \propto \langle S_z\rangle_0$. Even for a h_z eigenstate, for which no decay is expected in zeroth order in the transverse electron spin–nuclear spin flip–flop interaction, a long-time irreversible decay takes place, which is due to the spatial variation of the hyperfine coupling constant.

2.4.2. *Single-spin electron spin resonance: universal phase shift and power-law decay*

Here, we describe the situation in which the electron spin is coherently driven via pulsed magnetic resonance, while coupled to a nuclear long-time correlated spin bath. Recent remarkable experimental results [30] show a coherent electron spin oscillation, even for a Rabi period much longer than $T_2^* = 10{-}20$ ns. A non-exponential decay of the Rabi oscillations is observed, obeying a power-law decay with the appearance of a universal phase shift.

In order to measure the electron spin state in the experiment [30], a spin-charge conversion technique is implemented by operating a double quantum dot in the spin blockade regime [33,34] in which the transport through the dots can occur only via transitions from spin states with one electron per dot, $|(1,1)\rangle$, to the singlet state in the right dot, $|(0,2)\rangle$. The Pauli exclusion principle, which does not allow two electron with same spin state to occupy the same orbital, allows transport only for antiparallel spins. Transport of the spin-triplet states is therefore blocked. The oscillating transverse magnetic field rotates the spins, therefore unblocking an initial state with even parity spin state [34].

Consider a quantum dot in a time-independent magnetic field defining the z direction. In addition, an oscillating magnetic field is applied in the plane, along the x direction. For a large number of nuclei in the dot ($N \sim 10^6$ in GaAs dots) the field h_z is Gaussian distributed, with mean h_0 and variance σ (see [27,28,35]). In the case of strong external field ($b \gg \sigma$, with $b = g^*\mu_B B_z$), neglecting transverse electron spin–nuclear spin flip–flop terms in the hyperfine interaction, the Hamiltonian is ($\hbar = 1$)

$$\mathcal{H} = (b + h_z)S_z + b_{\rm ac}\cos(\omega t)S_x, \tag{72}$$

where $b_{\rm ac} = g^*\mu_B B_{\rm ac}$, ω and $B_{\rm ac}$ being the frequency and amplitude of the electron spin resonance (ESR) driving field. Here, h_z is considered static (justified for $t < 1\,\mu$s), and the assumption $\omega = b + h_0$ is made. In the rotating wave approximation (valid for $(b_{\rm ac}/b)^2 \ll 1$),

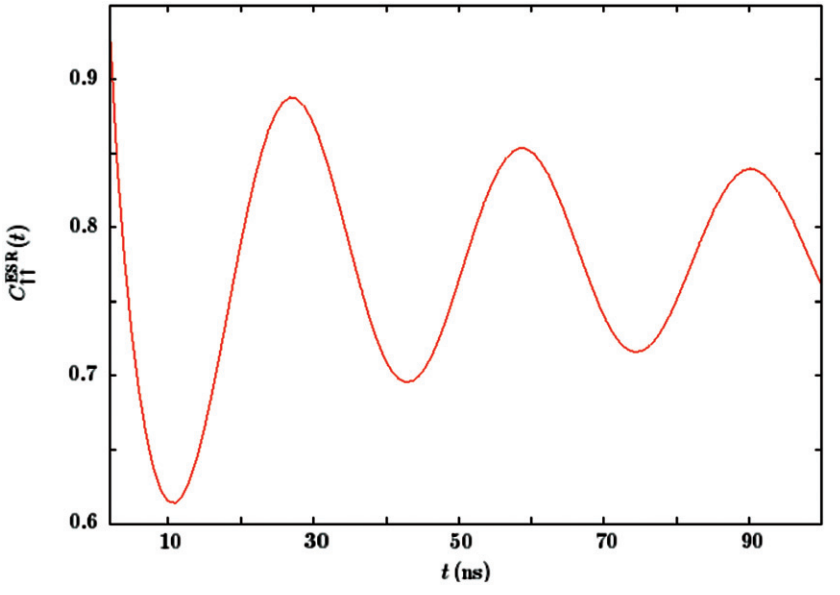

Figure 3. Decay of the driven Rabi oscillation in ESR showing a power-law decay $\propto 1/\sqrt{t}$ and a universal phase shift of $\pi/4$, as given by (73), valid for $t \gg \max(1/\sigma, 1/b_{ac}, b_{ac}/2\sigma^2)$. For the plot the value $b = \sigma = 0.4\,\mathrm{GHz}$ have been chosen.

after averaging over the Gaussian distribution of h_z, the decay of the driven Rabi oscillation is given by [30], see Figure 3

$$C_{\uparrow\uparrow}^{\mathrm{ESR}}(t) \sim 1 - C + \sqrt{\frac{b_{ac}}{8\sigma^2 t}}\cos\left(\frac{b_{ac}}{2}t + \frac{\pi}{4}\right) + \mathcal{O}\left(\frac{1}{t^{3/2}}\right), \tag{73}$$

for $t \gg \max(1/\sigma, 1/b_{ac}, b_{ac}/2\sigma^2)$, with $C = \exp(b_{ac}^2/8\sigma^2)\mathrm{erfc}(b_{ac}/\sqrt{8}\sigma)\sqrt{2\pi}b_{ac}/8\sigma$. The remarkable features appearing in the experiment are the $\sim 1/\sqrt{t}$ power-law decay and the universal $\pi/4$ phase shift. The reason for the appearance of these features is that the nuclear field h_z does not change over a timescale much longer than the Rabi period. Since different values of h_z determine different oscillation frequencies, an average over the distribution in h_z give rise to a decay in the coherence of the driven electron spin, and the off-resonant contributions also determine the phase shift. The fact that coherent Rabi oscillations are visible even when the Rabi period is much longer than the transverse spin decay time $\tau \sim 15\,\mathrm{ns}$ has its origin in the fact that the power-law decay sets in already after a short time $1/\sigma \sim 15\,\mathrm{ns}$.

2.4.3. *Single-triplet decoherence in a double quantum dot*

An alternative way to implement a qubit with electron spin in quantum dots is to consider a double quantum dot with two spins, one per dot, and encode the qubit in the subspace with zero z-projection of the total spin $S_{\mathrm{tot}}^z = S_1^z + S_2^z = 0$. The advantage of this scheme is the possibility of reducing the hyperfine coupling in the case of symmetric dots. At the same time additional decoherence due to the coupling to the orbital degree of freedom and leakage errors may appear.

The effective Hamiltonian for the one-electron-per-dot configuration can be written as

$$\mathcal{H}_{dd} = \epsilon_z S_z + \mathbf{h}\cdot\mathbf{S} + \delta\mathbf{h}\cdot\delta\mathbf{S} + \frac{J}{2}\mathbf{S}\cdot\mathbf{S} - J, \tag{74}$$

where $\mathbf{S}=\mathbf{S}_1+\mathbf{S}_2$, $\delta\mathbf{S}=\mathbf{S}_1-\mathbf{S}_2$, $\mathbf{h}=\mathbf{h}_1+\mathbf{h}_2$, and $\delta\mathbf{h}=\mathbf{h}_1-\mathbf{h}_2$. Here J is the Heisenberg exchange coupling between the two electron spins. For definiteness we work in a regime of large Zeeman splitting due to an external magnetic field, $\epsilon_z = g^*\mu_B \gg \max\{\langle\delta\mathbf{h}\rangle_{\rm rms}, \langle\mathbf{h}\rangle_{\rm rms}\}$, where $\langle\mathcal{O}\rangle_{\rm rms} = \langle\psi_I|\mathcal{O}|\psi_I\rangle^{1/2}$ denotes the root-mean-square expectation value of the operator $\mathcal{O}$ on the nuclear state $|\psi_I\rangle$. Requiring $\epsilon_z \gg J$, where J is taken to be positive without loss of generality, the large Zeeman splitting condition renders the relevant spin Hamiltonian block diagonal with respect to the eigensubspaces of S_z. In the $S_z=0$ subspace the spin Hamiltonian for the singlet $|S\rangle$ and $S_z=0$ triplet $|T_0\rangle$, to zeroth order in the inverse Zeeman splitting $1/\epsilon_z$, is given by $\mathcal{H}_0 = (J/2)\mathbf{S}\cdot\mathbf{S} + \delta h^z \delta S^z$. The effective qubit Hamiltonian in terms of the vector consisting of Pauli matrices $\boldsymbol{\tau} = (\tau^x, \tau^y, \tau^z)$, with the computational states $|S\rangle \to |\tau^z = -1\rangle$ and $|T_0\rangle \to |\tau^z = 1\rangle$, has the form

$$\mathcal{H}_0 = \frac{J}{2}(1+\tau^z) + \delta h^z \tau^x. \tag{75}$$

A systematic treatment of the dynamics induced by the Hamiltonian (75) can be found in [31,36]. The eigenstates of $\mathcal{H}_0$ are given by a product state between a nuclear eigenstate $|n\rangle$ of δh^z and a superposition of $|S\rangle$ and $|T_0\rangle$, therefore $\mathcal{H}_0$ does not lead to any dynamics in the nuclear field. The correlator C_{T_0S} is defined as the probability of finding the electron spins in the state $|T_0\rangle$ at time $t>0$, provided that the initial state $(t=0)$ was $|\psi(0)\rangle = |S\rangle \otimes |\psi_I\rangle$, with $|\psi_I\rangle = \sum_n a_n |n\rangle$ a superposition of δh^z eigenstates,

$$C_{T_0S}(t) = \sum_n \rho_I(n) |\langle n| \otimes \langle T_0| e^{-i\mathcal{H}_0 t} |S\rangle \otimes |n\rangle|^2, \tag{76}$$

where $\rho_I(n) = |a_n|^2$ are the diagonal matrix element of $\rho_I = |\psi_I\rangle\langle\psi_I| = \sum_n \rho_I(n)|n\rangle\langle n| + \sum_{n\neq n'} a_n^* a_{n'} |n'\rangle\langle n|$ in the $\{|n\rangle\}$ basis. For a Gaussian distributed field δh_z, with mean x_0 and variance σ_0, the asymptotics of C_{T_0S} saturates to finite value that deviates from the semiclassical results ($C_{T_0S}^{\rm semicl}(\infty) = 1/2$) for $J \ll x_0$ (see [36]),

$$C_{T_0S}(\infty) \sim \begin{cases} \dfrac{1}{2} - \dfrac{1}{8}\left(\dfrac{J}{x_0}\right)^2, & \sigma_0, J \ll x_0, \\ 2\left(\dfrac{x_0}{J}\right)^2, & \sigma_0 \ll x_0 \ll J. \end{cases} \tag{77}$$

At short times $C_{T_0S}(t)$ experiences a Gaussian decay on a timescale $\sqrt{J^2 + 4x_0^2}/4x_0\sigma_0$, while in the case of strong coupling $J \gg \max\{X_0, \sigma_0\}$ at long times $t \gg J/4\sigma_0^2$ a power-law decay appears (see [36]),

$$C_{T_0S}(t) \sim C_{T_0S}(\infty) - \frac{e^{-x_0^2/2\sigma_0^2}}{4\sigma_0\sqrt{Jt}} \cos\left(Jt + \frac{3\pi}{4}\right). \tag{78}$$

Those results show that the singlet-triplet correlator decays due to the quantum distribution of the nuclear spin system, even for a static system. For non-zero exchange

interaction $J \neq 0$ the asymptotic behaviour of the correlator $C_{T_0S}(t)$ changes from a short-time Gaussian behaviour to a long-time power-law ($\sim 1/t^{3/2}$) decay and acquires a universal phase shift which is $3\pi/2$, consistent with experimental findings for the correlator $C_{SS}(t)$ (see [37]). Qualitatively similar results appear when looking at the transverse correlator in the $S_z = 0$ subspace, although one finds different decay power and different value of the universal phase shift.

2.5. *Nuclear spin state manipulation*

As mentioned in the previous sections, for a system of N unpolarized nuclei and an effective hyperfine interaction strength A, the dephasing time in a weak magnetic field is $T_2^* \sim 1/\sigma \sim \sqrt{N}/A$, where σ is the width of the distribution of the nuclear field h_z. This decay T_2^* finds its origin in the ensemble average over the field distribution. In order to prolong the electron spin coherence, narrowing of the nuclear field distribution was proposed in [28] as an alternative to the strategy of polarizing the nuclear spins [24], that would require a polarization close to 100% to be efficient, which is currently not available [28]. Few methods for nuclear spin state narrowing have been studied: in [31] the narrowing is due to gate-controlled Rabi oscillations in a double quantum dot in which the exchange interaction oscillates; in [38] a scheme based on quantum phase estimation is envisioned for a single undriven spin in a single quantum dot; and in [32] the narrowing is achieved by optical preparation.

2.5.1. *Nuclear state narrowing by qubit state measurement*

Here we discuss a nuclear state narrowing technique that has been proposed in [31]. Consider for definiteness the ESR Hamiltonian (72). The effective Zeeman splitting is given by $b + h_z^n$, where $b = g^*\mu_B B_z$ and h_z^n is an eigenvalue of h_z. The idea behind state narrowing is that the ESR driving give rise to the resonance condition $b + h_z^n - \omega = 0$, such that the evolution of the electron spin depends on the nuclear spin state and thus a determination of the electron spin evolution results in a determination of the nuclear spin state.

The eigenvalues of the nuclear field, as already mentioned in the previous sections, are Gaussian distributed in equilibrium. The diagonal elements of the nuclear spin density matrix are $\rho_I(h_z^n, t=0) = \langle h_z^n|\rho_I|h_z^n\rangle = \exp(-(h_z^n - \langle h_z\rangle)^2/2\sigma^2)/\sqrt{2\pi}\sigma$, with mean $\langle h_z\rangle$ and variance σ. Therefore, initializing the electron spin in the state $|\uparrow\rangle$ at time $t=0$, the probability of finding the electron spin in the state $|\downarrow\rangle$ is given by

$$P_\downarrow(t) = \int \mathrm{d}h_z^n \, \rho_i(h_z^n, 0) P_\downarrow^n(t), \tag{79}$$

where $P_\downarrow^n(t)$ is the probability of finding the electron spin in the state $|\downarrow\rangle$, for a given eigenvalue h_z^n of the nuclear field h_z,

$$\begin{aligned} P_\downarrow^n(t) &= \left|\langle h_z^n| \otimes \langle\downarrow|U^{\mathrm{ESR}}(t)|\uparrow\rangle \otimes |h_z^n\rangle\right|^2 \\ &= \frac{1}{2}\frac{b_{\mathrm{ac}}^2}{b_{\mathrm{ac}}^2 + 4\delta_n^2}\left[1 - \cos\left(\frac{t}{2}\sqrt{b_{\mathrm{ac}}^2 + 4\delta_n^2}\right)\right]. \end{aligned} \tag{80}$$

If at time $t = t_m$ we perform a measurement of the electron spin and find $|\downarrow\rangle$, the diagonal element of the nuclear spin density matrix will change according to

$$\rho_I(h_z^n, 0) \to \rho_I^{(1,\downarrow)}(h_z^n, t_m) = \rho_I(h_z^n, 0)\frac{P_\downarrow^n(t_m)}{P_\downarrow(t_m)}. \tag{81}$$

In the case where a measurement is performed with a low time resolution Δt, $\Delta t \gg 1/b$, such that it gives the time averaged value, the probability turns out to be $P_\downarrow^n = \lim_{T\to\infty}(1/T)\int_0^T \mathrm{d}t P_\downarrow^n(t) = b_{\mathrm{ac}}^2/2(b_{\mathrm{ac}}^2 + 4\delta_n^2)$. Therefore, a measurement on the electron spin with outcome $|\downarrow\rangle$ results in a multiplication of the nuclear spin density matrix by a Lorentzian, with width b_{ac}, centred around the value h_z^n that satisfies the condition $b + h_z^n - \omega = 0$. The nuclear spin distribution, thus, undergoes a narrowing, resulting in an enhancement of the electron spin coherence, if $b_{\mathrm{ac}} < \sigma$. In the case that the measurement outcome is $|\uparrow\rangle$ the diagonal element of the nuclear spin density matrix will change according to

$$\rho_I(h_z^n, 0) \to \rho_I^{(1,\uparrow)}(h_z^n, t_m) = \rho_I(h_z^n, 0)\frac{1 - P_\downarrow^n(t_m)}{1 - P_\downarrow(t_m)}, \tag{82}$$

resulting in a reduced probability for the nuclear field to have a value that matches the resonance condition $b + h_z^n - \omega = 0$.

This procedure can be iterated many times before changes due to the slow internal dynamics start to affect the nuclear spin state. Many measurement of the electron spin are possible within this time, with re-initialization of the electron spin state between the measurements. Assuming that M cycles can be performed with a static nuclear field, we have

$$\rho_I(h_z^n, 0) \to \rho_I^{(M,\alpha_\uparrow)}(h_z^n, t_m) = \frac{1}{N}\rho_I(h_z^n, 0)\left(P_\downarrow^n\right)^{\alpha_\uparrow}(1 - P_\downarrow)^{M-\alpha_\uparrow}, \tag{83}$$

where $\alpha_\uparrow$ is the number of measurement outcomes $|\downarrow\rangle$. If the outcome is $|\downarrow\rangle$ the narrowing has been achieved; otherwise, it is necessary to wait for a re-equilibration of the nuclear system before the next measurement.

2.5.2. *Optical preparation of nuclear spins*

Here, we discuss the case of optical nuclear spin preparation that makes use of spin–flip two-photon Raman resonance in a driven three-level system (TLS) [32]. The lowest electronic states in GaAs quantum dots that are optically active under σ_+ circularly polarized excitation are the ground state of a single localized conduction-band (E_C) electron, in which a Zeeman field splits the up and down spin states, and the negatively charged exciton (trion) $|X\rangle$, given by two electrons with antiparallel spin plus one valence band heavy hole (hh) with angular momentum $J_{z'} = +3/2$, as schematically shown in Figure 4. The $J = 3/2$ subspace in the valence band splits up into heavy and light holes (hh and lh) along the direction z' of strong quantum dot confinement, that is in general different from the z-axis in the conduction band, chosen to be the direction of the magnetic field B. The two circularly polarized lasers stimulate the transition between $|\uparrow\rangle$ and $|X\rangle$ at frequency $\omega_p = \omega_X - \omega_\uparrow - \Delta_1$ and the transition between $|\downarrow\rangle$ and $|X\rangle$ at frequency $\omega_c = \omega_X - \omega_\downarrow - \Delta_2$, while the trion $J_{z'} = -3/2$ is not excited.

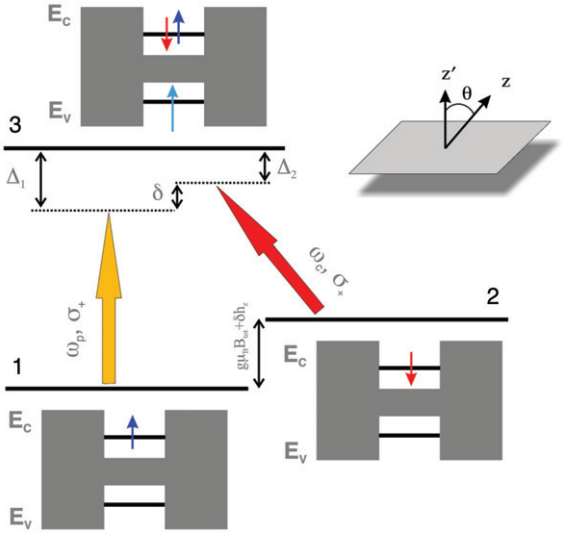

Figure 4. Three-level system. The state 1 (2) is the spin-up (-down) conduction-band (E_C) electron, with splitting given by $g\mu_B B_{\rm tot} + \delta h_z$, where δh_z is the z component of the nuclear field fluctuations. State 3 is a trion with $J_{z'} = 3/2$. Reprinted with permission from [32]. © 2004 by the American Physical Society.

The narrowing of the nuclear field distribution is based on light scattering in the TLS, where two long-lived spin states are resonantly coupled to the excited trion state $|X\rangle$ that decays spontaneously. For the two-photon resonance condition $\delta = \Delta_1 - \Delta_2 = 0$, where δ is the detuning of the difference of the frequency of the two lasers $\omega_c - \omega_p$ from the Zeeman splitting ω_z of the two spin states, the system is in a superposition of the two spin states with a vanishing excited state component, and the system is driven to a dark state with no photon emission. In presence of a nuclear spin field, the resonance moves to $\delta = \delta h_z$, where δh_z is the deviation of the Overhauser field from its mean. Monitoring the photon emission constitutes a continuous weak measurement of the Overhauser field h_z. The absence of photon emission in the limit $t \to \infty$, corresponding to the strong measurement limit, would project the nuclear state onto $|\delta h_z = 0\rangle$, with width $\sigma = 0$, therefore letting the dephasing time to diverge, $T_2^* \sim 1/\sigma \to \infty$. A continuous weak measurement of the Overhauser field, supported by an adaptive adjustment of the lasers frequencies every time a photon is detected, leads to a narrowing of the nuclear field distribution, and an enhancement of the phase coherence of the electron spin.

The relevant effective Hamiltonian of the TLS in the rotating wave approximation is block diagonal, with blocks labelled by the eigenvalues δh_z^k of the field δh_z

$$\mathcal{H}_k = -\frac{\hbar}{2}\begin{pmatrix} \delta h_z^k + \delta & 0 & \Omega_p \\ 0 & -\delta h_z^k - \delta & \Omega_c \\ \Omega_p & \Omega_c & -\Delta \end{pmatrix}, \tag{84}$$

where $\Delta = \Delta_1 + \Delta_2$. The combined system consisting of the TLS and the nuclear spins evolves in time according to a generalized master equation $\dot{\rho} = \mathcal{L}\rho$, where $\mathcal{L}$ is the

Liouvillian operator defined as

$$\dot{\rho} = \mathcal{L}\rho \equiv \frac{1}{i\hbar}[H, \rho] + \mathcal{W}\rho, \tag{85}$$

where H is the Hamiltonian of the system, and

$$\mathcal{W} = \sum_{\alpha=\uparrow,\downarrow} \Gamma_{X\alpha}(2\sigma_{\alpha X}\rho\sigma_{X\alpha} - \sigma_{XX}\rho - \rho\sigma_{XX})/2 + \sum_{\beta=\downarrow,X} \gamma_\beta(2\sigma_{\beta\beta}\rho\sigma_{\beta\beta} - \sigma_{\beta\beta}\rho - \rho\sigma_{\beta\beta})/2.$$

Here, the rate $\Gamma_{X\alpha}$ describes the radiative decay of $|X\rangle$ into $\alpha = |\uparrow\rangle, |\downarrow\rangle$, while γ_β is the pure dephasing rate of state $\beta = |\downarrow\rangle, |X\rangle$ with respect to $|\uparrow\rangle$.

Taking as the initial state a product of arbitrary density matrices χ_0 for the TLS and $\nu_0 = \sum_{kk'} \nu_{kk'} |\delta h_z^k\rangle\langle h_z^{k'}|$ for the nuclear field, the stationary solution is an entangled state $\bar{\rho}$.

In order to describe the state of the system conditional on a measurement record, a conditional density matrix is used. The *a posteriori* distribution ν_{kk} is found to be concentrated around the two photon resonance. The stationary emission rate is

$$\Gamma_{\text{em}} = \text{Tr}\mathcal{S}\bar{\rho}(t) = \Gamma \sum_k \nu_{kk}\langle X|\rho_{kk}|X\rangle, \tag{86}$$

where $\Gamma = \Gamma_{X\uparrow} + \Gamma_{X\downarrow}$ and $\mathcal{S}$ is the collapse operator, describing spontaneous emission of the state $|X\rangle$ into $|\uparrow\rangle$ and $|\downarrow\rangle$ at rates $\Gamma_{X\uparrow}$ and $\Gamma_{X\downarrow}$. The update rule for ν upon photon emission is

$$\nu'_{kk} = \frac{\nu_{kk}\langle X|\rho_{kk}|X\rangle}{\sum_j \nu_{jj}\langle X|\rho_{jj}|X\rangle}. \tag{87}$$

The population in the Overhauser field δh_z corresponding to the two-photon resonance $\delta h_z = \delta$ is depleted by the photon emission. The electron spin coherence is quantified by the time dependence of the transverse electron spin component, which in turn is given by the Fourier transform of the nuclear field distribution, $\langle S_+(t)\rangle = (\hbar/2)\sum_k \nu_{kk} \exp(it\delta h_z^k)$. The repeated observation of the quantum dot photon emission and consequent adaption of the laser frequencies after each photon detection leads to a narrowing in the nuclear distribution and consequent enhancement of the electron spin coherence time.

2.5.3. *Exponential decay in narrowed nuclear state*

We have seen that the nuclear spin bath induces a non-Markovian dynamics of the electron spin, with super-exponential or power-law decay of the correlation functions. On the other hand, it has been argued that a narrowing of the nuclear spin distribution is expected to prolong the electron spin coherence. In [39], it is shown that, in case of a large Zeeman splitting and for a particular narrowed nuclear spin state, a Markovian dynamics can arise from virtual flip–flops between the electron spin and the nuclear spin system, with simple exponential decay.

The Hamiltonian describing the interaction of the electron spin with the nuclear system in a large magnetic field is given by (69). The energy non-conserving term V can be

eliminated by means of a Schrieffer–Wolff transformation, $\bar{\mathcal{H}} = e^{S}\mathcal{H}e^{-S} \approx H = \mathcal{H}_0 + (1/2)[S, V]$, where $S = \mathcal{L}_0 V$, and $\mathcal{L}_0$ is the unperturbed Liouvillian, defined by $\mathcal{L}_0 O = [\mathcal{H}_0, O]$. The effective Hamiltonian H is given by

$$H = (\omega + X)S^z + D. \tag{88}$$

The operators ω, D, and X are nuclear spin operators and the first two are diagonal in a product-state basis of I_k^z-eigenstates, whereas X is purely off-diagonal and produces correlations between nuclear spins. Corrections of the order of around A^2/Nb in the diagonal terms of H are neglected, whereas the term of this size in X are retained. This assumption is valid as long as the bath correlation time τ_c is much shorter than the timescale after which the diagonal corrections become relevant for $b \gg A$, where a Born–Markov approximation is valid: $\tau_c \sim N/A \ll Nb/A^2$. As a result $\omega = b + h^z$.

The electron and nuclear states are assumed to be initially unentangled and the nuclear system is prepared in a narrowed state, $\omega|n\rangle = \omega_n|n\rangle$. For these initial conditions, the dynamics of the transverse electron spin component $\langle S_+\rangle_t$ is described by a GME, and can be written in a rotating frame defined by $x_t = \exp[-i(\omega_n + \Delta\omega)t]\langle S_+\rangle_t$, where $\Delta\omega$ is a frequency shift self-consistently defined by $\Delta\omega = -\mathrm{Re}\int_0^\infty \mathrm{d}t\Sigma(t)$, with $\tilde{\Sigma}(t) = \exp[-i(\omega_n + \Delta\omega)t]\Sigma(t)$, through the memory kernel $\Sigma(t)$ of the GME. The equation of motion for x_t is given by

$$\dot{x}_t = -i\int_0^t \mathrm{d}\tau\, \tilde{\Sigma}(\tau)x_{t-\tau}. \tag{89}$$

If $\Sigma(t)$ decays to zero sufficiently fast on the timescale $\tau_c \ll T_2$, where T_2 is in turn the decay time of x_t, it is possible to approximate $x_{t=\tau} \approx x_t$ and extend the upper limit of the integral to infinity, $t \to \infty$, obtaining a Markovian dynamics

$$x_t = \exp(= t/T_2)x_0 + \epsilon(t), \quad \frac{1}{T_2} = -\mathrm{Im}\int_0^\infty \mathrm{d}t\, \tilde{\Sigma}(t), \tag{90}$$

where $\epsilon(t)$ gives a small non-Markovian correction that can be bounded precisely if $\tilde{\Sigma}(t)$ is known.

For a homo-nuclear system, by expanding $\Sigma(t)$ in the perturbation $V = X\ S^z$ and retaining only leading orders in the Born approximation in the small parameter A/ω_n, the decoherence time T_2 can be cast in the compact form

$$\frac{1}{T_2} = \mathrm{Re}\int_0^\infty \mathrm{d}t\, e^{-i\Delta\omega t}\langle X(t)X\rangle, \quad X(t) = e^{-i\omega t}Xe^{i\omega t}, \tag{91}$$

where the average stands for an expectation value taken with respect to the initial nuclear state. Although the compact form resembles the standard result for pure dephasing valid in a weak coupling expansion, here there is no such weak coupling expansion. The decoherence rate $1/T_2$ depends on the correlator $C(t) = \langle X(t)X\rangle$. For an isotropic electron wavefunction of the form $\psi(r) = \psi(0)e^{-(r/r_0)^q/2}$ containing $N \gg 1$ nuclei within a radius r_0 in d dimension, the asymptotic dependence of $C(t)$ at long times is $C(t) \propto 1/t^{2\mathrm{d}/q}$, for $t \gg N/A$ and $d/q < 2$. For $d/q \leq 1/2$, $1/T_2$ given by (91) diverges and no Markov approximation is valid within the Born approximation. On the other hand, for

a two-dimensional dot with a Gaussian electron wavefunction and for unpolarized nuclear system, (91) gives the simple result

$$\frac{1}{T_2} = \frac{\pi}{3}\left(\frac{I(I+1)A}{3b}\right)^2 \frac{A}{N}. \tag{92}$$

The condition for the validity of the Markov approximation, $T_2 > \tau_c \sim N/A$ is satisfied whenever $A/b < 1$, which correspond to the range of validity of the Born approximation. Remarkably, from the last equation it follows that $1/T_2$ strongly depends on the magnitude of the nuclear spin, $1/T_2 \propto I^4$. Therefore, systems with large nuclear spin, such as In ($I_{\mathrm{In}} = 9/2$), will decay faster.

With these last results on exponential decay in a spin bath, we conclude the part on electron spin decoherence induced by the nuclear spin system and focus on phonon-mediated relaxation of the electron spin in quantum dots.

2.6. *Phonon-induced relaxation in quantum dots*

Electron spin relaxation in quantum dots takes place via transitions between spin states, with consequent energy dissipation in the environment. In a quantum dot the dissipative environment is represented mainly by the phonons in the surrounding crystal. Therefore, in order to fully understand relaxation and decoherence mechanisms that occur in quantum dots, it is important to understand the manner in which the electron spin interacts with phonons.

Spin-orbit (SO) interaction creates an admixture of orbital and spin degrees of freedom of the electron, and represents an effective coupling mechanism that mediates the spin–phonon interaction, and that, ultimately, is responsible for relaxation of the electron spin. Phonons can produce electric field fluctuations that can lead to spin relaxation of eigenstates of the SO Hamiltonian. Two kinds of electron–phonon interactions are taken into account, that arise, respectively, from an inhomogeneous deformation of the crystal potential, resulting in an alteration of the band-gap, and a homogeneous strain due to piezo-electric effect, the former taking place in all semiconductors, the latter only in crystals without structure inversion symmetry such as GaAs.

2.7. *Introduction to SO interaction*

An electron that moves in an electric field experiences an effective magnetic field in its rest frame which interacts with the spin of the electron. The internal magnetic field depends on the orbital the electron occupies and therefore the spin and orbit are coupled. This well-known effect comes directly from the relativistic Dirac theory of point particles and it goes under the name of SO interaction. The SO Hamiltonian has the general form [40]

$$\mathcal{H}_{\mathrm{SO}} = \frac{\hbar}{4m_0^2c^2}\mathbf{p}\cdot(\boldsymbol{\sigma}\times\nabla V), \tag{93}$$

where m_0 is the free electron mass, c is the speed of light, $\boldsymbol{\sigma} = (\sigma_x, \sigma_y, \sigma_z)$ is the Pauli matrix vector, and V is the electric potential. In the presence of an external magnetic field

$\mathbf{B} = \nabla \times \mathbf{A}$, the canonical momentum $\mathbf{p}$ is replaced by the kinetic momentum $\mathbf{P} = \mathbf{p} + e\mathbf{A}$, $\mathbf{A}$ being the vector potential.

In semiconductors such as Si or Ge the crystal lattice has spatial inversion symmetry. For such materials, states of a given momentum $\mathbf{k}$ are four-fold degenerate at $B = 0$. In fact due to time reversal symmetry, $\epsilon_{\mathbf{k},\uparrow} = \epsilon_{-\mathbf{k},\downarrow}$ holds, and from the inversion symmetry one has $\epsilon_{\mathbf{k},\boldsymbol{\sigma}} = \epsilon_{-\mathbf{k},\boldsymbol{\sigma}}$, such that $\epsilon_{\mathbf{k},\uparrow} = \epsilon_{\mathbf{k},\downarrow} =$ holds.

The double degeneracy can be broken either via the application of an external magnetic field, which breaks the time reversal symmetry, or via the braking of spatial inversion symmetry. This is indeed what happens in crystals that exhibit bulk inversion asymmetry (BIA), such as the zincblende structure of GaAs. This effect is know as Dresselhaus SO interaction [41,42]. The Hamiltonian for two-dimensional systems results from the three-dimensional bulk Hamiltonian [43] after integration over the growth direction z along [001]

$$\mathcal{H}_D \propto \left[-\sigma_x p_x \langle p_z^2 \rangle + \sigma_y p_y \langle p_z^2 \rangle + \sigma_x p_x p_y^2 - \sigma_y p_y p_x^2 \right] \tag{94}$$

where x and y point along the crystallographic directions [100] and [010]. Owing to the strong confinement along z, the terms cubic in momentum components appearing in the Hamiltonian are usually much smaller than the linear terms, and they are usually neglected. Retaining only the linear term

$$\mathcal{H}_D = \beta(-\sigma_x p_x + \sigma_y p_y) \tag{95}$$

where β depends on material properties and on $\langle p_z^2 \rangle$. The spin dynamics resulting from the Dresselhaus Hamiltonian is well understood in the case of a circular orbit, in which the spin rotates in the opposite direction with respect to the orbit, as shown in Figure 5.

In heterostructures such as GaAs/AlGaAs, an asymmetric confining potential additionally breaks the inversion symmetry, giving rise a further SO interaction due to structural inversion asymmetry (SIA), known as the Bychkov–Rashba term [44,45]. For a confining electric field along the z direction, the Bychkov–Rashba Hamiltonian ($\propto (\mathbf{E} \times \mathbf{p}) \cdot \boldsymbol{\sigma}$) is

$$\mathcal{H}_R = \alpha(\sigma_x p_y - \sigma_y p_x), \tag{96}$$

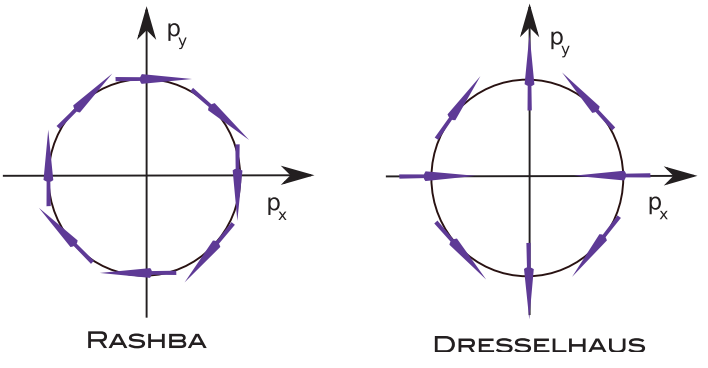

Figure 5. Schematic representation of the apparent momentum-dependent field $\boldsymbol{\Omega}(\mathbf{p})$ in the SO Hamiltonian, $\boldsymbol{\Omega}(\mathbf{p}) \cdot \boldsymbol{\sigma}$, for the Dresselhaus and Rashba SO interactions.

where α depends on the confining potential and on material properties. The spin dynamics resulting from the Bychkov–Rashba Hamiltonian can also be well understood in the case of a circular orbit, in which the spin rotates along in the same direction as the orbit, the spin always being antiparallel to the direction of motion, as explained in Figure 5.

2.8. *Electron spin relaxation and decoherence*

Owing to the fact that the most promising semiconductor devices that make use of the electron spin as the quantum two-level system (qubit) are realized on the basis of two-dimensional electron gases in GaAs heterostructures, the following discussion concentrates on spin flip mechanisms that are relevant for GaAs.

Spin relaxation of localized electrons in quantum dots shows remarkable differences from the case of delocalized bulk electrons. The most effective mechanisms in bulk 2D are related to the broken inversion symmetry, either the BIA or SIA case, which give rise to a strong SO splitting in the electron spectrum, ultimately responsible for spin flip. In addition, the piezoelectric interaction arising in non-inversion symmetric crystals provides a strong coupling of electrons to the bosonic bath of acoustic phonons. The interplay of these mechanisms results in an efficient spin-lattice relaxation for bulk carriers in III–V type semiconductors and heterostructures. The strong localization of electrons in quantum dots leads to suppression of the spin–flip rate. The phonon-assisted spin–flip mechanisms in semiconductor quantum dots have been studied in [21,22].

2.8.1. *Electron spin relaxation in quantum dots*

In the case of strong confinement in the z direction, corresponding to the [100] crystallographic axis, for a lateral dot size much larger than the degree of vertical confinement, the Hamiltonian derived from the Kane model [46] for two-dimensional electrons in the conduction band in the presence of an external magnetic field $\mathbf{B}$ is [21,22]

$$\mathcal{H} = \frac{\mathbf{p}^2}{2m} + U(\mathbf{r}) + U_{\mathrm{ph}}(\mathbf{r}, t) + \frac{1}{2} g \mu_{\mathrm{B}} \boldsymbol{\sigma} \cdot \mathbf{B} + \mathcal{H}_{\mathrm{SO}}^{D} + \mathcal{H}_{\mathrm{SO}}^{R}, \tag{97}$$

$$\mathcal{H}_{\mathrm{SO}}^{D} = \beta(-\sigma_x p_x + \sigma_y p_y), \quad \mathcal{H}_{\mathrm{SO}}^{R} = \alpha(\sigma_x p_y - \sigma_y p_x). \tag{98}$$

Here, $\mathbf{p} = -i\hbar\nabla + (e/c)\mathbf{A}$ is the kinetic momentum, m the effective mass, g the effective electron g-factor (in GaAs $g = -0.44$), and $\boldsymbol{\sigma}$ the Pauli matrix vector. The axes x, y, and z coincide with the main crystallographic axes, with z perpendicular to the two-dimensional plane. The first two terms of the Hamiltonian describe the quantum dot with confining potential $U(\mathbf{r})$, that is typically chosen to be parabolic. The third term describes the spin-independent interaction with acoustic phonon. The fourth term is the Zeeman Hamiltonian. Here, $\mathcal{H}_{\mathrm{SO}}$ describes the SO effects, $\mathcal{H}_{\mathrm{SO}}^{D}$ is the Dresselhaus term, due to BIA, and $\mathcal{H}_{\mathrm{SO}}^{D}$ is the Rashba term, due to SIA. For GaAs heterostructures $\beta \approx 10^5\,\mathrm{cm\,s^{-1}}$.

The Hamiltonian (97) should also contain a term describing 'direct' interaction between spin and phonons, such as that due to an inhomogeneous deformation of the lattice, and a term describing the spin–phonon coupling in the presence of a magnetic field due to a lattice-deformation-dependent admixture of valence-band and conduction-band states. Their contribution to spin relaxation rates turns out to be negligible with respect to

the dominant admixture mechanism contribution owing to the Dresselhaus and Rashba SO interaction. See [21,22,47] for a discussion of the direct spin–phonon coupling contribution.

The phonon-induced rate for the transition between $|\Psi_n^{\uparrow}\rangle$ and $|\Psi_n^{\downarrow}\rangle$ is given by Fermi's golden rule

$$\Gamma = \frac{2\pi}{\hbar}\sum_n \left|\langle \Psi_n^{\uparrow}|\mathcal{H}_{ph}|\Psi_n^{\downarrow}\rangle\right|^2 D(\epsilon_Z). \tag{99}$$

Here, $D(\epsilon_Z)$ is the phonon density of states at the Zeeman energy splitting ϵ_z. From experimental results, the relevant acoustic phonons can be treated as bulk-like phonons, showing a linear dispersion relation in the relevant energy range, for which the density of states increases quadratically with energy [48]. The states $|\Psi_n^{\uparrow}\rangle$ and $|\Psi_n^{\downarrow}\rangle$ are the effective spin states, containing more than one orbital and both the spin *up* and *down* states. This admixture of spin and orbit comes out in taking into account the SO interaction due to BIA and SIA as a perturbation. Owing to the localization of stationary states in a quantum dot, it follows that the SO interaction does not directly couple Zeeman-split sublevels in the same quantum dot orbital. It follows that within first-order perturbation theory in the SO Hamiltonian, the effective single electron quantum dot states are

$$|\Psi_n^{\uparrow}\rangle = |n\uparrow\rangle + \sum_{n'\neq n}\frac{(\mathcal{H}_{\rm SO})_{n'n}^{\downarrow\uparrow}}{E_n - E_{n'} + g\mu_{\rm B}B}|n'\downarrow\rangle, \tag{100}$$

$$|\Psi_n^{\downarrow}\rangle = |n\downarrow\rangle + \sum_{n'\neq n}\frac{(\mathcal{H}_{\rm SO})_{n'n}^{\uparrow\downarrow}}{E_n - E_{n'} - g\mu_{\rm B}B}|n'\uparrow\rangle, \tag{101}$$

where $(\mathcal{H}_{\rm SO})_{n'n}^{\downarrow\uparrow} = \langle n'\downarrow|\mathcal{H}_{\rm SO}|n\uparrow\rangle$ and $\{|n\rangle\}$ are the unperturbed quantum dot orbital states. Owing to the anisotropy of BIA and SIA SO interaction, the admixture of spin and orbit degrees of freedom turns out to be anisotropic [49].

For spin–flip transitions involving a small energy transfer, the dominant contribution comes from piezo-electric phonons. The electric field associated with a single phonon scales as $1/\sqrt{q}$ for piezo-phonons and as $\sqrt{q}$ for deformation potential phonons, q being the phonon wave number. This is due to the fact that piezo-phonons come from a homogeneous lattice strain, in which long wavelengths play a major role. *Vice versa*, a local deformation would involve short wavelengths, and so higher energies. On the other hand, wavelengths much longer than the dot size give rise to a global shift of the entire dot potential, therefore the effective phonon wavelengths are those comparable with the dot size, as seen in [50].

The electron–phonon coupling for piezo-electric phonons has the form

$$U_{ph}^{\mathbf{q}\alpha}(\mathbf{r},t) \propto \exp(i\mathbf{q}\cdot\mathbf{r} - i\omega_{\mathbf{q}\alpha}t)A_{\mathbf{q}\alpha}b_{\mathbf{q}\alpha}^{\dagger} + \text{h.c.}, \tag{102}$$

where $\mathbf{q}\alpha$ are the wavelength and the branch of the phononic modes, $A_{\mathbf{q}\alpha}$ is effective anisotropic piezo-electric modulus of wave $\mathbf{q}\alpha$. The matrix elements of the phonon Hamiltonian between the Zeeman split sublevels of orbital level n, that describe the

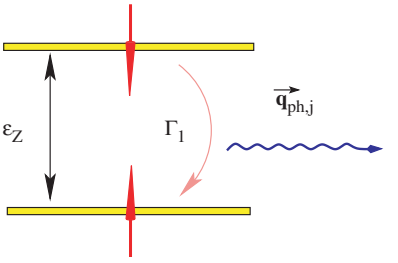

Figure 6. Schematic representation of the spin–flip process associated with the emission of a phonon of energy ϵ_Z and momentum $\mathbf{q}_{ph,j}$, where j is the branch index, at rate Γ_1.

spin–flip process with emission of phonon $\mathbf{q}\alpha$, are given at first order in the SO interaction by

$$\left\langle \Psi_n^{\uparrow} \middle| U_{ph}^{\mathbf{q}\alpha} \middle| \Psi_n^{\downarrow} \right\rangle = \sum_{k \neq n} \left[\frac{\left(U_{ph}^{\mathbf{q}\alpha}\right)_{nk} (\mathcal{H}_{\mathrm{SO}})_{kn}^{\uparrow\downarrow}}{E_n - E_k - g\mu_{\mathrm{B}} B} + \frac{\left(U_{ph}^{\mathbf{q}\alpha}\right)_{nk} (\mathcal{H}_{\mathrm{SO}})_{kn}^{\downarrow\uparrow}}{E_n - E_k + g\mu_{\mathrm{B}} B} \right]. \tag{103}$$

As a consequence of Kramer's theorem, in case of no external magnetic field, (103) is zero. Considering only Dresselhaus SO interaction, for small Zeeman splitting, $g\mu_{\mathrm{B}} B \ll \sqrt{ms^2\hbar\omega_0}$, it is possible to obtain an effective spin–flip Hamiltonian which acts on the subspace of Zeeman sublevels of orbital level n (see [22]), where a phonon-induced electric field arise as a gradient of U_{ph}. For a parabolic dot confinement potential, and for the particular case of a circular dot with level spacing ω_0, the spin–flip rate for the transition between the Zeeman sublevels of the dot ground state, associated with the emission of a piezo-phonon as depicted in Figure 6, is [22]

$$\Gamma_1 = \frac{(g\mu_{\mathrm{B}} B)^5}{\hbar(\hbar\omega_0)^4} \Lambda_p (1 + \cos^2(\vartheta)), \quad \Lambda_p \equiv \frac{2}{35\pi} \frac{(eh_{14})^2 \beta^2}{\rho\hbar} \left(\frac{1}{s_{\mathrm{l}}^5} + \frac{4}{3s_{\mathrm{t}}^5} \right), \tag{104}$$

where β is the strength of the Dresselhaus SO interaction, ϑ is the angle between the direction of confinement in the quantum dot z, and the direction of the applied magnetic field z', and Λ_p is the strength of the effective spin–piezo-phonon coupling. For given longitudinal and transverse sound speed s_{l} and s_{t}, crystal mass density ρ, and modulus of the piezo-tensor eh_{14} ($eh_{14} = 1.3 \times 10^7\,\mathrm{eV\,cm^{-1}}$ for GaAs), it ranges from around 7×10^{-3} to about 6×10^{-2}, depending on β. Equation (104) shows a strong dependence on the magnetic field and the lateral dot confinement energy ω_0. For $\hbar\omega_0 = 10\,\mathrm{K}$ and magnetic field $B = 1\,\mathrm{T}$, $\Gamma_1 \approx 1.5 \times 10^3\,\mathrm{s^{-1}}$. These theoretical expectations, in particular the B-dependence, have been confirmed in experiments [51–53], and long spin relaxation times, up to 1 s, have been measured [23].

The effect of the Rashba SO interaction has so far not been taken into account. As the Dresselhaus term, it contributes to the admixing of spin and orbital states, and therefore to relaxation due to phonon scattering. The effect of the interplay of these two terms can show up in a strong difference in the their associated relaxation rates [23,54–56]. For a quantum dot in an external magnetic field, the first and second lowest levels show a crossing behaviour as a function of the applied magnetic field,

with the ground state unaffected. In a perturbative treatment of the SO interaction [54], Dresselhaus and Rashba terms show a qualitative difference, in which the latter couples the crossing levels, giving rise to an anticrossing of the levels at the point of accidental degeneracy. For magnetic fields much smaller than the crossing level value, the these two levels have a well-defined spin orientation, that is, a low degree of admixture. In the region of anticrossing the admixture leads to equally weighted superposition of the *up* and *down* states, and eventually to a reversed situation in the limit of the magnetic field much larger than the crossing value, in which the two levels have again well-defined spin, but reversed. Therefore, sweeping the magnetic field over the crossing region leads to spin–flip. In particular at the avoided crossing point, the strong admixture between spin states lead to a cusp-like behaviour of the relaxation rate as a function of the magnetic field, at the anticrossing point.

2.8.2. *Phonon-induced electron spin decoherence*

In a Markovian dynamics the decoherence time T_2 is limited by both spin–flip and dephasing processes, though its upper bound is $T_2 \leq 2T_1$. A systematic analysis of phonon-induced spin decay was carried out in [57]. Both the Rashba and Dresselhaus SO interactions were also treated perturbatively. The deformation potential phonons were also considered. For a SO length $\lambda_{SO} = \hbar/m^*\beta$ much larger than the electron orbit size λ, the contribution to the spin–phonon coupling in the Hamiltonian linear in $\lambda/\lambda_{SO} \propto \alpha$, β is due only to a finite Zeeman splitting. For B field in the range $m^*\beta^2 \ll g\mu_B\, B \ll \hbar\omega_0$, the effective Hamiltonian is

$$\mathcal{H}_{\text{eff}} = \frac{1}{2} g\mu_B[\mathbf{B} + \delta\mathbf{B}(t)] \cdot \boldsymbol{\sigma}, \quad \delta\mathbf{B}(t) = 2\mathbf{B} \times \boldsymbol{\Omega}(t), \tag{105}$$

where $\boldsymbol{\Omega}(t) = \langle\psi|[(\hat{L}_d^{-1}\boldsymbol{\xi}), U_{\text{ph}}(t)]|\psi\rangle$, $|\psi\rangle$ is the electron orbital wavefunction, $\hat{L}_d$ is the dot Liouvillian, $\hat{L}_d A = [\mathcal{H}_d, A]$. The vector $\boldsymbol{\xi}$ lies in the two-dimensional dot plane and depends on α, β, and m^*. The most important consequence of (105) is that within first order in the SO coupling parameter there can only be transverse fluctuations of the effective field.

In the case of many uncorrelated scattering events, the expectation values $\langle\mathbf{S}\rangle$ of the spin obeys the Bloch equation [7]

$$\langle\dot{\mathbf{S}}\rangle = \boldsymbol{\omega} \times \langle\mathbf{S}\rangle - \Gamma\langle\mathbf{S}\rangle + \boldsymbol{\Upsilon}, \tag{106}$$

where $\boldsymbol{\omega} = \omega\mathbf{B}/B$, $\omega = g\mu_B\, B/\hbar$. In the Born–Markov approximation, for a generic $\delta\mathbf{B}$ such that $\langle\delta\mathbf{B}\rangle = 0$, the tensor Γ can be expressed in terms of the spectral function

$$J_{ij}(w) = \frac{g^2\mu_B^2}{2\hbar^2} \int_0^\infty \mathrm{d}t\, \langle\delta B_i(0)\delta B_j(t)\rangle e^{-iwt}, \tag{107}$$

and it is diagonal in a frame (X, Y, Z), with Z oriented along $\mathbf{B}$. The symmetric part of Γ is responsible for the decay of the spin components, and it can be expressed just as function of $J_{ij}^{\pm}(w) = \text{Re}[J_{ij}(w) \pm J_{ij}(-w)]$. Here, Γ can be split in two contributions, $\Gamma = \Gamma^r + \Gamma^d$, where Γ^r contains the spectral function $J_{ij}(\omega)$ at the Zeeman frequency ω, and describes spin decay due to emission or absorption of a phonon, whereas Γ^d is due to elastic scattering of spin. The relaxation time T_1 is completely determined by Γ^r, while the

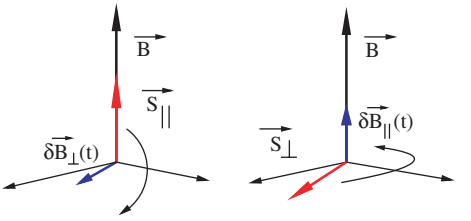

Figure 7. Schematic representation of the relaxation process (left-hand side), due to magnetic field fluctuations $\delta B_\perp(t)$ orthogonal to the applied B field, and of the dephasing process (right-hand side), due to magnetic field fluctuations $\delta B_\parallel(t)$ parallel to the applied B field.

decoherence time T_2 is affected by both Γ^r and Γ^d, the latter describing pure dephasing. In the general case, the solution of (106) yields

$$\frac{1}{T_1} := \Gamma_{ZZ} = \Gamma^r_{ZZ}, \quad \frac{1}{T_2} := \frac{1}{2}(\Gamma_{XX} + \Gamma_{YY}). \tag{108}$$

In many cases the contribution of Γ^r to spin decoherence is negligible, the decoherence rate being determined entirely by Γ^d. However, it turns out that, at first-order perturbation theory in the SO interaction, no dephasing takes place [57]. Owing to the transverse nature of the fluctuations in the magnetic field in the effective Hamiltonian, the tensor Γ^d is identically zero, $\Gamma^d = 0$ (Figure 7 illustrates an intuitive picture of the effect of the longitudinal and the transverse fluctuations). As a result

$$\frac{1}{T_1} = \frac{2}{T_2} = J^+_{XX}(\omega) + J^+_{YY}(\omega). \tag{109}$$

Contributions to the decoherence time T_2 due to pure dephasing arise when two-phonon processes are taken into account in the next order in the electron–phonon interaction [58]. Therefore, if only SO decay mechanisms are taken into account, the decoherence time T_2 for the decay of the transverse component of an electron spin in GaAs quantum dots is $T_2 = 2T_1$.

2.9. *SO interaction for heavy holes*

The electron spin in GaAs quantum dots has been shown to have a long relaxation time, due to inefficient phonon-induced relaxation mechanisms. On the other hand, the decoherence time is mainly dominated by hyperfine-induced decay, owing to the fact that the decay of the longitudinal electron spin component can be strongly suppressed by the application of an external magnetic field. In order to circumvent this problem, the use of hole spins as carriers has been recently proposed. The valence band in III–V semiconductors has a p symmetry, for which the electron has zero probability of being found on the position of the nucleus. According to (65), it follows that the hyperfine interaction between holes and nuclei is strongly suppressed with respect to that of nuclei and conduction band electrons. However, the hole spin relaxation time turns out to be much smaller than that of the electrons by several order of magnitude. The reason for this is due to the fact that, in addition to the SO coupling due to bulk inversion asymmetry and

the structural inversion asymmetry, there is a strong SO coupling between the heavy-hole (HH) and the light-hole (LH) subbands [59].

On the other hand, investigations of hole spin relaxation in quantum dots, exclusively due to SO coupling of LH and HH subbands, have shown that SO coupling between HH and LH is negligible for two-dimensional quantum dots, if the energy splitting between the HH and LH subbands is much larger than the level spacing in these subbands [60,61]. Therefore, other SO mechanisms start to play a significant role in those cases.

In [62], HH spin relaxation was analysed in the presence of Rashba and Dresselhaus SO coupling, as well as SO between HH and LH. From the two-band Kane model, the Hamiltonian for the valence band of III–V semiconductors is given by

$$\mathcal{H}_{\text{bulk}} = \mathcal{H}_{\text{LK}} + \eta \mathbf{J} \cdot \mathbf{\Omega} + \mathcal{H}_{\text{Z}}, \tag{110}$$

where $\mathcal{H}_{\text{LK}}$ is the Luttinger–Kohn Hamiltonian [63], $\eta \propto (E_{\text{g}} + \Delta_{\text{so}})/\Delta_{\text{so}}$, Δ_{so} is the split-off gap energy, and E_{g} is the band gap energy. Here, $\mathbf{J} = (J_x, J_y, J_z)$ are the 4×4 matrices corresponding to spin 3/2, $\Omega_z = P_z(P_x^2 - P_y^2)$, and Ω_x, Ω_y are obtained by cyclic permutations. The last term in (110) $\mathcal{H}_Z = -2\kappa\mu_{\text{B}}\, \mathbf{B} \cdot \mathbf{J} - 2q\mu_{\text{B}}\, \mathbf{B} \cdot \mathcal{J}$ is the Zeeman term for the valence band [64], with κ and q Luttinger parameters [64], and $\mathcal{J} = (J_X^3, J_y^3, J_z^3)$.

In the case of structure inversion asymmetry along the growth direction, due to an asymmetric confinement, there is an additional contribution to the SO interaction, the Bychkov–Rashba term. For the two-band Kane model it is given by [65,66] $\alpha_R(\mathbf{P} \times \mathbf{E}) \cdot \mathbf{J}$, where $\mathbf{E}$ is the effective electric field along the growth direction, and α_R is the Bychkov–Rashba SO coupling constant. We consider a two-dimensional system grown along the [001]-direction. Owing to confinement, the valence band splits into a HH subband, with $J_z = \pm 3/2$, and a LH subband, with $J_z = \pm 1/2$ (see [59,62]), where z is the growth direction. In the case of large splitting Δ between HH and LH, the properties of the two subbands can be described separately, the $J_z = \pm 3/2$ subspace for HHs and the $J_z = \pm 1/2$ subspace for LHs, using only the 2×2 submatrices. The HHs submatrices have the properties $\tilde{J}_x = \tilde{J}_y = 0$, and $\tilde{J}_z - (3/2)\sigma_z$ (see [67]). For low temperatures only the HH subband is significantly occupied. Considering only HHs, starting from the bulk Hamiltonian (110) with the addition of the Bychkov–Rashba term, at the lowest order in perturbation theory [68], it is possible to derive an effective Hamiltonian for a quantum dot with lateral confinement potential $U(x, y)$

$$\mathcal{H} = \frac{1}{2}\left(P_x^2 + P_y^2\right) + U(x, y) + \mathcal{H}_{\text{SO}}^{\text{HH}} - \frac{1}{2} g_{zz} \mu_{\text{B}} B_z \sigma_z, \tag{111}$$

where m is the effective HH mass, g_{zz} is the component of the g factor tensor along the growth direction, and the effect of an in-plane component of the magnetic field can be neglected due to strong anisotropy in the HH g factor, $g_{\parallel} \ll g_{zz}$ (see [67]), as well as the orbital effect of the in-plane magnetic field, as long as $B_{\parallel} \ll c\hbar/eh^2$, h being the height of the quantum dot. Here $\mathbf{P} = \mathbf{p} + (|e|/c)\mathbf{A}(\mathbf{r})$, with $\mathbf{A}(\mathbf{r}) = (-yB_z/2, xB_z/2, yB_x - xB_y)$, and

$$\mathcal{H}_{\text{SO}}^{\text{HH}} = i\alpha\sigma_+ P_-^3 + \beta P_- P_+ P_- \sigma_+ + \gamma B_- P_-^2 \sigma_+ + \text{h.c.} \tag{112}$$

The first two terms in the SO interaction for HHs consist in the Rashba and Dresselhaus contribution, respectively, while the last term (γ) describes the combination of two effects: the orbital coupling via non-diagonal elements in the Luttinger–Kohn Hamiltonian ($\propto P_{\pm}^2$), taken into account perturbatively, and magnetic coupling via non-diagonal

elements in the Zeeman term, ($\propto B_{\pm}$) (see [64]). This new SO term is unique for HHs [69]. In (112) $\alpha - 3\gamma_0\alpha_R\langle E_z\rangle/2m_0\Delta$, $\beta = -3\gamma_0\eta\langle P_z^2\rangle/2m_0\Delta$, $\gamma = 3\gamma_0\kappa\mu_B/m_0\Delta$, $\sigma_{\pm} = (\sigma_x \pm \sigma_y)/2$, $P_{\pm} = P_x \pm P_y$, and $B_{\pm} = B_x \pm B_y$, m_0 is the free electron mass, γ_0 is the Luttinger parameter [64], $\langle E_z\rangle$ is the average electric field, and Δ is the splitting between HH and LH subbands, $\Delta \propto h^{-2}$, where h is the quantum-dot height. For a quantum dot with characteristic lateral size l, the ratio $\langle \mathcal{H}_{SO}^{el}\rangle/\langle \mathcal{H}_{SO}^{HH}\rangle \propto (l/h)^2$. Therefore, for flat quantum dots, $l/h \gg 1$, the SO coupling for HHs can be weaker than that for conduction electrons [54,57]. This observation has also been confirmed experimentally [70], where the spin relaxation rate for heavy holes was shown to be comparable to that of electrons.

For vanishing SO interaction, the spectrum of the Hamiltonian (111) for a parabolic lateral confinement can be found through a canonical transformation [71], and it is the Fock–Darwin spectrum split by the Zeeman term [72,73]. For $U(x, y) = m\omega_0^2(x^2 + y^2)/2$, defining $\Omega = \sqrt{\omega_0^2 + \omega_c^2/4}$, with $\omega_c = |e|B_z/cm$ being the cyclotron frequency, the spectrum of the Hamiltonian (111) is given by

$$E_{k,l,s} = \hbar\Omega(2k + 1) + \hbar\left(\Omega - \frac{\omega_c}{2}\right)\ell - \hbar\omega_Z s/3, \tag{113}$$

where $s = \pm 3/2$, k is a level quantum number (in the case $\omega_0 \to 0$ it becomes the Landau-level quantum number), and ℓ is the z-component of the orbital angular momentum, with $-\ell \le k$ and $k \ge 0$. Defining $n_1 = k + l$, $n_2 = k$, and $\omega_{1,2} = \Omega \pm \omega_c/2$, the spectrum can be brought in the form $E_{n_1,n_2} = \hbar\omega_1(n_1 + 1/2) + \hbar\omega_2(n_2 + 1/2) - \hbar\omega_Z s_z$, and the orbital part of the wavefunction is therefore given by the product of two independent harmonic oscillator wavefunctions. In the literature an other representation is often used, in which the principal-level quantum number is introduced, $n = 2k + l$, and the quantum number labelling the levels are n, ℓ, s, with the spectrum given by $E = \hbar\Omega(n + 1) - \hbar\omega_c\ell/2 - \hbar\omega_Z s/3$, with the restriction $|\ell| \le n$.

In the framework of perturbation theory [54], it can be seen that the corrections to the spectrum due to $\mathcal{H}_{SO}^{HH}$ arise only at second order, and the SO interaction influences the wavefunctions more strongly than the energy levels. Here, $\mathcal{H}_{SO}^{HH}$ couples the two lowest states $|0, \pm 3/2\rangle$ to the states with opposite spin orientations and different orbital momenta $|l, \mp 3/2\rangle$. The different SO interactions appearing in (112) differ by symmetry in the momentum space [54,74], and thus produce a mixing of spin-up and spin-down states, with resulting avoided crossings between energy levels. We mention here that the levels cross only if $g_{zz} > 0$, therefore in the case of GaAs ($g_{zz} > 0$) quantum dots an anticrossing appears, with consequent peak of the relaxation rate as a function of the magnetic field, at the point where the crossing takes place, while for InAs ($g_{zz} < 0$) quantum dot no crossing and no cusp-like behaviour of the relaxation rate appear. The SO mixing of the HH states provides a mechanism of transitions between the states $|0, \pm 3/2\rangle$ through emission or absorption of an acoustic phonon, that ultimately represents the main source of relaxation and decoherence for HHs [62].

Taking into account piezoelectric and deformation potential phonons, the potential of a phonon with mode $\mathbf{q}\alpha$ is given by [22,68]

$$U_{\mathbf{q}\alpha}^{ph} = \sqrt{\frac{\hbar}{2\rho s_\alpha q V}} F(q_z) e^{i\mathbf{q}_\parallel \cdot \mathbf{r}} \times \left\{ w A_{\mathbf{q}\alpha} + i\left[\left(a + \frac{b}{2}\right)\mathbf{q} \cdot \mathbf{d}^{\mathbf{q}\alpha} - \frac{3}{2} b q_z d_z^{\mathbf{q}\alpha}\right]\right\}, \tag{114}$$

where $\mathbf{q}_\parallel = (q_x, q_y)$, a and b are constants of the deformation potential, V the quantum dot volume, s_α the sound velocity, ρ the crystal mass, $A_{\mathbf{q}\alpha}$ the effective piezoelectric modulus, $\mathbf{d}_{\mathbf{q}\alpha}$ the phonon polarization vector, $F(q_z)$ the form factor, which is determined by the spread of the electron wavefunction in the z direction.

2.9.1. *Spin decoherence and relaxation for HHs*

For a single-particle quantum dot, in which a HH can occupy one of the low-lying levels, some energy levels with same spin orientation cross, with increasing B, the upper Zeeman-split ground-state level. Therefore, we consider an n-level system, in which the first $n-1$ levels have same spin orientation, while the n-level has opposite spin. In the context of Bloch–Redfield theory, the Bloch equations for the spin motion of a heavy hole in such a system are given, in the interaction picture, by

$$\langle \dot{S}_z \rangle = (S_T - \langle S_z \rangle)/T_1 - R(t), \tag{115}$$

$$\langle \dot{S}_x \rangle = -\langle S_x \rangle/T_2, \quad \langle \dot{S}_y \rangle = -\langle S_y \rangle/T_2, \tag{116}$$

where $R(t) = W_{n1}\rho_{nn}(t) + \sum_{i=1}^{n-1} W_{ni}\rho_{ii}(t)$, $\rho(t)$ is the density matrix, W_{ij} is the transition rate from state j to state i, S_T is a constant that takes the value $\langle S_z \rangle$ in the thermodynamic equilibrium $R(t) = 0$. The spin motion involves $n-1$ states and therefore there are $n-1$ transition rates. It can be shown, by solving the master equation, that for low temperature $\hbar q_\alpha \gg k_B T$, $R(t) \approx 0$ and phonon absorption is strongly suppressed. In this case only one relaxation rate contributes to the relaxation time T_1, and the relaxation time T_1 and decoherence time T_2 are given by

$$\frac{1}{T_1} = W_{n1}, \quad \frac{1}{T_2} = \frac{1}{2T_1}. \tag{117}$$

The relaxation rates for the different SO interactions are [62]

$$\frac{1}{T_1^{\mathrm{BR}}} \propto \alpha^2 \omega_z^7 \left(\frac{\omega_+^3}{3\omega_+ + \omega_Z} - \frac{\omega_-^3}{3\omega_- - \omega_Z} \right)^2, \tag{118}$$

$$\frac{1}{T_1^{\mathrm{D}}} \propto \beta^2 \omega_z^3 \left(\frac{\omega_+}{\omega_+ + \omega_Z} - \frac{\omega_-}{\omega_- - \omega_Z} \right)^2, \tag{119}$$

$$\frac{1}{T_1^{\parallel}} \propto \gamma^2 B_\parallel^2 \omega_z^5 \left(\frac{\omega_+^2}{2\omega_+ + \omega_Z} + \frac{\omega_-^2}{2\omega_- - \omega_Z} \right)^2, \tag{120}$$

where $\omega_\pm = \Omega \pm \omega_c/2$, $\Omega = \sqrt{\omega_0^2 + \omega_c^2/4}$ $\omega_c = |e|B/mc$ is the cyclotron frequency, $\omega_Z - g_{zz}\mu_B B_z$, and $B_\parallel - \sqrt{B_x^2 + B_y^2}$. In contrast to the case of conduction electrons [57], no interference takes place for HHs, and the rates originating from different SO terms sum up, giving the total spin relaxation rate $1/T_1 = 1/T_1^{\mathrm{BR}} + 1/T_1^{\mathrm{D}} + 1/T_1^{\parallel}$. For the case of GaAs quantum dots the crossing between levels takes place at $\omega_Z = \omega_-$, $2\omega_-$, and $3\omega_-$, and the strong spin mixing arising causes cusp-like peaks in the relaxation rate as a function of the external field B.

2.9.2. *Electric dipole spin resonance for HHs*

The possibility of coherent manipulating the spins is of great importance for spintronics and quantum computation. In case of conduction electron spin-based electronics, such control is obtained by the ESR. Through the application of short resonant microwave pulses, arbitrary superpositions of spin-up and spin-down states can be created. Therefore, ESR provides a necessary tool for single-qubit operations, an essential requirement for quantum computation. In Rabi oscillations and spin echo experiments [75], that are based on this technique, the ESR signal can be detected by measuring the absorption of radiofrequency (rf) power [76]. ESR methods involve magnetic-dipole transitions induced by oscillating magnetic fields. In addition, an alternative is provided by alternating electric fields, which give rise to electric-dipole spin resonance (EDSR).

Considering the SO coupling as a perturbation, at first order the two states corresponding to the Zeeman-split ground state $|\pm\rangle$ are given as a superposition of few unperturbed Fock–Darwin states and spin states, $|n,\ell\rangle|s\rangle$, with $n\in\mathbb{N}$ the principal quantum number, $|\ell|\leq n$ the azimuthal quantum number, and $s=\pm 3/2$ as introduced in Section 2.9 (for details see [69]). In the case of HHs it can be shown [69] that magnetic-dipole transition ($\Delta_n=0, \Delta\ell=0$, and $\Delta s=\pm 1$) are forbidden, while, because of SO coupling between states with different orbital momenta and opposite spin orientations, $|0,0,\pm 3/2\rangle$ and $|1,\pm 1,\mp 3/2\rangle$, electric-dipole transitions ($\Delta_n=\pm 1, \Delta\ell=\pm 1$, and $\Delta s=0$) are most likely to occur. HHs are thus affected by the oscillating electric field component, but not by the magnetic field component. EDSR for HHs appears to be an essential tool for the control of spin dynamics and for the determination of important parameters, as the effective g factor, effective mass m, SO coupling constants, and spin relaxation and decoherence time.

The Hamiltonian for the interaction of HHs with a circularly polarized electric field, that rotates with frequency ω in the XY plane, $\mathbf{E}(t)=E(\sin\omega t,-\cos\omega t,0)$, is given by $\mathcal{H}^{\mathrm{E}}=(|e|E/m\omega)(P_x\cos\omega t+P_y\sin\omega t)$. The coupling between the states $|\pm\rangle$ is given by $\langle+|\mathcal{H}^{\mathrm{E}}|-\rangle=d_{\mathrm{SO}}Ee^{-i\omega t}$, where

$$d_{\mathrm{SO}}=(|e|l/2\omega)\left(\beta_1^+\omega_+ +\beta_1^-\omega_-\right), \tag{121}$$

is an effective dipole moment of a HH and it depends on Dresselhaus SO coupling constant, perpendicular magnetic field $B_\perp$, lateral quantum dot size, and frequency ω of the rf electric field. For details on $\beta_1^\pm$ and l see [69].

The effective master equation for the density matrix ρ_{nm}, in the context of Bloch–Redfield theory, takes the form of Bloch equations, with a rf field detuned from ω_Z, $\delta_{\mathrm{rf}}=\omega_Z-\omega$, Larmor frequency $2d_{\mathrm{SO}}E/\hbar$, spin relaxation time $T_1=1/(W_{+-}+W_{-+})$, W_{nm} being the transition rate from state m to state n, decoherence time $T_2=2T_1$, and equilibrium value of ρ_z without rf field given by $\rho_z^T=(W_{+-}-W_{-+}T_1)$.

The coupling energy between a HH and an oscillating field is given by

$$\left\langle\mathcal{H}^{\mathrm{E}}(t)\right\rangle=-\mathbf{d}_{\mathrm{SO}}\cdot\mathbf{E}(t), \tag{122}$$

where $\mathbf{d}_{\mathrm{SO}}=d_{\mathrm{SO}}(i\rho_{-+}-i\rho_{+-}+\rho_{-+},0)$ is the dipole moment of a HH. The rf power $P=-d\langle\mathcal{H}^{\mathrm{E}}(t)\rangle/\mathrm{d}t=-\omega d_{\mathrm{SO}}E\rho_-$ absorbed by a HH spin system in a stationary state is given by [77]

$$P=\frac{2\omega(d_{\mathrm{SO}}E)^2T_2\rho_z^T/\hbar}{1+\delta_{\mathrm{rf}}^2T_2^2+(2d_{\mathrm{SO}}E/\hbar)^2T_1T_2}. \tag{123}$$

The dependence of P on perpendicular magnetic field $B_\perp$ and frequency of the oscillating field ω shows three resonances and one resonant dip. The first resonance corresponds to the Zeeman energy of the HH $B_\perp = \hbar\omega/g_{\perp}\mu_B$, the second to the first anticrossing between the unperturbed $E_{0,-3/2}$ and $E_{1,3/2}$ energy levels, $\omega_Z - \omega_-$, the third resonance reflects the peak in the decoherence rate T_2^{-1} due to an applied in-plane magnetic field at the second anticrossing $\omega_Z = 2\omega_-$. The resonant dip takes place at zero dipole moment.

The study of the position of these resonances allows us to determine $g_\perp$, m, and ω_0, while the shape and height provide information about the SO interaction constants α, β, and SO interaction strength due to in-plane magnetic field. In addition, it is possible to extract information about the dependence of spin relaxation and decoherence times on $B_\perp$.

3. Superconducting qubits

In addition to spin qubits in semiconductor quantum dots, superconducting qubits represent a category of promising candidates for the implementation of artificial two-level systems as qubits. The key ingredient in building superconducting qubits is the strong nonlinearity of the current–voltage relation of a Josephson junction. The ability to isolate few charge states on a superconducting island, together with the possibility to let them interact through the coherent tunnelling of Cooper pairs through the junction, represent a promising way to control and operate a purely quantum system (charge qubits). The flux quantization together with the strong non-linear potential, arising from the current–voltage relation, provide a way to isolate few current states and coherently superimpose them (flux qubit).

Superconducting qubits can be included in a more general framework of quantum circuits, that are electrical circuits showing, in the low-temperature regime, quantum behaviour, including quantum fluctuations [78]. In this context, as LC-circuits provide electrical realizations of quantum harmonic oscillators, showing a linear current–voltage relation, Josephson junctions provide a full anharmonic counterpart, showing a more rich spectrum, with groups of few energy levels well separated from higher bands of the spectrum.

Several types of superconducting qubits based on Josephson junctions have been so far theoretically proposed and experimentally realized (for comprehensive reviews see [79,80]). Apart from the particular design of each device, superconducting qubits can be classified according to the working regime of the Josephson elements that constitute the circuit. Every Josephson junction is characterized by two features: (i) a critical current I_c, that is the maximal supercurrent that can flow through the junction; and (ii) an effective capacitance that the two superconducting faces have to accumulate charge. Together the energy associated with the critical current $E_J = I_c\Phi_0/2\pi$ and the charging energy of the associated capacitance $E_C = e^2/2C$ are the two most important parameters that determine the qubit working regime. For $E_C \gg E_J$ the charge degrees of freedom are well defined and the number of Cooper pairs in a superconducting island is a well-defined quantum number. Qubits that work in this regime are called charge qubits [81–90]. In contrast, for $E_C \ll E_J$ flux degrees of freedom have well-defined values, and current states are well defined. Qubits that operate in this regime are called flux qubits [91–94]. Other realizations of superconducting qubits, for different values of the ratio E_J/E_C, and many kinds of

possible accessible parameter regimes have been explored. The so-called phase qubit [95,96] operates in the flux regime, but is completely represented by the superconducting phase, and it has no magnetic flux or circulating current associated. The quantronium [97], consists of a split Cooper pair box arranged in a loop containing an extra large junction for the read-out.

Experimental observations of Rabi oscillations in driven quantum circuits have shown several periods of coherent oscillations, confirming, to some extent, the validity of the two-level approximation and possibility to coherently superimpose the computational two states of the system. Nevertheless, the unavoidable coupling to a dissipative environment surrounding the circuit represents a source of relaxation and decoherence that limit the performance of the qubit for quantum computation tasks. Therefore, for the implementation of superconducting circuits as quantum bits, it is necessary to understand the way the system interacts with the environmental degrees of freedom, and to reduce their effect, if possible.

3.1. *The quantronium*

A very successful realization of a superconducting qubit is the so-called quantronium [11]. Its circuit consists in a split Cooper pair box (CPB), constituting the qubit, and a hysteretic current-biased Josephson junction that is used for the readout. The main superconducting loop is interrupted by two adjacent tunnel junctions, having Josephson energies $E_J/2(1 \pm d)$, where d, that parametrizes the asymmetry of the two junctions, is made as small as possible, and by a much bigger readout junction. The superconducting island of the CPB is located between the two small junctions an its charge energy is $E_C = (2e)^2/2C$, with C the total capacitance to the ground. The island is voltage bias and a magnetic flux Φ_{ext} is applied through the loop. The working regime of the qubit is determined by the parameters $N_g = C_g V$, with C_g the gate capacitor, by $\phi = 2\pi\Phi_{\text{ext}}/\Phi_0$, with the superconducting flux quantum $\Phi_0 = h/2e$, and by the bias current I_B. The quantum Hamiltonian of the total system is

$$\mathcal{H} = \mathcal{H}_{\text{CPB}} + \mathcal{H}_{\text{readout}}, \tag{124}$$

$$\mathcal{H}_{\text{CPB}} = E_C(\hat{N} - N_g)^2 - E_J \cos(\hat{\delta}/2)\cos\hat{\theta} + dE_J \sin(\hat{\delta}/2)\sin\hat{\theta}, \tag{125}$$

$$\mathcal{H}_{\text{readout}} = \mathcal{E}_C\hat{q}^2 - \mathcal{E}_J \cos\hat{\gamma} - \Phi_0 I_B\hat{\gamma}/2\pi, \tag{126}$$

where $\hat{N}$ is the number operator of the excess Cooper pair on the island, $\hat{\gamma}$ is the superconducting phase operator across the readout junction, $\hat{\theta}$ and $\hat{q}$ their respective conjugate variables, $\hat{\delta} = \hat{\gamma} + \phi$, and $\mathcal{E}_C$ and $\mathcal{E}_J$ are the charging and Josephson energies of the readout junction. The quantronium works in a regime in which $E_C \approx E_J$, therefore neither the excess Cooper pair $\hat{N}$ nor the superconducting phase $\hat{\theta}$ are well-defined quantum numbers. Nevertheless, for a large range of bias conditions, determined by N_g and $\delta \approx \phi + \arcsin(I_B/I_0)$, the energy spectrum of the CPB is anharmonic, and the low-temperature dynamics of the system is well described in the two-level approximation, with $|0\rangle$ and $|1\rangle$ the two eigenstates of the Hamiltonian, with energy splitting $\hbar\omega_{01}(N_g, \delta)$, in an

eigenbasis that depends on (N_g, δ). In particular, there exists an optimal point $(\delta = 0, N_g = 1/2)$ for which $\partial\omega_{01}/\partial N_g = \partial\omega_{01}/\partial\delta = 0$, and the qubit results immune at first order to fluctuations of the bias parameters.

3.1.1. *Noise affecting the control parameters*

Many sources of noise in the environment surrounding the qubit affect its dynamics, inducing decoherence, that can manifest themselves as energy exchange between the qubit and the noise source, and as random dephasing between the two states of the system. Contributions of charge noise due to finite impedance Z_g of the voltage source $\kappa_g V_g$ coupled to $\hat{N}$, in the weak-coupling limit $\kappa_g \ll 1$, is quantified by the spectral density [11]

$$S_{N_g}(\omega) \approx \kappa_g^2 \frac{\hbar^2 \omega}{E_C^2} \frac{\mathrm{Re}[Z_g(\omega)]}{R_k} \left[1 + \coth\left(\frac{\hbar\omega}{2k_B T} \right) \right], \tag{127}$$

with $R_k = h/e^2$, and the background charge noise dominates at low frequency. An analogous analysis shows that noise in the superconductive phase due to the admittance in parallel with the Josephson readout junction is characterized by a similar spectral density.

Fluctuations of the Josephson energies of the two small junctions are empirically described by a noise source with a $1/f$ spectral density. Critical current fluctuations are thought to be due to atomic defects in the oxide barrier of the tunnel junctions. These defects are usually well described as two-level fluctuators (TLFs), that switch between two states, and have a spectral density that follows approximately a $1/f$ law. The fact that the distribution in energy splitting of these fluctuators can extend above the qubit transition frequency, supported by the observation of avoided level crossing in the spectroscopic qubit line, suggests that TLFs located in the tunnel junctions can lead to dephasing due to low-frequency E_J noise, and can play a significant role in the relaxation of the quantronium. Collections of microscopically charged TLFs, partially located in the substrate, partially in the oxide layer covering the electrodes, and partially in the oxide barriers of the Josephson junctions, can also produce background charge noise, whose spectral density follows a $1/f$ law.

3.1.2. *Decoherence due to 1/f noise in the quantronium*

In [11] an extensive treatment of the theory of $1/f$ noise-induced decoherence for qubits is carried on. A spectral density with a low-frequency ω_{ir} and high-frequency ω_c cutoff is chosen, $S_X(\omega) = A/|\omega|$, with $\omega_{ir} < |\omega| < \omega_c$, and several scenarios are analysed. For $1/f$ noise at times $t \ll 1/\omega_{ir}$ the Ramsey decay is dominated by the quasistatic contribution, $\omega < 1/t$. The pure dephasing of the quantronium is dominated by low frequencies $\omega \ll 1/t$, characteristic of a noise spectral density that is strongly peaked at low frequencies. In the static approximation [98,99], for $\omega \ll 1/t$, $\mathrm{sinc}(\omega t/2) \approx 1$ ($\mathrm{sinc}\, x = \sin x/x$), and the decay law (44) reduces to a Gaussian

$$f_{z,R}(t) = \exp\left(-\frac{t^2}{2} D_{X,z}^2 \sigma_X^2 \right), \tag{128}$$

with $\sigma_X^2 = \int_{-\infty}^{\infty} d\omega S_X(\omega)$, that for the case of interest of $1/f$ noise reduces to $\sigma_X^2 = 2A\ln(\omega_c/\omega_{ir})$, valid if $D_{X,z}^2\sigma_X^2 A\ln(\omega_c/\omega_{ir}) \gg \omega_c$, whereas for $t > 1/\omega_c$ it reduces to $\sigma_X^2 = A\ln(1/\omega_{ir}t)$, the so-called quasistatic contribution

$$f_{z,R}(t) = \exp\left[-t^2 D_{X,z}^2 A\left(\ln\frac{1}{\omega_{ir}t} + O(1)\right)\right]. \tag{129}$$

In general, in the static approximation, valid for static and quasistatic noise with distribution function $P(\delta X)$, the Ramsey decay is given by the Fourier transform of $P(\delta X)$,

$$f_{z,R}^{\text{stat}}(t) = \int d(\delta X)\, P(\delta X) e^{iD_{X,z}\delta X t}. \tag{130}$$

Concerning the echo decay given by (46), the quasistatic contribution of $1/f$ noise, valid for $t \ll 1/\omega_{ir}$ yields

$$f_{z,E}(t) = \exp(-t^2 D_{X,z}^2 A\ln 2). \tag{131}$$

Whereas for low ω_c it yields

$$f_{z,E}(t) = \exp\left(-\frac{A}{32} D_{X,z}^2 \omega_c^2 t^4\right). \tag{132}$$

3.1.3. *Decoherence at optimal point*

As already defined, the optimal point is defined as the point in the space of external parameters that enter $\hbar\omega_{01}$ for which $D_{X,y} = \partial\omega_{01}/\partial X = 0$. This way, the coherence time T_2 reaches its upper bound given by the relaxation time T_1, $T_2 = 2T_1$ to first order in perturbation theory. It can happen, though, that, due to a singularity at low frequencies, the second-order contribution of the longitudinal noise has to be taken into account [11,98,99]. The decay of the Ramsey and the echo signals are therefore given by

$$f_z(t) = \left\langle \exp\left(i\frac{1}{2}\frac{\partial^2\omega_{01}}{\partial X^2}\int_0^t d\tau\chi(\tau)\delta x^2(\tau)\right)\right\rangle, \tag{133}$$

with $\chi(\tau) = 1$ for the Ramsey signal, and $\chi(\tau < t/2) = -1$ and $\chi(\tau > t/2) = 1$ for the echo signal.

The Ramsey decay for $1/f$ noise with $\omega_c t \gg 1$ can be approximated by the product of a quasistatic low-frequency ($\omega < 1/t$) and a high-frequency ($\omega > 1/t$) contributions, $f_{z,R}(t) = f_{z,R}^{lf}(t) f_{z,R}^{hf}(t)$, given by [11,98,99]

$$f_{z,R}^{lf}(t) = \frac{1}{\sqrt{1 - i(\partial^2\omega_{01}/\partial X^2)\sigma_X^2 t}}, \tag{134}$$

$$\ln f_{z,R}^{hf}(t) \approx -t\int_{\sim 1/t}^{\infty}\frac{d\omega}{2\pi}\ln\left(1 - 2\pi i\frac{\partial^2\omega_{01}}{\partial x^2}S_X(\omega)\right). \tag{135}$$

In the quasistatic approximation, $\omega_c < 1/t$, for quasistatic noise with distribution $P(\delta X)$, the Ramsey decay is given by the Fresnel-type transform

$$f_{z,R}^{st}(t) = \int \mathrm{d}(\delta X)\, P(\delta X) e^{i(\partial^2\omega_{01}/\partial 2X^2)\delta X^2 t}. \tag{136}$$

For a Gaussian distribution $P(\delta X) = \exp(-\delta X^2/2\sigma_X^2)$ and $1/f$ noise, the Ramsey decay reduces to the low-frequency contribution (134), with $\sigma_X^2 = 2A\ln(1/\omega_{ir}t)$, whereas the echo decay follows

$$f_{z,E}(t) = \frac{1}{\sqrt{1 + (\partial^2\omega_{01}/\partial X^2)^2\sigma_X^2 A\omega_c^2 t^4/16}}. \tag{137}$$

3.2. *The superconducting flux qubit: the Delft design*

In the working regime $E_J \gg E_C$, three types of circuit designs have been proposed, the Delft flux qubit [91,94], the IBM flux qubit [100], and its gradiometer variety [101]. The phase qubit operates in the same regime, see Section 3.3.

The flux qubit realized at Delft [94] consists of a superconducting loop interrupted by three Josephson junctions (see Figure 8). The strong flux regime $E_J \gg E_C$ allows flux quantization of the flux through the loop, $\varphi_1 + \varphi_2 + \varphi_3 = 2\pi n$. Therefore, only two of the three phases of the junctions play the role of dynamical variables. For sufficiently low temperatures, in the small loop inductance limit, the inductive degree of freedom associated with the loop is frozen, and the effective potential $U(\varphi)$ is periodic and shows a double well shape. The charging energy of the system here plays the role of the kinetic energy, and the Hamiltonian is written as

$$\mathcal{H} = -2e^2\nabla_{\boldsymbol{\varphi}}^T\mathcal{C}^{-1}\nabla_{\boldsymbol{\varphi}} + \left(\frac{\Phi_0}{2\pi}\right)^2 U(\boldsymbol{\varphi}). \tag{138}$$

The lowest energy states are two flux states localized in the two well minima φ_L and φ_R, and they correspond to clockwise and counter-clockwise circulating currents in the loop, $|L\rangle$ and $|R\rangle$, encoding the logical $|0\rangle$ and $|1\rangle$ states of the qubit. Tunnelling through the

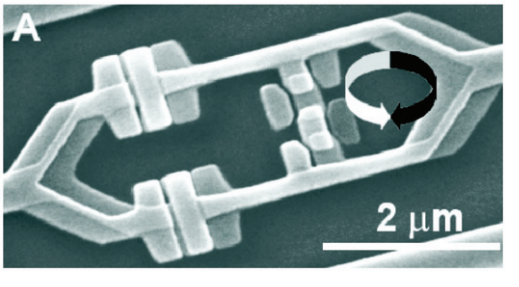

Figure 8. Scanning electron micrograph of the Delft flux qubit (small loop with three Josephson junctions) and attached SQUID (large loop). From [94]. © 2000 Reprinted with permission from AAAS.

potential barrier between the wells lifts the degeneracy between the two current states, giving rise to a splitting $\Delta = \langle L|\mathcal{H}|R\rangle$ between the lowest states of the system, which become the symmetric and antisymmetric superpositions of the current states. An external bias flux can create asymmetry in the double well, $\epsilon = \langle L|\mathcal{H}|L\rangle - \langle R|\mathcal{H}|R\rangle$. The qubit Hamiltonian written in the $\{|L\rangle, |R\rangle\}$ basis takes the form

$$\mathcal{H} = \frac{\Delta}{2}\sigma_x + \frac{\epsilon}{2}\sigma_z. \tag{139}$$

3.2.1. *Markovian dynamics due to dissipative circuitry*

The regime of working of flux qubits, in which the charging energy is much smaller than the Josephson energy, $E_C \ll E_J$, makes the flux qubits substantially insensitive to background charge fluctuations. Still, however, other mechanisms can affect their phase coherence and in order to implement them as building blocks for quantum computation schemes, it is necessary to understand which sources of decoherence affect the short-time dynamics of flux qubits and reduce their effect as much as possible.

Several sources of dissipation for flux qubits have been discussed throughout the literature [102], background charge fluctuations ($\tau_\varphi \approx 0.1$s), as well as quasiparticle tunnelling in the superconductor with a non-vanishing subgap conductance ($\tau_\varphi \approx 1$ms). Nuclear spins in the substrate have also been considered as a possible source of dissipation. The static random magnetic field produced by the nuclear spins may induce shifts in qubit frequencies, but no dephasing is expected until a typical nuclear relaxation time, which can be very long, up to minutes, due to the slow dynamics of nuclear spins.

However, the most efficient source of dissipation for flux qubits is represented by fluctuations in the external circuit that produce fluctuating magnetic fluxes through the loop. The coupling of flux degrees of freedom of the qubit to the dissipative environmental elements is well described in the graph formalism described in [100]. In the Born–Markov approximation, it can be shown that the Redfield tensor, written in the eigenbasis $\{|n\rangle\}$ of $\mathcal{H}_S$, is entirely determined by

$$\mathrm{Re}\,\Gamma^{(+)}_{lmnk} = (\mathbf{m}\cdot\boldsymbol{\varphi})_{lm}(\mathbf{m}\cdot\boldsymbol{\varphi})_{nk} J(|\omega_{nk}|)\frac{e^{-\beta\omega_{nk}/2}}{\sinh\beta|\omega_{nk}|/2}, \tag{140}$$

$$\mathrm{Im}\,\Gamma^{(+)}_{lmnk} = -(\mathbf{m}\cdot\boldsymbol{\varphi})_{lm}(\mathbf{m}\cdot\boldsymbol{\varphi})_{nk} J(|\omega_{nk}|)\frac{2}{\pi}P\int_0^\infty \mathrm{d}\omega\,\frac{J(\omega)}{\omega^2-\omega_{nk}^2} \tag{141}$$

$$\times\left(\omega - \omega_{nk}\coth\frac{\beta\omega}{2}\right), \tag{142}$$

where $\beta = k_B T$ and the $\mathbf{m}\cdot\boldsymbol{\varphi}$ appears in the Hamiltonian for the system–bath coupling, $\mathbf{m}$ being related to the topology of the dissipative circuitry.

In the two-level approximation, the rates for transitions from the two-level subspace to higher states can be neglected, and (140) and (142) simplify and the dynamics of the 2×2 density matrix of the system can be cast in the form of Bloch equations for the dynamics of a pseudo-spin 1/2. In this framework the relaxation matrix contains just two rates, T_1^{-1} and

T_2^{-1} for the decay of the longitudinal and transverse pseudo-spin component, respectively. The latter, in turn, is limited by relaxation time T_1 and pure dephasing time T_ϕ, $1/T_2 = 1/2T_1 + 1/T_\phi$, and the two rates are given by [100]

$$\frac{1}{T_1} = 4|\langle 0|\mathbf{m}\cdot\boldsymbol{\varphi}|1\rangle|^2 J(\omega_{01})\coth\frac{\omega_{01}}{2k_{\mathrm{B}}T}, \tag{143}$$

$$\frac{1}{T_\phi} = |\langle 0|\mathbf{m}\cdot\boldsymbol{\varphi}|0\rangle - \langle 1|\mathbf{m}\cdot\boldsymbol{\varphi}|1\rangle|^2\frac{J(\omega)}{\omega}\bigg|_{\omega\to 0} 2k_{\mathrm{B}}T. \tag{144}$$

Typically, T_ϕ can be made to diverge for an appropriate choice of external fluxes such that $\langle 0|\mathbf{m}\cdot\boldsymbol{\varphi}|0\rangle = \langle 1|\mathbf{m}\cdot\boldsymbol{\varphi}|1\rangle$. However, this divergence is not expected to show up experimentally, since it will be cutoff by other mechanisms.

The two lowest energy states, eigenstates of the Hamiltonian (139), are given by

$$|0\rangle = \frac{1}{\sqrt{2}}\left(\sqrt{1+\frac{\epsilon}{\omega_{01}}}|L\rangle + \sqrt{1-\frac{\epsilon}{\omega_{01}}}|R\rangle\right), \tag{145}$$

$$|1\rangle = \frac{1}{\sqrt{2}}\left(\sqrt{1-\frac{\epsilon}{\omega_{01}}}|L\rangle - \sqrt{1+\frac{\epsilon}{\omega_{01}}}|R\rangle\right), \tag{146}$$

where $\omega_{01} = \sqrt{\epsilon^2+\Delta^2}$. Approximating the localized flux states $|L\rangle$ and $|R\rangle$ as Gaussians centred in the minima of the double well, the relaxation rate T_1^{-1} and the pure dephasing rate T_ϕ^{-1} are given by

$$\frac{1}{T_1} \approx \left(\frac{\Delta}{\omega_{01}}\right)^2 |\mathbf{m}\cdot\Delta\boldsymbol{\varphi}|^2\left(1+\frac{S^2}{2}\right)^2 J(\omega_{01})\coth\frac{\omega_{01}}{2k_{\mathrm{B}}T}, \tag{147}$$

$$\frac{1}{T_\phi} \approx \left(\frac{\epsilon}{\omega_{01}}\right)^2 |\mathbf{m}\cdot\Delta\boldsymbol{\varphi}|^2\left(1+\frac{S^2}{2}\right)^2 \frac{J(\omega)}{\omega}\bigg|_{\omega\to 0} 2k_{\mathrm{B}}T, \tag{148}$$

where $S = \langle L|R\rangle$ is the overlap between the two Gaussians. The vector $\Delta\varphi$ connects the two minima of the double well. These relation are valid in the Markov limit and in the Born approximation, where the system–bath interaction is considered only at first order. By inspection of the previous formula it is clear that a symmetric double well potential, for which $\epsilon = 0$, let the dephasing time to diverge. This is realized for a value of the external applied magnetic flux $\Phi_{\mathrm{ext}} = \Phi_0/2$, being $\epsilon \propto (\Phi_{\mathrm{ext}}/\Phi_0 - 1/2)$. Moreover, for $\mathbf{m}\cdot\Delta\boldsymbol{\varphi} = 0$ the environment is decoupled from the system, and both the relaxation and dephasing time diverge.

In [100] an estimate of the leakage rate due to transition from the qubit states $k = 0, 1$ to higher energy levels $n = 2, 3, \ldots$ outside the qubit subspace can be quantified from (140) and (142),

$$\frac{1}{T_{L,k}} = 4\sum_n |\langle n|\mathbf{m}\cdot\boldsymbol{\varphi}|k\rangle|^2 J(\omega_{kn})\coth\frac{\omega_{kn}}{2k_{\mathrm{B}}T}. \tag{149}$$

In the regime $\eta \gg \Delta, \delta, \epsilon$, where η is the energy splitting between the lowest two states $|L\rangle$ and $|R\rangle$ and the third energy level, and δ is the coupling between the qubit subspace and the next higher level, the dominant leakage occurs with rate

$$\frac{1}{T_L} \approx 4\left(\frac{\delta}{\eta}\right)^2 |\mathbf{m} \cdot \Delta\boldsymbol{\varphi}|^2 J(\eta) \coth \frac{\eta}{2k_B T}, \tag{150}$$

and in the regime in which the two-level approximation is well defined, $\Delta \gg k_B T$, thermally activated leakage is strongly suppressed.

3.2.2. *Asymmetry in the double-layer structure*

In the design of the Delft flux qubit [94] particular attention has been spent in order to render the qubit immune to current fluctuations from the current bias line. In case of zero dc bias current ($I_B = 0$), a small fluctuating current $\delta I_B(t)$, generated by the finite impedance of the current source, would equally divide into the two arms of the superconducting quantum interference device (SQUID) loop, such that no net current would cross the three-junction qubit line. Small geometrical asymmetry in the SQUID loop has been shown to be insufficient to cause decoherence at zero bias current [100], and the effects of a small asymmetry in the SQUID junctions are effectively negligible.

An artifact of the fabrication technique for producing superconducting Josephson junction circuits gives rise to another important asymmetry in the circuit, that affects the coherent dynamics of the qubit. The double-layer structure, resulting from the shadow evaporation technique, in which a Josephson junction is obtained introducing an insulating layer between a top and a bottom superconducting layers, always produces circuit loops with an even number of junctions. Therefore, a further unintentional asymmetry characterizes the Delft three-junction qubit. As proposed in [103], using a fourth much larger Josephson junction, for which the Josephson energy can be usually neglected, symmetry in the double-layer structure is restored and effects of fluctuations in the bias current are suppressed. Experimental data show [104] the behaviour of the decoherence time for two samples having the first three and the second four Josephson junctions. Both samples are studied at the *optimal point*, for which $\epsilon = 0$ so that $\partial E/\partial\epsilon = 0$, and at the *decoupling* bias current I_B^*, such that $\partial E/\partial I_B = 0$, that ensure decoupling of the qubit from the fluctuating bias current. For the first (three junction) qubit the dephasing time is $T_2 = 120\,\text{ns}$, obtained by fitting the exponentially decaying Ramsey fringes. In this case thermal fluctuation are shown to be negligible, and flux noise is believed to be responsible of strong decreasing of the dephasing time for $\epsilon \neq 0$. For the second (four junction) qubit the decoherence time is measured by means of a spin–echo technique, and it provides $T_{\text{echo}} = 3.9\,\mu\text{s}$ at the decoupled optimal point. In this case dephasing at the optimal point is produced by thermal fluctuations of the photon number in the plasma mode of the SQUID detector. As theoretically shown in [103], the restored symmetry of the four junction design leads to a shift of the maxima of T_1 and T_2 towards $I_B = 0$ and to an increase of their maximal values, which means a strong improvement due to the four junction design.

3.2.3. *Thermal photon noise-induced dephasing*

In addition to magnetic flux fluctuations, an important source of dephasing is represented by thermal photon noise in the read-out part of the circuit. To measure the state of the

qubit a SQUID is coupled to the qubit via mutual inductance. When the SQUID is biased by a current that has a value smaller than the critical current, the SQUID acts just as an effective inductor, whose linear inductance depends on the qubit current state. The critical current at which the SQUID switches to a normal state can have two values $I_c^{|0\rangle}$ and $I_c^{|1\rangle}$, according to the two qubit possible current states. A bias current pulse of amplitude I_B, $I_c^{|0\rangle} < I_B < I_c^{|1\rangle}$, allows us to discriminate between the two qubit states. The read-out apparatus consisting of a dc-SQUID and a shunt capacitor C_s forms a weakly damped harmonic oscillator of frequency $\omega_{\rm ho}$, that is detuned from the qubit frequency ω_q. The presence of n photons in the harmonic oscillator induces a shift in the qubit frequency, $\omega_{q,n} - \omega_{q,0} = n\delta\omega_0$, where the shift per photon depends on the effective qubit–oscillator coupling. Assuming that the pure dephasing time τ_ϕ is much larger than the inverse of the damping rate κ, $\tau_\phi \gg 1/\kappa$, thermally excited photons in the oscillator produce a dephasing [88,105,106]

$$\tau_\phi = \frac{\kappa}{\bar{n}(\bar{n}+1)\delta\omega_0^2}, \tag{151}$$

where $\bar{n} = (\exp(\hbar\omega_{\rm ho}/k_{\rm B}T) - 1)^{-1}$ is the thermal average number of photon in the oscillator. A similar effect has been observed in an experimental work [89] in which a charge qubit is coupled to a superconducting waveguide resonator, slightly detuned from the qubit frequency. There, opposite to the case described here, the oscillator is driven and a shift and a broadening in the qubit resonance frequency appear, as a consequence of an ac-Stark shift and of photon shot noise.

The flux qubit of [106] has been engineered with four Josephson junctions to ensure a symmetric qubit–SQUID coupling [103]. The qubit energy bias can be written as the sum of two contributions, $\epsilon = \eta + \lambda$, where $\eta = 2I_p(\Phi_{\rm ext} - \Phi_0/2)$ (I_p is the qubit persistent current) is controlled by the external flux $\Phi_{\rm ext}$ and $\lambda = 2I_pMJ(I_B)/h$ which depends on I_B via the SQUID circulating current. This dependence has two crucial consequences: first the qubit bias point $\Phi^*_{\rm ext}$ for which $\partial\omega_q/\partial\Phi_{\rm ext} = 0$ results shifted by the measurement pulse. Therefore, it is possible to operate the qubit at the flux-insensitive point, while keeping a difference in the expectation value of the current in the two qubit states, which is a crucial requirement for measuring the qubit state. Second a coupling between the qubit and the external harmonic oscillator, the so-called plasmon mode, arise, with an interaction Hamiltonian

$$\mathcal{H}_{\rm q-ho} \propto \left[g_1(I_B)(a + a^\dagger) + g_2(I_B)(a + a^\dagger)^2\right]\sigma_z, \tag{152}$$

where $g_1(I_B) \propto (\mathrm{d}\lambda/\mathrm{d}I_B)$ and $g_2(I_B) \propto (\mathrm{d}^2\lambda/\mathrm{d}I_B^2)$) (see [105]). For a particular I_B^* that realizes $\mathrm{d}\lambda/\mathrm{d}I_B = 0$, it is possible to switch $g_1(I_B)$ off [103,106].

Working at these optimal point, the qubit is immune from external flux and bias current fluctuations at first order, $\partial\omega_q/\partial\Phi_{\rm ext}(\Phi^*_{\rm ext}, I^*_B) = \partial\omega_q/\partial I_B(\Phi^*_{\rm ext}, I^*_B) = 0$. The shift per photon of $\delta\omega_0$ is given, at second-order perturbation theory in $\mathcal{H}_{\rm q-ho}$ (see [105,106]), by

$$\delta\omega_0 = 4\left[(g_1(I_B)\sin\theta)^2\frac{\omega_q}{\omega_{\rm ho}^2 - \omega_q^2} - g_2(I_B)\cos\theta\right], \tag{153}$$

where $\cos\theta = \epsilon/\omega_q$. For some value $\epsilon^*(I_B) < 0$ one obtains $\delta\omega_0 = 0$. In [106], via spectroscopy the authors demonstrated the existence of a line $\epsilon^*(I_B)$, that includes

$I_B = I_B^*$ and $\epsilon = 0$, providing an optimal point with respect to bias current noise, flux noise, and photon noise. Measurements of the qubit spectral line shape at the optimal point showed, for the particular sample [106], a twin peak structure, which could arise from strong coupling to one microscopic fluctuator. An effective dephasing time $t_2 = 2/\pi(w_1 + w_2)$ is obtained by fitting the peaks with two Lorentzians of width w_1 and w_2. Measurements of the spin–echo decay time T_{echo}, particularly indicated in case of relatively high-frequency noise, as photon noise in the plasma mode that occurs at $\kappa \approx 130\,\text{MHz}$, gives at the optimal point $T_{\text{echo}} = 3.9\,\mu\text{s}$. By studying the variation of T_{echo} and t_2 as a function of ϵ, a sharp peak is found at $\epsilon = 0$ for $I_B = I_B^*$, while for $I_B = 0$ the peak shifts towards $\epsilon < 0$. The variation of the maximum in t_2 as a function of I_B shows that the maximal coherence time is not obtained at $\epsilon = 0$, as it would be expected for flux or bias current noise. On the other hand, it fits with the line $\epsilon^*(I_B)$ for which $\delta\omega_0 = 0$, suggesting that thermally induced photon noise, rather than flux noise or bias current noise, is responsible for the qubit dephasing. For a temperature $T = 70\,\text{mK}$ and quality factor $Q = 150$, which yields a mean photon number $\bar{n} = 0.15$, the dephasing time τ_ϕ (151) closely matches the spin–echo measurements.

3.2.4. *Decoherence due to 1/f flux noise in flux qubits*

Recent remarkable experimental results have shown that low-frequency flux noise constitutes one of the main mechanisms of decoherence for flux qubits [107,108]. Experimentally, identification of the dominant sources of noise and the way they couple to the qubit degrees of freedom is achieved by changing the bias parameters and observing how the qubit dynamics results affected.

In [107] a Delft-like flux qubit is studied, in which the qubit shares a four junction line with a current biased SQUID shunted by an on-chip capacitance. The measurements of energy relaxation, free induction decay, and echo decay reveal that, at the optimal external flux $\Phi_{\text{ext}} = \Phi_{\text{ext}}^*$, and current $I_B = I_B^*$ bias conditions, where both $\partial E_{01}/\partial\Phi_{\text{ext}}$ and $\partial\Phi_{\text{ext}}/\partial I_B$ were set to zero in order to minimize dephasing due to fluctuations of Φ_{ext} and I_B, the energy-relaxation and echo signals decay exponentially with rates Γ_1 and Γ_{2E}. Moreover, since $\Gamma_{2E} \approx \Gamma_1/2$, the coherence in echo measurement is mainly limited by energy relaxation. Moving away from I_B^*, but remaining on the line $\Phi_{\text{ext}}^*(I_B)$, it is found that, although the rates Γ_1 and Γ_{2E} strongly depend on I_B, the decay curves are always exponential. This suggests that the fluctuations introduced by I_B have a relatively uniform spectrum, and that the I_B-dependent contributions are uniquely due to bias current fluctuations, which well decouple at $I_B = I_B^*$.

On the other hand, measurement at $\Phi_{\text{ext}} \neq \Phi_{\text{ext}}^*$, with the bias current kept at the optimal point $I_B = I_B^*$, show a qualitatively different behaviour. The energy relaxation rate Γ_1 is almost independent on Φ_{ext}, while the dephasing is strongly enhanced when slightly departing from $|\Phi_{\text{ext}} - \Phi_{\text{ext}}^*|$. Moreover, remarkably, the decay curves are no more exponential, but rather fitted with a Gaussian, $\exp[-(\Gamma_{\varphi E}^g t)^2]$, with a decay rate $\Gamma_{\varphi E}^g$ that increases almost linearly with $|\Phi_{\text{ext}} - \Phi_{\text{ext}}^*|$. Assuming Gaussian fluctuations of Φ_{ext} with spectrum density $S_{\Phi_{\text{ext}}}(\omega) = A_{\Phi_{\text{ext}}}/|\omega|$, the average echo decay is

$$\left\langle e^{i\varphi(t)} \right\rangle_E = e^{-(\Gamma_{\varphi E}^g t)^2}, \tag{154}$$

with the decay rate given by $\Gamma_{\varphi E}^{g} = \sqrt{A_{\Phi_{\rm ext}} \ln 2}|\partial E_{01}/\partial \Phi_{\rm ext}|/\hbar$. The linear dependence of $\Gamma_{\varphi E}^{g}$ on $\Phi_{\rm ext}$ follows from $|\partial E_{01}/\partial \Phi_{\rm ext}| = \epsilon/\sqrt{\epsilon^2 + \Delta^2}$, that for $\Phi_{\rm ext} - \Phi_{\rm ext}^{*} \approx 0$ is basically linear.

Similar results in [108] confirm the linear dependence of the $\Gamma_2^{\rm echo} = 1/T_2^{\rm echo}$ rate on the applied magnetic flux, and a very weak dependence of the relaxation rate $\Gamma_1 = 1/T_1$ on the external magnetic flux. Here, the qubit and the SQUID do not share a current line and the coupling between the qubit and the SQUID is purely inductive. The maximal $T_2^{\rm echo}$ is obtained, as expected, at the optimal point $\Phi_{\rm ext}^{*} = \Phi_0/2$, where $\partial E_{01}/\partial \Phi_{\rm ext} = 0$. From the Korringa relations (32), energy relaxation is related to the dephasing process via $\Gamma_2^{\rm echo} = \Gamma_1/2 + \Gamma_\varphi$, where Γ_φ represents the pure dephasing rate due to fluctuations in the energy splitting of the qubit. Splitting the pure dephasing rate Γ_φ in a non-magnetic contribution Γ_φ^0 and a first-order contribution due to magnetic fluctuations Γ_φ^Φ, $\Gamma_\varphi = \Gamma_\varphi^0 + \Gamma_\varphi^\Phi$, at the optimal point, where $\Gamma_\varphi^\Phi = 0$, the dephasing time $T_2^{\rm echo}$ of the qubit is found to be almost completely determined by the energy relaxation process, that is, $T_2^{\rm echo} = 250\,{\rm ns}$, and $T_1 = 140\,{\rm ns}$, with $T_2^{\rm echo} \approx 2T_1$, meaning that the dephasing of the flux qubit at the optimal point is mostly determined by the high-frequency noise $S_\Phi(\omega \approx \Delta/h)$. On the other hand, in the proximity of the optimal point, the linearity of the dephasing rate $\Gamma_2^{\rm echo}$, as a function of the applied magnetic field, suggests a departure from a Markovian dynamics, typical of noise with a short correlation time, and that the magnetic fluctuations have a $1/f$-type spectrum in a frequency range of the order of $1/T_2^{\rm echo}$.

3.3. *The superconducting phase qubit*

The phase qubit works in a regime in which $E_J \gg E_C$ and the circuit consists of a loop with a single large Josephson junction, as shown in Figure 9(a). The circuit is biased with a current I typically driven close to the critical current I_0 of the junction. The Hamiltonian of the system is

$$H = \frac{\hat{Q}^2}{2C} - \frac{I_0 \Phi_0}{2\pi}\cos\hat{\delta} - \frac{I\Phi_0}{2\pi}\hat{\delta}, \tag{155}$$

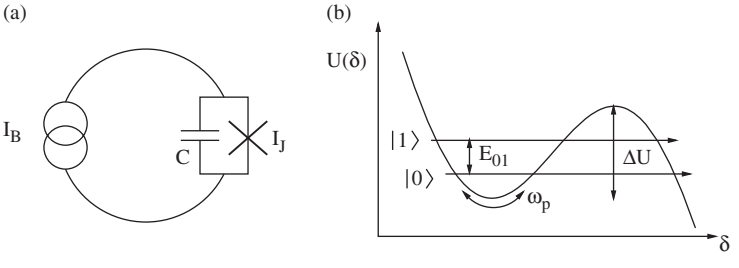

Figure 9. (a) Schematic representation of the phase qubit circuit, constituted by a current-biased Josephson junction. (b) Anharmonic potential $U(\delta)$ showing the two lowest-energy states $|0\rangle$ and $|1\rangle$, separated by an energy splitting E_{01}. The plasma frequency ω_p is given by the local quadratic curvature of the potential at the bottom of the well, and ΔU is the potential barrier that separates the two energy levels in the well from a continuum of levels on the right-hand side of the barrier.

where $\Phi_0/2\pi = \hbar/2e$ is the superconducting flux quantum. Charge and phase operators, $\hat{Q}$ and $\hat{\delta}$, that correspond to the charge on the Josephson junction capacitance and the superconducting phase across the Josephson junction, respectively, are conjugate variables that satisfy the canonical commutation rule $[\hat{\delta}, \hat{Q}] = 2ei$. For a large area junction $I_0\Phi_0/2\pi = E_J \gg E_C = e^2/2C$ the superconducting phase has a well-defined value and quantum mechanical behaviour can be observed. The Josephson inductance and the junction capacitance form an anharmonic 'LC' resonator. The anharmonic potential as a function of the superconducting phase across the junction can be approximated by a cubic potential parametrized by the potential barrier $\Delta U(I) = (2\sqrt{2I_0\Phi_0/3\pi})[1 - I/I_0]^{3/2}$ and a classical plasma oscillation frequency at the bottom of the potential well $\omega_p(I) = 2^{1/4}(2\pi\ I_0/\Phi_0 C)^{1/2}[1 - I/I_0]^{1/4}$. The two qubit states $|0\rangle$ and $|1\rangle$ are encoded in the two lowest quantum states in the potential well, and have energy splitting $E_{01} = \hbar\omega_p(1 - 5\hbar\omega_p/36\Delta U)$. Unlike in a flux or charge qubit, in a phase qubit the state ($|0\rangle$ or $|1\rangle$) is exclusively distinguished by the phase wavefunction, and not by any macroscopic quantity, such as current or charge. Transitions are driven by applying microwaves at frequency $\omega_{01} = E_{01}/\hbar$. For more details on the phase qubit we refer to [96].

Coherent control of the qubit is obtained through the bias current

$$I(t) = I_{\mathrm{dc}} + I_{1/f}(t) + I_{\mu wc}(t)\cos(\omega_{01}t) + I_{\mu ws}(t)\sin(\omega_{01}t), \tag{156}$$

where $I_{1/f}$, $I_{\mu wc}$, and $I_{\mu ws}$ are varied in time slowly compared with $2\pi/\omega_{01}$. In the frame rotating with frequency ω_{01}, the qubit Hamiltonian is given by

$$H = \epsilon\frac{\Phi_0}{2\pi}I_{\mu wc}(t)\sigma_x + \epsilon\frac{\Phi_0}{2\pi}I_{\mu ws}(t)\sigma_y + \frac{1}{2}\frac{\partial E_{01}}{\partial I_{\mathrm{dc}}}I_{1/f}(t)\sigma_z, \tag{157}$$

where $\epsilon = \sqrt{E_C/E_{01}}$, and $\sigma_{x,y,z}$ are the Pauli operators.

3.3.1. *Decoherence of a phase qubit due to an arbitrary noise source*

Since the qubit is controlled by the bias current, noise in the bias current can represent a source of decoherence for the qubit. In [109] a physical picture of decoherence is presented for a phase qubit.

In a Bloch picture, the state of the qubit is represented by $|\psi\rangle = \cos(\theta/2)|0\rangle + e^{i\phi}\sin(\theta/2)|1\rangle$. Low-frequency noise induces fluctuations is the longitudinal z component of the pseudo-spin representing the qubit that lead to dephasing of the qubit. The phase noise after time t is

$$\phi_n(t) = \frac{\partial\omega_{01}}{\partial I_{\mathrm{dc}}}\int_0^t \mathrm{d}t'\, I_n(t'), \tag{158}$$

and it arises from current noise $I_n(t)$. The magnitude of the phase noise is described by $\langle\phi_n^2(t)\rangle$, and it can be obtained through the noise spectral density $S_I(f)$,

$$\langle\phi_n^2(t)\rangle = \left(\frac{\partial\omega_{01}}{\partial I_{\mathrm{dc}}}\right)^2\int_0^{\omega_{01}/2\pi}\mathrm{d}f S_I(f)W_0(f), \tag{159}$$

where $S_I(f)$ is given by the Fourier transform of the noise correlator $\langle I_n(t)I_n(0)\rangle = \int_0^\infty \mathrm{d}f\, S_I(f)\cos(2\pi ft)$, the spectral weight $W_0(f) = \sin^2(\pi ft)/(\pi f)^2$, and the integral on the frequency has been cutoff for frequencies greater than $\omega_{01}/2\pi$. This last

assumption is justified since for those frequencies the noise current flows mainly through the junction capacitance, rather than the junction itself, thus not substantially affecting ω_{01}. The magnitude of noise is defined as the mean-square amplitude of the current noise at frequency f per 1 Hz bandwidth. For low frequencies $f \leq 1/t$, $W_0(f)$ is rather constant, whereas it decreases as $1/f^2$ at higher frequencies. As a consequence, phase noise affects the qubit dynamics only at low frequencies for most noise sources. For constant (white) noise S_I^0, one has

$$\langle \phi_n^2(t) \rangle = \left(\frac{\partial \omega_{01}}{\partial I_{\mathrm{dc}}} \right)^2 \frac{S_I^0 t}{2}. \tag{160}$$

At higher frequencies close to ω_{01}, noise induces transitions between the two qubit states $|0\rangle$ and $|1\rangle$. The current that controls these transitions is given by $I_{\mu wc}(t) \cos(\omega_{01} t) + I_{\mu ws}(t) \sin(\omega_{01} t)$, and mixing from noise around frequency ω_{01} can be understood as low-frequency noise in $I_{\mu wc}(t)$ and $I_{\mu ws}(t)$. Random fluctuations along the transverse x and y components of the qubit induce transitions between the qubit states. For constant spectral density around ω_{01} given by $2S_I(\omega_{01}/2\pi)$, an application of the previous results gives

$$\langle \theta_x^2(t) \rangle = \left\langle \theta_y^2(t) \right\rangle = \frac{E_C}{E_{01}} \left(\frac{\Phi_0}{2\pi} \right)^2 S_I(\omega_{01}/2\pi) t. \tag{161}$$

The random angles $\chi = \phi$, θ_x and θ_y are assumed to be Gaussian distributed, with zero mean and mean squared noise $\langle \chi^2 \rangle$ calculated previously, $\mathrm{d}p(\chi)/\mathrm{d}\chi = \exp(-\chi^2/2\langle \chi^2 \rangle)/\sqrt{2\pi \langle \chi^2 \rangle}$.

If the qubit is initially in the ground state, that is when it is parallel to the z direction in the Bloch sphere, when the noise is small, it is immune to phase noise at low frequencies. However, transverse noise around a frequency ω_{01} can induce transitions in between the qubit states. The probability p_0 to be in the state $|0\rangle$ is given in the Bloch picture by $\cos^2(\theta/2) \simeq \cos^2[\sqrt{\theta_x^2 + \theta_y^2}/2]$. With the values previously obtained for the mean-square noise, averaging over the Gaussian distribution gives

$$p_0 = \frac{1}{2}\left(1 + e^{-t/T_1}\right), \quad \frac{1}{T_1} = \frac{E_C}{E_{01}} \left(\frac{\Phi_0}{2\pi} \right)^2 S_I(\omega_{01}/2\pi). \tag{162}$$

The rate $1/T_1$ describes the absorption and emission rate for the stimulated transitions $0 \to 1$ and $1 \to 0$. Since low-frequency noise cannot add energy $\hbar\omega_{01}$, there is no contribution from phase noise.

The effects of noise on a superposition state can be understood within a 'Ramsey fringe' picture. Through a $\pi/2$ pulse the qubit is rotated from the ground state $|0\rangle$ to the state $(|0\rangle + |1\rangle)/\sqrt{2}$, that points in the x direction in the Bloch sphere, and left evolving for a time t, after which a subsequent $\pi/2$ pulse is performed and the qubit state is finally measured. During the evolution between the two $\pi/2$ pulses, the state of the qubit can change due to noise in ϕ and θ_y, therefore, both phase and stimulated transitions noise affect the qubit dynamics. In this case, the total decoherence rate is given by the Korringa relation [10] $1/T_2 = 1/T_\phi + 1/2T_1$, where $1/T_\phi$ is directly extracted from (160) $1/T_\phi = (\partial \omega_{01}/\partial I_c)^2 S_I^0/4$.

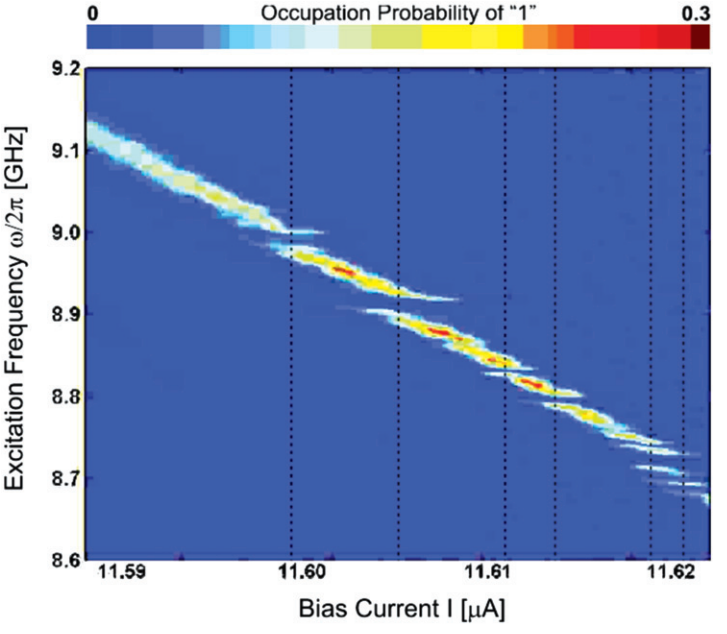

Figure 10. Measured probability of state '1' versus microwave excitation frequency $\omega/2\pi$ and bias current I for a fixed microwave power for a phase qubit. The dotted vertical lines indicate spurious resonators. Reprinted with permission from [110]. © 2005 by the American Physical Society.

3.3.2. *1/f noise in superconducting phase qubit*

In this section we review recent results on the decoherence of superconducting phase qubits [95,96]. Recent experiments [110,111] have pointed out that a dominant source of decoherence for the phase qubit is represented by low-frequency $1/f$ noise, that is believed to arise from two level systems in the insulating barrier of the tunnel junction as well as in the dielectric material surrounding the circuit. In Figure 10 a measurement of the transition frequency ω_{01} between the two qubit state, as a function of the bias current I and the microwave excitation frequency $\omega/2\pi$, shows a qubit line in which a number of spurious resonators appear, characteristic of the energy-level repulsion predicted for coupled two-state systems. Near the resonators, the Rabi oscillations show beating, loss, and recovery of the oscillations with time, and a rapid decrease in coherence amplitude. The beating behaviour is consistent with the interaction of a qubit with another two-level system, but not with harmonic oscillator modes in the read-out SQUID. Moreover, each different sample has its own set of resonator frequencies and strengths, indicating that the two-level systems have a microscopic origin.

A new method to measure $1/f$ noise in Josephson junction qubits was presented recently in [112]. It uses the resonant response of the qubit to directly measure the spectrum of the low-frequency noise, and allows us to distinguish between flux and critical-current fluctuations by comparison of the noise taken at positive and negative bias. Remarkably it can yield low-frequency spectra below 1 Hz. Dephasing is produced by

low-frequency fluctuations in the qubit energy, which in this study are believed to arise from magnetic flux noise in the qubit loop, with a spectral density that scales inversely with frequency, $1/f$. It turns out that the flux-like noise predominates over critical-current noise.

The possibility that the flux noise is due to two-level system defects in the native oxides of the superconductive film, as proposed in [113], is examined in [112]. Following [114] for a standard two-level system model [115] a theoretical estimation of the flux noise spectral density, for a realistic geometry of the circuit loop, gives $S_\Phi(1\text{Hz}) \approx 10^{-3}(\mu\Phi_0)^2/\text{Hz}$, about four orders of magnitude smaller than the measured flux noise. This estimate is based on the assumption that the two-level system fluctuations randomize the defect magnetic moment; this assumption is highly questionable because two-level system defects in typical oxides are not considered to be magnetic.

4. Conclusion

Decoherence in solid-state devices is a fascinating and currently very relevant topic. From the point of view of fundamental research, it is interesting to study the quantum-classical boundary and the mechanisms that play a dominant role in the disappearance of coherence in the time-evolution of quantum systems. Solid-state devices are particularly interesting since they are typically complex and consist of many particles. From the point of view of possible applications, the relevant coherence and relaxation times of the quantum hardware (for example, T_1 and T_2 for Markovian systems) is what ultimately limits the performance for quantum computing. In order to be able to perform long quantum computations, a thorough understanding and optimization of decoherence plays a key role, together with quantum error correction and fault-tolerant quantum computation schemes. Owing to their potential for scaling, solid-state systems are among the most promising candidates for the implementation of quantum information processing. Therefore, the decoherence mechanisms that affect those devices needs to be fully understood and suppressed where this is possible.

We have reviewed the current state of knowledge regarding decoherence in solid-state qubits, mainly from a theoretical point of view, but also reporting on some particularly significant experimental results and achievements. After having introduced the main concepts of quantum coherence, quantum open systems, and system–environment interactions, and the mathematical framework needed to study the physics of open quantum systems, we have reviewed the current status of our understanding of decoherence both in spin qubits and superconducting qubits.

Many coherent oscillations have been experimentally observed for spin qubits and superconducting qubits, showing coherence times much longer than the time needed to perform a single quantum operation. Therefore, it can be expected that these two leading solid-state embodiments of quantum hardware will also play an important role in the years to come. While the latest experimental and theoretical achievements are promising indications that further progress in this direction is possible, the up-scaling to more qubits, fault-tolerant quantum computing under physically realistic conditions, control and preparation of the environment (for example, nuclear spins), and others, represent the challenges that lie ahead.

References

[1] N.F. Ramsey, Phys. Rev. 78 (1950), pp. 695–699.
[2] S. Nakajima, Progr. Theor. Phys. 20 (1958), p. 948.
[3] R. Zwanzig, J. Chem. Phys. 33 (1960), p. 1338.
[4] ———, *Lectures in Theoretical Physics*, Vol. 3, W.E. Brittin, B.W. Downs, and J. Downs, eds., Interscience, New York, 1961.
[5] A.G. Redfield, Adv. Magn. Reson. 1 (1965), p. 1.
[6] K. Blum, *Density Matrix Theory and Applications*, Plenum Press, New York, 1981.
[7] C.P. Slichter, *Principles of Magnetic Resonance*, Amsterdam, North-Holland, 1987.
[8] G. Lindblad, Commun. Math. Phys. 48 (1976), p. 119.
[9] A.G. Redfield, IBM J. Res. Dev. 1 (1957), p. 19.
[10] A. Abragam, *The Principles of Nuclear Magnetism*, Clarendon Press, Oxford, 1961.
[11] G. Ithier, E. Collin, P. Joyez, P.J. Meeson, D. Vion, D. Esteve, F. Chiarello, A. Shnirman, Y. Makhlin, J. Schriefl et al., Phys. Rev. B 72 (2005), p. 134519.
[12] R.P. Feynman and F.L. Vernon, Ann. Phys. 24 (1963), p. 118.
[13] A.O. Caldeira and A.J. Leggett, Ann. Phys. (San Diego) 149 (1983), p. 374.
[14] A.J. Leggett, S. Chakravarty, A.T. Dorsey, M.P.A. Fisher, A. Garg, and W. Zwerger, Rev. Mod. Phys. 59 (1987), pp. 1–85.
[15] U. Weiss, *Quantum Dissipative Systems*, World Scientific, London, 1999.
[16] D.P. DiVincenzo and D. Loss, Phys. Rev. B 71 (2005), p. 035318.
[17] ———, Exact Born approximation for the spin-boson model, Preprint (2003), cond-mat/0304118.
[18] J.R. Petta et al., Phys. Rev. Lett. 100 (2008), p. 067601.
[19] D. Loss and D.P. DiVincenzo, Phys. Rev 57 (1998), p. 120.
[20] J.R. Petta, J.M. Taylor, A.C. Johnson, A. Yacoby, M.D. Lukin, C.M. Marcus, M.P. Hanson, and A.C. Gossard, Dynamic nuclear polarization with single electron spins, Phys. Rev. Lett. 100 (2008), p. 067601.
[21] A.V. Khaetskii and Y.V. Nazarov, Phys. Rev. B 61 (2000), p. 12639.
[22] ———, Phys. Rev. B 64 (2001), p. 125316.
[23] S. Amasha, K. MacLean, P.R. Iuliana, D.M. Zumbuhl, M.A. Kastner, M.P. Hanson, and A.C. Gossard, Electrical control of spin relaxation in a quantum dot, Phys. Rev. Lett. 100 (2008), p. 046803.
[24] G. Burkard, D. Loss, and D.P. DiVincenzo, Phys. Rev. B 59 (1999), p. 2070.
[25] W.A. Coish, E.A. Yuzbashyan, B.L. Altshuler, and D. Loss, J. Appl. Phys 101 (2007), p. 081715.
[26] D. Paget, G. Lampel, B. Sapoval, and V.I. Safarov, Phys. Rev. B 15 (1977), p. 7580.
[27] A.V. Khaetskii, D. Loss, and L. Glazman, Phys. Rev. Lett. 88 (2002), p. 186802.
[28] W.A. Coish and D. Loss, Phys. Rev. B 70 (2004), p. 195340.
[29] J.R. Petta, A.C. Johnson, J.M. Taylor, E.A. Laird, A. Yacoby, M.D. Lukin, C.M. Marcus, M.P. Hanson, and A.C. Gossard, Science 309 (2005), p. 2180.
[30] F.H.L. Koppens, D. Klauser, W.A. Coish, K.C. Nowack, L.P. Kouwenhoven, D. Loss, and L.M.K. Vandersypen, Phys. Rev. Lett. 99 (2007), p. 106803.
[31] D. Klauser, W.A. Coish, and D. Loss, Phys. Rev. B 74 (2006), p. 205302.
[32] D. Stepanenko, G. Burkard, G. Giedke, and A. Imamoglu, Phys. Rev. Lett. 96 (2006), p. 136401.
[33] K. Ono and S. Tarucha, Phys. Rev. Lett. 92 (2004), p. 256803.
[34] F.H.L. Koppens, C. Buizert, K.J. Tielrooij, I.T. Vink, K.C. Nowack, T. Meunier, L.P. Kouwenhoven, and L.M.K. Vandersypen, Nature (London) 442 (2006), p. 766.
[35] I.A. Merkulov, A.L. Efros, and J. Rosen, Phys. Rev. B 65 (2002), p. 205309.
[36] W.A. Coish and D. Loss, Phys. Rev. B 72 (2005), p. 125337.

[37] E.A. Laird, J.R. Petta, A.C. Johnson, C.M. Marcus, A. Yacoby, M.P. Hanson, and A.C. Gossard, Phys. Rev. Lett. 97 (2006), p. 056801.
[38] G. Giedke, J.M. Taylor, D. D'Alessandro, M.D. Lukin, and A. Imamoğlu, Phys. Rev 74 (2006), p. 032316.
[39] W.A. Coish, J. Fischer, and D. Loss, Exponential decay in a spin bath, Phys. Rev. B 77 (2008), p. 125329.
[40] J.J. Sakurai, *Advanced Quantum Mechanics*, Addison-Wesley, Reading, MA, 1967.
[41] G. Dresselhaus, Phys. Rev. 100 (1955), p. 580.
[42] M.I. Dyakonov and V.Yu. Kachorovskii, Sov. Phys. Semicond. 20 (1986), p. 110.
[43] M.I. Dyakonov and V.I. Perel, Sov. Phys. JETP 33 (1971), p. 1053.
[44] E.I. Rashba, Sov. Phys. Solid State 2 (1960), p. 1109.
[45] Yu.A. Bychkov and E.I. Rashba, JETP Lett. 39 (1984), p. 78.
[46] G.E. Pikus and A.N. Tikov, *Optical Orientation*, Amsterdam, North-Holland, 1984, p. 73.
[47] L.M. Roth, Phys. Rev. 118 (1960), p. 1534.
[48] T. Fujisawa, T.H. Oosterkamp, W.G. van der Wiel, B.W. Broer, R. Aguado, S. Tarucha, and L.P. Kouwenhoven, Science 282 (1998), p. 932.
[49] V.I. Fal'ko, B.L. Altshuler, and O. Tsyplyatyev, Phys. Rev. Lett. 95 (2005), p. 076603.
[50] T. Meunier, I.T. Vink, L.H. Willems van Beveren, K.-J. Tielrooij, R. Hanson, F.H.L. Koppens, H.P. Tranitz, W. Wegscheider, L.P. Kouwenhoven, and L.M.K. Vandersypen, Phys. Rev. Lett. 98 (2007), p. 126601.
[51] D. Rugar, R. Budakian, H.J. Mamin, and B.W. Chui, Nature (London) 430 (2004), p. 329.
[52] J.M. Elzerman, R. Hanson, L.H. Willems van Beveren, B. Witkamp, L.M.K. Vandersypen, and L.P. Kouwenhoven, Nature (London) 430 (2004), p. 431.
[53] M. Kroutvar, Y. Ducommun, D. Heiss, M. Bichler, D. Schuh, G. Abstreiter, and J.J. Finley, Nature (London) 432 (2004), p. 81.
[54] D.V. Bulaev and D. Loss, Phys. Rev. B 71 (2005), p. 205324.
[55] P. Stano and J. Fabian, Phys. Rev. B 72 (2005), p. 155410.
[56] ———, Phys. Rev. Lett. 96 (2006), p. 186602.
[57] V.N. Golovach, A. Khaetskii, and D. Loss, Phys. Rev. Lett. 93 (2004), p. 016601.
[58] P. San-Jose, G. Zarand, A. Shnirman, and G. Schöon, Phys. Rev. Lett. 97 (2006), p. 076803.
[59] Al.L. Efros and M. Rosen, Phys. Rev. B 58 (1998), p. 7120.
[60] L.M. Woods, T.L. Reinecke, and R. Kotlyar, Phys. Rev. B 69 (2004), p. 125330.
[61] C. Lü, J.L. Cheng, and M.W. Wu, Phys. Rev. B 71 (2005), p. 075308.
[62] D.V. Bulaev and D. Loss, Phys. Rev. Lett. 95 (2005), p. 076805.
[63] J.M. Luttinger and W. Kohn, Phys. Rev. 97 (1955), p. 869.
[64] J.M. Luttinger, Phys. Rev. 102 (1956), p. 1030.
[65] R. Winkler, Phys. Rev. B 62 (2000), p. 4245.
[66] R. Winkler, H. Noh, E. Tutuc, and M. Shayegan, Phys. Rev. B 65 (2002), p. 155303.
[67] H.W. van Kesteren, E.C. Cosman, W.A.J.A. van der Poel, and C.T. Foxon, Phys. Rev. B 41 (1990), p. 5283.
[68] B.P. Zakharchenya and F. Meier, *Optical Orientation*, Amsterdam, North-Holland, 1984.
[69] D.V. Bulaev and D. Loss, Phys. Rev. Lett. 98 (2007), p. 097202.
[70] D. Heiss, S. Schaeck, H. Huebel, M. Bichler, G. Abstreiter, J.J. Finley, D.V. Bulaev, and D. Loss, Observation of extremely slow hole spin relaxation in self-assembled quantum dots, Preprint (2007), arXiv:0705.1466.
[71] N.G. Ganichev, V.A. Margulis, and A.V. Shorokhov, Phys. Rev. B 69 (2004), p. 113312.
[72] V. Fock, Z. Phys. 47 (1928), pp. 446–448.
[73] C.G. Darwin, Proc. Cambridge Philos. Soc. 27 (1930), pp. 86–90.
[74] S.D. Ganichev, V.V. Bel'kov, L.E. Golub, E.L. Ivchenko, P. Schneider, S. Giglberger, J. Eroms, J. De Boeck, G. Borghs, W. Wegscheider et al., Phys. Rev. Lett. 92 (2004), p. 256601.

[75] F.H.L. Koppens, C. Buizert, K.J. Tielrooij, I.T. Vink, K.C. Nowack, T. Meunier, L.P. Kouwenhoven, and L.M.K. Vandersypen, Nature 442 (2006), p. 766.
[76] R. Meisels, Semicond. Sci. Technol. 20 (2005), p. R1.
[77] A. Abragam, *The Principles of Nuclear Magnetism*, Plenum, New York, 1996.
[78] M.H. Devoret, *Quantum Fluctuations in Electrical Circuits*, S. Reynaud, E. Giacobino, and J. Zinn-Justin, eds., Elsevier, Amsterdam, 1997.
[79] Y. Makhlin, G. Schöon, and A. Shnirman, Rev. Mod. Phys. 73 (2001), p. 357.
[80] M.H. Devoret, A. Wallraff, and J.M. Martinis, Superconducting qubits: a short review, Preprint (2004), cond-mat/0411174.
[81] D.V. Averin, Solid State Commun. 105 (1998), p. 659.
[82] Y. Makhlin, G. Schön, and A. Shnirman, Nature 398 (1999), pp. 305–307.
[83] Y. Nakamura, Yu.A. Pashkin, and J.S. Tsai, Nature 398 (1999), pp. 786–788.
[84] Yu.A. Pashkin, T. Yamamoto, O. Astafiev, Y. Nakamura, D.V. Averin, and J.S. Tsai, Nature 421 (2003), pp. 823–826.
[85] A. Shnirman, G. Schön, and Z. Hermon, Phys. Rev. Lett. 79 (1997), pp. 2371–2374.
[86] D. Vion, A. Aassime, A. Cottet, P. Joyez, H. Pothier, C. Urbina, D. Esteve, and M.H. Devoret, Science 296 (2002), p. 886.
[87] A. Wallraff, D.I. Schuster, A. Blais, L. Frunzio, R.-S. Huang, J. Majer, S. Kumar, S.M. Girvin, and R.J. Schoelkopf, Nature 431 (2004), pp. 162–167.
[88] A. Blais, R.-S. Huang, A. Wallraff, S.M. Girvin, and R.J. Schoelkopf, Phys. Rev. A 69 (2004), p. 062320.
[89] D.I. Schuster, A. Wallraff, A. Blais, L. Frunzio, R.-S. Huang, J. Majer, S.M. Girvin, and R.J. Schoelkopf, Phys. Rev. Lett. 94 (2005), p. 123602.
[90] A. Blais, J. Gambetta, A. Wallraff, D.I. Schuster, S.M. Girvin, M.H. Devoret, and R.J. Schoelkopf, Phys. Rev 75 (2007), p. 032329.
[91] T.P. Orlando, J.E. Mooij, L. Tian, C.H. van der Wal, L.S. Levitov, S. Lloyd, and J.J. Mazo, Phys. Rev. B 60 (1999), pp. 15398–15413.
[92] J.E. Mooij, T.P. Orlando, L. Levitov, L. Tian, C.H. van der Wal, and S. Lloyd, Science 285 (1999), p. 1036.
[93] C.H. van der Wal, A.C.J. ter Haar, F.K. Wilhelm, R.N. Schouten, C.J.P.M. Harmans, T.P. Orlando, S. Lloyd, and J.E. Mooij, Science 290 (2000), p. 773.
[94] I. Chiorescu, Y. Nakamura, C.J.P.M. Harmans, and J.E. Mooij, Science 299 (2003), p. 1869.
[95] L.B. Ioffe, V.B. Geshkenbein, M.V. Feigel'man, A.L. Fauchère, and G. Blatter, Nature 398 (1999), pp. 679–681.
[96] J.M. Martinis, S. Nam, J. Aumentado, and C. Urbina, Phys. Rev. Lett. 89 (2002), p. 117901.
[97] A. Cottet, D. Vion, A. Aassime, P. Joyez, D. Esteve, and M.H. Devoret, Physica C 367 (2002), p. 197.
[98] Yu. Makhlin and A. Shnirman, Phys. Rev. Lett. 92 (2004), p. 178301.
[99] G. Falci, A. D'Arrigo, A. Mastellone, and E. Paladino, Phys. Rev. A 70 (2004), p. 040101(R).
[100] G. Burkard, R.H. Koch, and D.P. DiVincenzo, Phys. Rev. B 69 (2004), p. 064503.
[101] R.H. Koch, J.R. Rozen, G.A. Keefe, F.M. Milliken, C.C. Tsuei, J.R. Kirtley, and D.P. DiVincenzo, Phys. Rev. B 72 (2005), p. 092512.
[102] L. Tian, L.S. Levitov, C.H. van der Wal, J.E. Mooij, T.P. Orlando, S. Lloyd, C.J.P.M. Harmans, and J.J. Mazo, *Quantum Mesoscopic Phenomena and Mesoscopic Devices in Microelectronics*, *NATO Science Series C: Mathematical and Physical Science No. 559*, I. Kulik and R. Elliatioglu, eds., Kluwer Academic, Dordrecht, 2000, p. 429.
[103] G. Burkard, D.P. DiVincenzo, P. Bertet, I. Chiorescu, and J.E. Mooij, Phys. Rev. B 71 (2005), p. 134504.
[104] P. Bertet, I. Chiorescu, G. Burkard, K. Semba, C.J.P.M. Harmans, D.P. DiVincenzo, and J.E. Mooij, Relaxation and dephasing in a flux qubit, Preprint (2004), cond-mat/0412485.

[105] P. Bertet, I. Chiorescu, C.J.P.M. Harmans, and J.E. Mooij, Dephasing of a flux-qubit coupled to a harmonic oscillator, Preprint (2005), cond-mat/0507290.
[106] P. Bertet, I. Chiorescu, G. Burkard, K. Semba, C.J.P.M. Harmans, D.P. DiVincenzo, and J.E. Mooij, Phys. Rev. Lett. 95 (2005), p. 257002.
[107] F. Yoshihara, K. Harrabi, A.O. Niskanen, Y. Nakamura, and J.S. Tsai, Phys. Rev. Lett. 97 (2006), p. 167001.
[108] K. Kakuyanagi, T. Meno, S. Saito, H. Nakano, K. Semba, H. Takayanagi, F. Deppe, and A. Shnirman, Phys. Rev. Lett. 98 (2007), p. 047004.
[109] J.M. Martinis, S. Nam, J. Aumentado, and K.M. Lang, Phys. Rev. B 67 (2003), p. 094510.
[110] R.W. Simmonds, K.M. Lang, D.A. Hite, S. Nam, D.P. Pappas, and J.M. Martinis, Phys. Rev. Lett. 93 (2004), p. 077003.
[111] J.M. Martinis, K.B. Cooper, R. McDermott, M. Steffen, M. Ansmann, K.D. Osborn, K. Cicak, S. Oh, D.P. Pappas, R.W. Simmonds et al., Phys. Rev. Lett. 95 (2005), p. 210503.
[112] R.C. Bialczak, R. McDermott, M. Ansmann, M. Hofheinz, N. Katz, E. Lucero, M. Neeley, A.D. O'Connel, H. Wang, A.N. Cleland et al., Phys. Rev. Lett. 99 (2007), p. 187006.
[113] R.H. Koch, D.P. DiVincenzo, and J. Clarke, Phys. Rev. Lett. 98 (2007), p. 267003.
[114] A. Shnirman, G. Schön, I. Martin, and Y. Makhlin, Phys. Rev. Lett. 94 (2005), p. 127002.
[115] S. Hunklinger and A.K. Raychaudhuri, *Amorphous Solids: Low-temperature Properties*, W.A. Phillips, ed., Springer, Berlin, 1981.
[116] G. Burkard, Phys. Rev. B 71 (2005), p. 144511.

Appendix A: Circuit theory and system Hamiltonian

A systematic approach to obtain the Lagrangian and the Hamiltonian of a generic circuit containing many different lumped elements, as well as Josephson junctions, has been proposed in [100,116]. In this way, it is possible to construct the full classical Hamiltonian of the system, quantize it and study its quantized spectrum, in the two-level approximation.

A.1. *Network graph theory and the equations of motion*

By means of classical network theory, an electric circuit is represented by an oriented graph, consisting of nodes and branches. Each branch corresponds to a single two-terminal element, such as a resistor, capacitor, inductor, current source, voltage source, etc. The branches are then divided into two groups, the tree, representing a set of branches of the graph connecting all nodes without containing any loop, and the chords, represented by all of the rest of the branches. In this way every time a chord branch is added to the tree a loop is obtained. The grouping in chords and tree depends on the formalism adopted, that in turn is functional to the kind of circuit described, either a flux qubit or a charge qubit. All of the topological information of the circuit is contained in the fundamental loop matrix $\mathbf{F}$, which connects tree branches and loops (that is, chords), such that the matrix elements F_{XY} can be 1, -1, 0, depending whether the tree branch X and the chord branch Y have the same orientation, different orientation in the loop, or do not belong to the same loop.

The equations of motion are represented by Kirchhoff's laws, and can be at once written as

$$\mathbf{F}\mathbf{I}_{\mathrm{ch}} = -\mathbf{I}_{\mathrm{tr}}, \quad \mathbf{F}^T\mathbf{V}_{\mathrm{tr}} = \mathbf{V}_{\mathrm{ch}} - \dot{\mathbf{\Phi}}_{\mathrm{ext}}. \tag{A1}$$

Here $\mathbf{\Phi}_{\mathrm{ext}}$ takes into account the possibility of having time-dependent applied external fluxes. The fluxes and charges of the circuit represent the canonical variables of system, and they can be formally defined for the generic element X as

$$\mathbf{I}_X(t) = \dot{\mathbf{Q}}_X(t), \quad \mathbf{V}_X(t) = \dot{\mathbf{\Phi}}_X(t). \tag{A2}$$

From the last equation and from the second Josephson relation, it is possible to identify the formal flux associated to the Josephson junction as the superconducting phase difference φ across the junction,

$$\frac{\mathbf{\Phi}_J}{\Phi_0} = \frac{\boldsymbol{\varphi}}{2\pi}, \quad \mathbf{I}_J = \mathbf{I}_c \sin \boldsymbol{\varphi}, \tag{A3}$$

where $\sin \boldsymbol{\varphi} = \{\sin \varphi_1, \sin \varphi_2, \ldots\}$, and the second formula represents the first Josephson relation. With current–voltage relations for the various types of other branches, it is possible to obtain the classical equations of motion for the superconducting phases

$$\mathbf{C}\ddot{\boldsymbol{\varphi}} = -\mathbf{L}_J^{-1} \sin \boldsymbol{\varphi} - \mathbf{M}_0 \boldsymbol{\varphi} - \mathbf{M}_d * \boldsymbol{\varphi} - \frac{2\pi}{\Phi_0}(\mathbf{N}\mathbf{\Phi}_{\text{ext}} + \mathbf{S}\mathbf{I}_B), \tag{A4}$$

where $\mathbf{L}_J^{-1} = 2\pi \mathbf{I}_c / \Phi_0$ is a diagonal matrix for the Josephson inductances of the junctions, $\mathbf{M}_0$ is the matrix of linear inductance, describing their energy and mutual interaction, $\mathbf{N}$ and $\mathbf{S}$ describing the inductive coupling of the phases φ with external fluxes and currents, respectively. Here $\mathbf{M}_d(t)$ is a symmetric matrix containing all of the dissipative dynamics of φ (see [100]).

A.2. *Two-level approximation*

Dissipative elements present in the circuit are incompatible with a Hamiltonian description of the system, therefore for the moment we omit them. In order to derive the Lagrangian for the electric circuit, a complete set of unconstrained flux and charge degrees of freedom has to be isolated, such that every assignment of values to those charges and fluxes represents a possible dynamical state of the system. The Hamiltonian of the circuit follows straightforwardly from the Lagrangian by means of a Legendre transformation, and can be formally written as

$$\mathcal{H} = \frac{1}{2}(\mathbf{Q} - C_{\mathbf{V}}\mathbf{V})^T \mathbf{C}^{-1} (\mathbf{Q} - C_{\mathbf{V}}\mathbf{V}) + \left(\frac{\Phi_0}{2\pi}\right)^2 U(\boldsymbol{\varphi}), \tag{A5}$$

$$U(\boldsymbol{\varphi}) = -\sum_i \frac{2\pi I_{c;i}}{\Phi_0} \cos \varphi_i + \frac{1}{2}\boldsymbol{\varphi}^T \mathbf{M}_0 \boldsymbol{\varphi} + \frac{2\pi}{\Phi_0}\boldsymbol{\varphi}^T(\mathbf{N}\mathbf{\Phi}_{\text{ext}} + \mathbf{S}\mathbf{I}_B), \tag{A6}$$

where $\mathcal{C}$ is the capacitance matrix, collecting all of the capacitive elements of the circuit, and describing the effective charge energy of the system, $C_{\mathbf{V}}$ describes the coupling of the charges $\mathbf{Q}$ to externally applied voltages $\mathbf{V}$. The number of Cooper pairs, that accumulate on a junction capacitance, and the phase of the superconducting order parameter through the junction, for sufficiently low temperatures, become quantized and satisfy canonical commutation rules,

$$\left[\hat{\Phi}_i, \hat{Q}_j\right] = \left[\frac{\Phi_0}{2\pi}\hat{\varphi}_i, 2e\hat{N}_j\right] = i\hbar\delta_{ij}, \tag{A7}$$

where $2e$ is the charge of a Cooper pair, and $\Phi_0/2\pi$ is flux quantum. Therefore, once a Hamiltonian is obtained from circuit theory, its quantization follows straightforwardly. The energy of an isolated system is a conserved quantity, therefore strictly speaking the Hamiltonian should be time independent. However time-dependent circuit elements, such as alternating currents and voltages, can be included in the Hamiltonian description as time-dependent parameters.

Care should be taken when dissipative elements such as resistors are present in the circuit. In this case a more general approach must be adopted, in which the system considered is coupled to a environmental bath, and the dynamics of the circuit under analysis is obtain as the dynamics of part of a larger isolated system, as discussed in Section 1.6.1.

Once the Hamiltonian has been obtained and quantized it is possible to study the temperature regime, in which few low-energy states are taken into consideration. A two-level

approximation can be carried out by considering only the ground state and first excited state, and neglecting higher levels of the spectrum. The goodness of the two-level approximation is controlled by the ratio of the temperature and the energy gap between the first and second excited state, $k_B T/\Delta_{12} \ll 1$. The Hamiltonian of the two-level system can therefore be expressed in the form of a pseudo-spin 1/2

$$\mathcal{H} = \frac{\Delta}{2}\sigma_x + \frac{\epsilon}{2}\sigma_z, \tag{A8}$$

where Δ denotes the tunnel coupling between the two qubit states $|0\rangle$ and $|1\rangle$, eigenstates of σ_z, and ϵ the bias, owing to asymmetry.